

**Study of New Metabolites Produced by Endophytic Fungi
from Merapi Volcano Area in Java Island, Indonesia**

インドネシア・ジャワ島のメラピ火山の麓で採取した植物内生
菌類が生産する新規二次代謝産物に関する研究

DOCTORAL THESIS

Nanang Rudianto Ariefta
from Republic of Indonesia

**Division of Biomolecular Function
Specialty of Bioresources Science
The United Graduate School of Agricultural Sciences
Iwate University
2020**

**Study of New Metabolites Produced by Endophytic Fungi
from Merapi Volcano Area in Java Island, Indonesia**

インドネシア・ジャワ島のメラピ火山の麓で採取した植物内生菌類が生産
する新規二次代謝産物に関する研究

DOCTORAL THESIS

Submitted to Fulfill A Part of The Requirements for the Title Doctor of Philosophy
in the United Graduate School of Agricultural Sciences at Iwate University

Presented by

Nanang Rudianto Ariefta

from Republic of Indonesia

Major Advisory Professor:

Prof. Dr. Yoshihito Shiono (Yamagata University)

Advisory Professor:

Prof. Dr. Takuya Koseki (Yamagata University)

Prof. Dr. Ken-ichi Kimura (Iwate University)

Division of Biomolecular Function

Specialty of Bioresources Science

The United Graduate School of Agricultural Sciences

Iwate University

2020

List of Contents

List of Contents	i
List of Figures	iv
List of Tables	vi
Summary	vii
List of Abbreviations	x
Chapter 1 Introduction	1
1.1 Natural products as source of drugs	1
1.2 Endophytic fungi	4
1.3 Mount Merapi, a volcano in Java Island, Indonesia	8
1.4 Objectives and overview of this study	9
1.5 General experimental procedures	10
Chapter 2 Metabolites from <i>Nectria pseudotrichia</i> 120-1NP	11
2.1 Introduction	11
2.2 Experimental	11
2.2.1 Fungal material and fermentation	11
2.2.2 Extraction and isolation	11
2.2.3 Experimental X-ray of nectrianolin A (1)	12
2.2.4 Chiral investigation of C-3" of nectrianolin B (2)	13
2.2.5 Preparation of the MTPA ester derivatives for 11	13
2.3 Antimicrobial assay	14
2.4 Phytotoxic assay	15
2.5 Cell culture and cytotoxicity assay	15
2.6 Physicochemical properties	15
2.6.1 Nectrianolin A (1)	15
2.6.2 Nectrianolin B (2)	16
2.6.3 Nectrianolin C (3)	16
2.6.4 6,8-Dihydroxy-3,4,7-trimethylisocoumarin (5)	16
2.6.5 8-Hydroxy-6-methoxy-3,4,7-trimethylisocoumarin (6)	16
2.6.6 Nectriaquinone A (7)	16
2.6.7 Nectriaquinone B (8)	17
2.6.8 Zythiostromic acid C (11)	17
2.7 Results and Discussion	17
Chapter 3 Metabolites from <i>Fusarium solani</i> B-18	31
3.1 Introduction	31
3.2 Material and methods	31

3.2.1 Fungal material and fermentation.....	31
3.2.2 Extraction and isolation	32
3.2.3 Preparation of acetyl derivatives	33
3.2.4 Preparation of MTPA ester derivatives for 12	34
3.2.5 Preparation of MTPA ester derivatives for 15	35
3.2.6 Preparation of MTPA ester derivatives for 20	35
3.2.7 Preparation of MTPA ester derivatives for 22	36
3.2.8 Osteoclastic differentiation assay	36
3.2.9 ECD calculations for 21–23	37
3.3 Physicochemical properties	37
3.3.1 Fusaspirol A (12).....	37
3.3.2 Fusaspirol B (13).....	38
3.3.3 Fusaspirol C (14).....	38
3.3.4 Fusaspirol D (15).....	38
3.3.5 (-)-Lanyulactone (18).....	38
3.3.6 Fusopoltide B (20).....	38
3.3.7 Fusopoltide C (21).....	39
3.3.8 Fusopoltide D (22).....	39
3.3.9 Fusopoltide E (23).....	39
3.4 Results and Discussion	39
Chapter 4 Metabolites from <i>Colletotrichum boninense</i> AM-12-2.....	60
4.1 Introduction	60
4.2 Material and methods.....	60
4.2.1 Fungal material and fermentation.....	60
4.2.2 Extraction and isolation	60
4.2.3 Preparation of MTPA ester derivatives for 26	61
4.2.4 Preparation of MTPA ester derivatives for 27	62
4.2.5 Preparation of MTPA ester derivatives for 28	63
4.2.6 NMR calculation for 26	63
4.2.7 Preparation of X-ray crystalline sponge for 27–30	64
4.2.8 Insecticidal assay	64
4.3 Physicochemical properties	65
4.3.1 3-(3-hydroxy-2-(hydroxymethyl)phenyl)propanoic acid (24).....	65
4.3.2 2-hydroxymethyl-3-hydroxy-(<i>E</i>)-cinnamic acid (25)	65
4.3.3 Colletofuran A (26)	65
4.3.4 Colletofuran B (27)	66
4.3.5 Colletofuran C (28).....	66
4.3.6 Colletofuran D (29).....	66
4.3.7 Colletofuran E (30)	66
4.4 Results and Discussion	66
Chapter 5 Conclusions.....	80
References	83
Acknowledgements	90
Supplemental Data	92
Appendix. 1. ¹H NMR spectrum of 1 (Pyridine-<i>d</i>₅, 600 MHz).....	92

Appendix 2. ^1H NMR spectrum of 2 (Pyridine- d_5 , 600 MHz).....	93
Appendix 3. ^1H NMR spectrum of 3 (Pyridine- d_5 , 600 MHz).....	94
Appendix 4. ^1H NMR spectrum of 5 (Pyridine- d_5 , 600 MHz).....	95
Appendix 5. ^1H NMR spectrum of 6 (CDCl_3 , 600 MHz).....	96
Appendix 6. ^1H NMR spectrum of 7 (CDCl_3 , 600 MHz).....	97
Appendix 7. ^1H NMR spectrum of 8 (CDCl_3 , 600 MHz).....	98
Appendix 8. ^1H NMR spectrum of 11 (CD_3OD , 600 MHz).....	99
Appendix 9. ^1H NMR spectrum of 12 (CDCl_3 , 600 MHz).....	100
Appendix 10. ^1H NMR spectrum of 13 (CDCl_3 , 600 MHz).....	101
Appendix 11. ^1H NMR spectrum of 14 (CDCl_3 , 600 MHz).....	102
Appendix 12. ^1H NMR spectrum of 15 (CD_3OD , 600 MHz).....	103
Appendix 13. ^1H NMR spectrum of 18 (CDCl_3 , 600 MHz).....	104
Appendix 14. ^1H NMR spectrum of 20 (CDCl_3 , 600 MHz).....	105
Appendix 15. ^1H NMR spectrum of 21 (CDCl_3 , 600 MHz).....	106
Appendix 16. ^1H NMR spectrum of 22 (CDCl_3 , 600 MHz).....	107
Appendix 17. ^1H NMR spectrum of 23 (CDCl_3 , 600 MHz).....	108
Appendix 18. ^1H NMR spectrum of 24 (CD_3OD , 600 MHz).....	109
Appendix 19. ^1H NMR spectrum of 25 (CD_3OD , 600 MHz).....	110
Appendix 20. ^1H NMR spectrum of 26 (CDCl_3 , 600 MHz).....	111
Appendix 21. ^1H NMR spectrum of 27 (CDCl_3 , 600 MHz).....	112
Appendix 22. ^1H NMR spectrum of 28 (CDCl_3 , 600 MHz).....	113
Appendix 23. ^1H NMR spectrum of 29 (CDCl_3 , 600 MHz).....	114
Appendix 24. ^1H NMR spectrum of 30 (CDCl_3 , 600 MHz).....	115

List of Figures

Figure 1.1 Structures of important drugs from plants.	1
Figure 1.2 Structures of important drugs from microorganisms.	2
Figure 1.3 Outline of taxol biosynthesis. ²⁰	5
Figure 1.4 Structures of trichothecrotocins A–C from <i>T. crotochinigenum</i> . ²⁸	6
Figure 1.5 Structures of isopenicins A–C from <i>Penicillium</i> sp. sh18. ²⁹	7
Figure 1.6 Structures of cytorhizins A–C from <i>C. rhizophorae</i> A761.....	7
Figure 1.7 The Circum-Pacific “Ring of Fire”. ³⁴	8
Figure 2.1 Structures of 1–11	18
Figure 2.2 ¹ H- ¹ H COSY and key HMBC correlations of 1–3	20
Figure 2.3 Key NOE correlations of 1	20
Figure 2.4 ORTEP drawing of 1 , showing 50% probability ellipsoids.....	21
Figure 2.5 ¹ H- ¹ H COSY and key HMBC correlations observed for 5–8 and 11	24
Figure 2.6 (a) Key NOE correlations observed for 11 , (b) chemical shift differences for mono-(<i>S</i>)-MTPA ester (11a) and mono-(<i>R</i>)-MTPA ester (11b) and (c) chemical shift differences for di-(<i>S</i>)-MTPA ester (11c) and di-(<i>R</i>)-MTPA ester (11d) (in ppm).	28
Figure 2.7 Seedling growth inhibition of 4–11 using lettuce (<i>Lactuca sativa</i> L.) seeds. NC (negative control); PC (positive control).....	30
Figure 3.1 Structures of 12–15 , 12a , 15a , and I–II	41
Figure 3.2 ¹ H- ¹ H COSY and key HMBC correlations observed for 12 , 13 , and 15	43
Figure 3.3 Key NOE correlations observed for 12 , 13 , and 15	43
Figure 3.4 Chemical shift differences for (a) (<i>S</i>)-MTPA ester (12c) and (<i>R</i>)-MTPA ester (12d) of 12b and (b) chemical shift differences for (<i>S</i>)-MTPA ester (15b) and (<i>R</i>)-MTPA ester (15c) of 15 (in ppm).....	44
Figure 3.5 The key NOE correlations and coupling constant values (<i>J</i> ₁₀₋₉) of 12a , 15a , and II	47
Figure 3.6 The effect of isolated compounds and its derivatives on osteoclastic differentiation. RAW264.7 cells were induced osteoclastic differentiation in the presence of 1 μM of each compound, 0.1% DMSO (solvent), or 1 μM kenpaullone as a positive control. After 4 days, TRAP-positive multinucleated cells in each well were counted. The data represent mean values (±S.D., n=4) and were analyzed by ANOVA and Tukey-Kramer’s multiple-comparison tests (* <i>P</i> <0.01). ...	48
Figure 3.7 Typical images of TRAP-stained mature osteoclasts. The images show TRAP-stained multinucleated cells in 96-well plate in the presence of 1 μM of 0.1% DMSO (control), 12 , and 12a . The black square in each well was magnified to show the TRAP-stained mature osteoclasts, which are in magenta color as shown by black arrows. ...	49
Figure 3.8 Structures of 16–23	50
Figure 3.9 ¹ H- ¹ H COSY and key HMBC correlations observed for 18 and 20–23	51
Figure 3.10 Key NOE correlations observed for 19–23	53
Figure 3.11 Chemical shift differences for (a) (<i>S</i>)-MTPA ester (20a) and (<i>R</i>)-MTPA ester (20b) of 20 , and (b) chemical shift differences for (<i>S</i>)-MTPA ester (22b) and (<i>R</i>)-MTPA ester (22c) of 22 (in ppm).....	54

Figure 3.12 Populations and B3LYP/611G+(d) optimized lowest energy 3D conformers of 21	55
Figure 3.13 Experimental and calculated ECD spectra of 21	56
Figure 3.14 (a) experimental and calculated ECD spectra of 22 , 22a , 23 and 23a , and (b) structures of truncated model of 22a and 23a	58
Figure 4.1 The structures of 24–30	67
Figure 4.2 The ^1H – ^1H COSY, key HMBC, and key DIFF-NOE correlations of 24–30	69
Figure 4.3 The comparison of ^1H NMR spectra of 26 , 26a , and 26b (CDCl_3) in ppm.	72
Figure 4.4 Chemical shift differences for (S)-MTPA ester (26a) and (R)-MTPA ester (26b) of 26 (in ppm).	72
Figure 4.5 a) The key diff-NOE correlations of 26 and Newman projections of dihedral angles between H-10–H-11 and H-11–H12; b) Comparison between calculated and observed ^{13}C NMR chemical shifts, MAE, ME, and correlation coefficient r^2 for the proposed stereochemical models of 26 . Slope, intercept, and r^2 values determined by least-squares linear regression between the calculated chemical shift and the experimental ^{13}C NMR.	73
Figure 4.6 Chemical shift differences for a) (S)-MTPA ester (26a) and (R)-MTPA ester (26b) of 26 , b) chemical shift differences for (S)-MTPA ester (27a) and (R)-MTPA ester (27b) of 27 , and c) chemical shift differences for (S)-MTPA ester (28a) and (R)-MTPA ester (28b) of 28 (in ppm).	76
Figure 4.7 3D conformations model for guests 27–30	77

List of Tables

Table 1.1	Approximate number of known synthetic compounds, natural, and microbial products. ⁶	3
Table 2.1	¹³ C NMR (150 MHz) and ¹ H NMR (600 MHz) spectral data of 1–3 in pyridine- <i>d</i> ₅	19
Table 2.2	¹³ C NMR (150 MHz) and ¹ H NMR (600 MHz) spectral data for 5 and 6 .	23
Table 2.3	¹³ C NMR (150 MHz) and ¹ H NMR (600 MHz) spectral data for 7–8 in CDCl ₃	25
Table 2.4	¹³ C NMR (150 MHz) and ¹ H (600 MHz) spectral data for 11 in CD ₃ OD.	26
Table 3.1	¹³ C NMR (150 MHz) and ¹ H NMR (600 MHz) spectral data for 12–15 .	42
Table 3.2	¹³ C NMR (150 MHz) and ¹ H NMR (600 MHz) spectral data for 12a and 15a (in CDCl ₃)	45
Table 3.3	¹³ C NMR (150 MHz) and ¹ H NMR (600 MHz) spectral data for 18	51
Table 3.4	¹³ C NMR (150 MHz) and ¹ H NMR (600 MHz) spectral data for 20 and 21 (in CDCl ₃)	53
Table 3.5	¹³ C NMR (150 MHz) and ¹ H NMR (600 MHz) spectral data for 22 and 23 (in CDCl ₃)	57
Table 4.1	¹³ C NMR (150 MHz) and ¹ H (600 MHz) spectral data of 24 and 25 (CD ₃ OD).	68
Table 4.2	¹³ C NMR (150 MHz) and ¹ H (600 MHz) spectral data of 26 (CDCl ₃)	71
Table 4.3	¹³ C NMR (150 MHz) and ¹ H (600 MHz) spectral data of 27–30 (CDCl ₃)	74
Table 4.4	Insecticidal activity of compounds 26–30 against two aphid species	79

Summary

Natural products have played a major role in the search for new drugs or drug candidates throughout the course of many years. Because of their enormous structural diversity and complexity, they are a continuing and inspiring source for researchers. Fungi are one important source of pharmacologically active and structurally diverse natural products. This thesis describes investigations of new compounds from endophytic fungi, through fermentation process. The isolation of secondary metabolites from the fermentation products have done utilizing several steps of chromatography. The structures of the isolated compounds were established by extensive spectral analyses of 1D/2D-NMR and HRESITOFMS. The absolute configurations were determined using a combination of the modified Mosher's ester method, X-ray crystallography, experimental and calculated ECD analysis, X-ray crystalline sponge method, and/or comparison with reported data.

Mount Merapi in Java island, Indonesia, is known as the most active and hazardous volcano in the world. Merapi is 25–30 km north of Yogyakarta City and is home to approximately 1.6 million people. One of the most feared aspects of Merapi is the pyroclastic flow eruption type, which consists of revolving clouds of superheated gases. A recent large eruption in 2010 caused many changes to the environment, including plants and microorganisms. It was assumed that during the post-eruption in this area, fungal endophytes were not investigated as metabolite sources. We explored new metabolite sources from the damaged area, which led to the isolation of several fungal strains. Three of them, *Nectria pseudotrichia* 120-1NP, *Fusarium solani* B-18, and *Colletotrichum boninense* AM-12-2, were described in this thesis.

N. pseudotrichia 120-1NP is an endophytic fungus isolated from the stem of *Gliricidia sepium*. Seven new compounds, nectrianolins A–C (**1–3**); 6,8-dihydroxy-3,4,7-trimethylisocoumarin (**5**); 8-hydroxy-6-methoxy-3,4,7-trimethylisocoumarin (**6**); nectriaquinone B (**8**); and zythiostromic acid C (**11**), were isolated from the brown rice culture of this strain, along with four known compounds (**4**, **7**, **9**, and **10**). To the best of our knowledge, this is the first isolation of **7** from a natural source. Compounds **1** and **2** have a rearranged monocyclo-farnesyl skeleton (which is uncommon to sesquiterpene-epoxycyclohexane conjugates) instead of a bicyclo-farnesyl skeleton. Compounds **1–3** were evaluated for their in vitro cytotoxicity against HL60 and HeLa cell lines by the MTT method. Compounds **1–3** exhibited cytotoxic activity against the HL60 cell lines with IC₅₀ values of 1.7, 1.5 and 10.1 μ M, respectively. Compound **1–3** also exhibited cytotoxicity against the HeLa cell lines with IC₅₀ values of 34.7, 16.6 and 52.1 μ M, respectively. Additionally, compounds **4–11** were evaluated for their antimicrobial activity against *Staphylococcus aureus*, *Pseudomonas aeruginosa*, *Candida albicans*, and *Aspergillus clavatus*, phytotoxicity, and in vitro cytotoxicity. Unlike the other

compounds, **8** and **9** exhibited antibacterial activity against *S. aureus* and *P. aeruginosa* with MIC values ($\mu\text{g/mL}$) of >50 and 6.25, and of >50 and 3.125, respectively. The phytotoxicity was tested using lettuce seeds; notably, only **9** induced significant seedling growth inhibition compared to control. Moreover, **7-10** exhibited cytotoxicity against HL60 cells with IC_{50} values (μM) of 11.9, 1.33, 1.93, and 11.6, respectively. The higher cytotoxicity of **8** and **9** compared to that of the related compounds **7** and **10** was attributed to their increased cell membrane permeability due to the presence of the hydroxyl group.

F. solani B-18 is an endophytic fungus isolated from an unidentified forest litter. Four new compounds with γ -methylidene-spirobutanolide core, fusaspirols A–D (**12–15**), were isolated from the brown rice culture of *Fusarium solani* B-18. Oxaspirol analogues have been reported to possess various biological activities, **12–15** and its derivatives did not show cytotoxicity against murine macrophage derived RAW264.7 cells. Thus, they were tested for osteoclastic differentiation activity using the same cells. After four days of the osteoclastic induction, mature osteoclasts of multinucleated-TRAP (tartrate-resistant acid phosphatase)-positive cells were counted. Compounds **12** and **12a** significantly increased the number of mature osteoclasts at the comparable levels to the positive control (kenpauillone) and the negative control (DMSO), suggesting that **12** and **12a** activated a signaling pathway in osteoclastic differentiation. In the scale-up fermentation based on this strain, with the same method, additional four new polyketides, fusopoltides B–E (**20–23**), were isolated along with four known compounds (**16–19**). Fusopoltide B (**20**) is a diastereomer of its co-isolated known compound, fusopoltide A (**19**), featuring a pentaleno[1,2-*c*]pyran ring system. Fusopoltide C (**21**) and fusopoltides D–E (**22–23**) are incorporated the first natural polyketides featured decahydro-pentaleno[1,2-*c*]pyran and pentaleno[1,2-*c*]furan ring systems, respectively.

C. boninense AM-12-2 is an endophytic fungus isolated from the stem of *Acacia mangium*. Seven new compounds, 3-(3-hydroxy-2-(hydroxymethyl)phenyl)propanoic acid (**24**), 2-hydroxymethyl-3-hydroxy-(*E*)-cinnamic acid (**25**), and colletofurans A–E (**26–30**), were isolated from brown-rice culture of *Colletotrichum boninense* AM-12-2. Colletofurans A–E (**26–30**) are first natural compounds featured an unprecedented 1-octyl-1,3-dihydroisobenzofuran core. Additionally, colletofuran A (**26**) contained a unique 1,6-dioxaspiro[4.4]nonane ring system. Compounds **24–30** were evaluated for their anti-aphicidal activity. Aphids are a serious insect pest in agriculture worldwide. This assay was performed to test the susceptibility of *Aphis gossypii* (Glover) and *Myzus persicae* (Sulzer), against **26–30**. The commercial insecticide milbemectin was tested as the positive control. Compound **26** and **29** exhibited strong aphicidal activities against *A. gossypii* with the LC_{50} ($\mu\text{g/mL}$) values of 1 and 0.5, respectively. Furthermore, **27**, **29**, and **30** showed moderate activity against *M. persicae* with the LC_{50} ($\mu\text{g/mL}$) values of 169, 118, and 26, respectively. Notably, **29** exhibited

strong aphicidal activity ($LC_{50} = 0.5 \mu\text{g/mL}$) against *A. gossypii* and weak activity ($LC_{50} = 118 \mu\text{g/mL}$) against *M. persicae*. In contrast, **30** exhibited moderate aphicidal activity against *M. persicae* ($LC_{50} = 26 \mu\text{g/mL}$), but inactive against *A. gossypii*. Other compounds displayed either weak or no aphicidal activity ($LC_{50} > 200 \mu\text{g/mL}$) against tested aphids. In general, the data showed dose dependent responses and *M. persicae* was more resistant than *A. gossypii* to the treatments.

This thesis describes the chemical investigation of 30 fungal metabolites, including 22 new compounds and two compounds firstly isolated from fungal cultures. Complex interactions with their host may involve the presence of these fungi in volcanic areas. The interactions possibly related to their chemistry in some respects and have been shown to produce or elicit secondary metabolites that are new, attractive, and biologically active. Since endophytic fungi from Merapi volcano area are unexplored, there is a high likelihood that new metabolites will be discovered. Although certain new compounds exhibited no activity in bioassay, the new chemistry faced difficulties in the determination of the structure that had to be addressed. These results also disclosed that endophytic fungi from Merapi volcano area, harbor an enormous reservoir of new compounds for drug discovery.

List of Abbreviations

$[\alpha]_{\text{D}}^{\text{T}}$	specific rotation at the sodium D-line at T °C
λ_{max}	maximum wavelength, in UV-vis spectroscopy
ν_{max}	maximum transmittance, in FTIR spectroscopy
1D	one-dimensional, in NMR
2D	two-dimensional, in NMR
Abs	absorbance
br	broad, in NMR
c	concentration in specific rotation, g/100 mL
calcd.	calculated, in HRESITOFMS
CD	circular dichroism
CDCl_3	deuterated chloroform, NMR solvent
CD_3OD	deuterated methanol, NMR solvent
CHCl_3	chloroform
COSY	correlation spectroscopy, in NMR
d	doublet, in NMR
δ	chemical shift, in NMR
dd	doublet of doublet, in NMR
ddd	doublet of doublet of doublet, in NMR
DEPT	distortion less enhancement by polarization transfer, in NMR
Diff-NOE	difference nuclear overhauser effect, in NMR
DNA	deoxyribonucleic acid
EtOAc	ethyl acetate
FTIR	fourier-transform infrared spectroscopy
g	gram(s)
H_2O	water
HMBC	heteronuclear multiple bond connectivity, in NMR
HMQC	heteronuclear multiple quantum coherence, in NMR
HPLC	high performance liquid chromatography
HRESITOFMS	high-resolution electrospray ionization time of flight mass spectroscopy
Hz	hertz

IC ₅₀	half maximal inhibitory concentration
IR	infrared spectroscopy
<i>J</i>	coupling constant, in NMR
KBr	potassium bromide, in IR spectroscopy
LC ₅₀	half maximal lethal concentration
Log ϵ	natural logarithm of molar absorptivity or extinction coefficient, in UV-vis spectroscopy
M	molar, mol/L
m	multiplet, in NMR
MeOH	methanol
MERS	middle east respiratory syndrome
mg	milligram(s)
MHz	megahertz
mL	milliliter(s)
mm	millimeter(s)
MS	mass spectroscopy
<i>m/z</i>	mass per charge
μ L	microliter(s)
nm	nanometer(s)
NMR	nuclear magnetic resonance
ppm	parts per million
pyridine- <i>d</i> ₅	deuterated pyridine
q	quartet, in NMR
rRNA	ribosomal ribonucleic acid
t _R	retention time, in HPLC
s	singlet, in NMR
sp.	species
t	triplet, in NMR
TLC	thin layer chromatography
TMS	tetramethylsilane
UV-vis	ultraviolet-visible spectroscopy

Chapter 1 Introduction

1.1 Natural products as source of drugs

The therapeutic use of natural products—compounds derived from natural sources, including plants, animals or microorganisms—leads undoubtedly recorded in human history by thousands of years. The importance of natural products for medicine and health has been immense throughout our evolution.¹ Analytical and structural chemistry provided the tools for purifying different compounds and evaluating their structures, which in turn gave insights into their action on the human body. Subsequently, a large number of well-known natural compounds were identified, analyzed, and synthesized (Fig. 1.1): salicin from *Salix alba* (white willow), emetine from *Cephaelis ipecacuanha* (ipecacuanha), strychnine and brucine from *Strychnos nuxvomica* (strychnos), quinine from *Cinchona ledgeriana* (cinchona bark), colchicine from *Colchicum autumnale* (colchicum), caffeine from *Coffea arabica*, nicotine from *Nicotiana tabacum*, atropine from *Atropa belladonna*, and cocaine from *Erythroxylum coca*. Many of these compounds are still widely used as drugs.^{2,3}

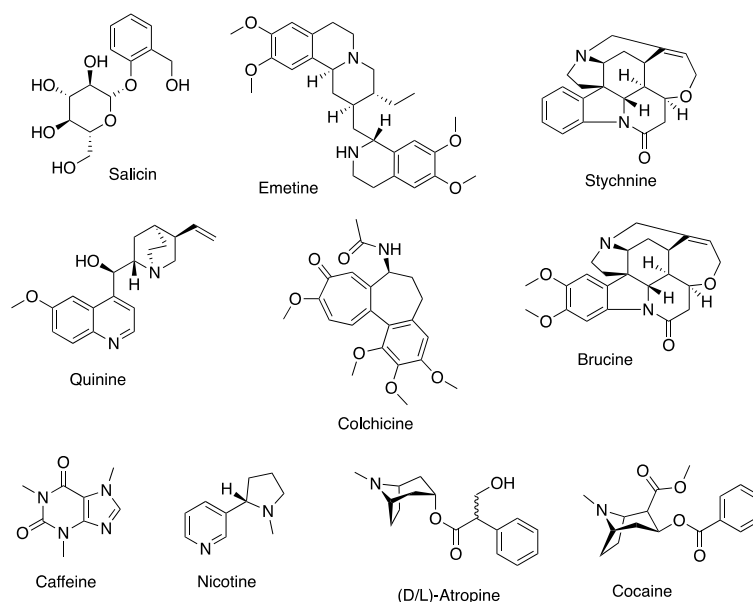


Figure 1.1 Structures of important drugs from plants.

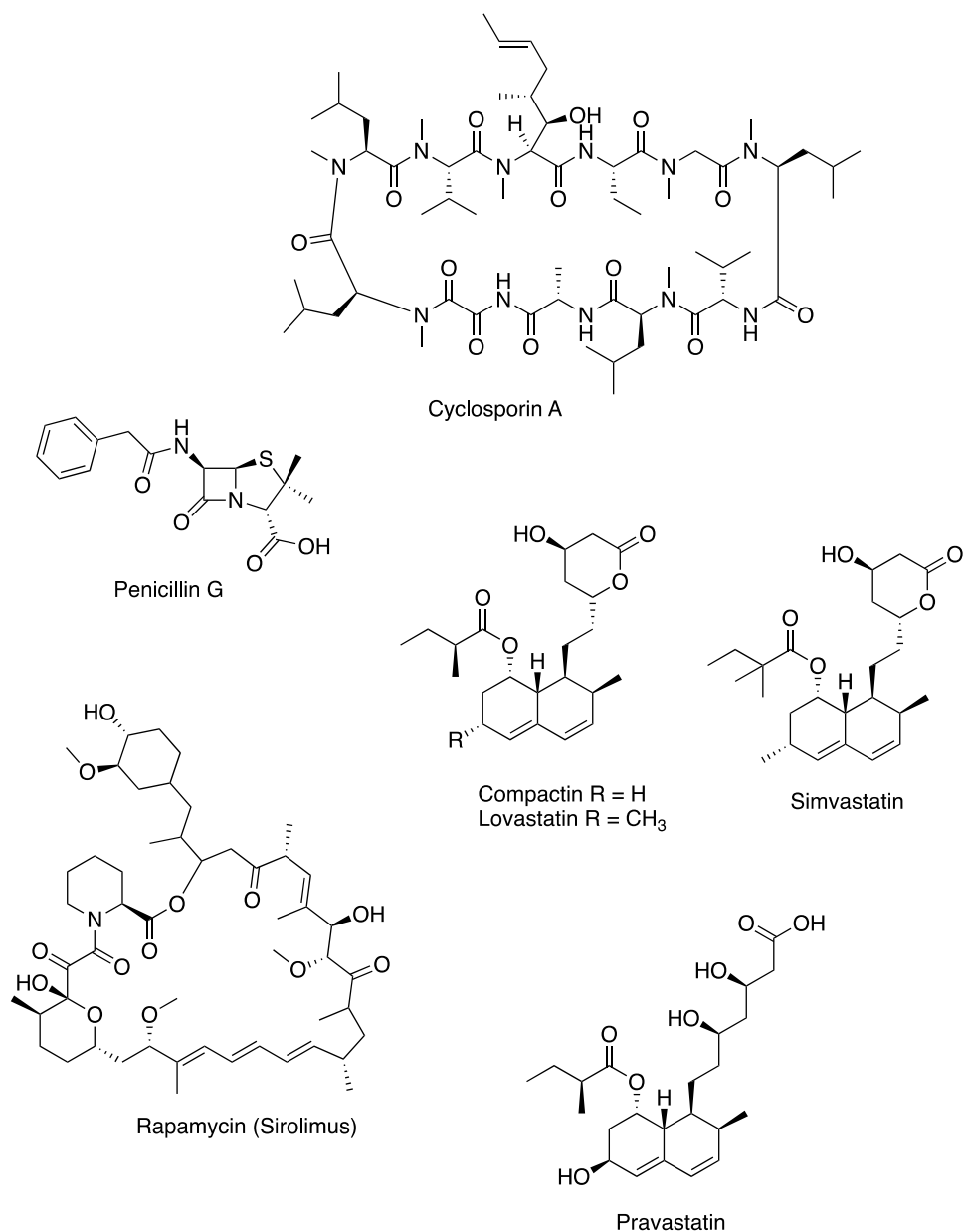


Figure 1.2 Structures of important drugs from microorganisms.

The unexpected discovery of penicillin G from the filamentous fungus, *Penicillium notatum*, by Alexander Fleming in 1929 at St. Mary's Hospital, and the observation of the broad therapeutic use of this agent in the 1940s by Howard Florey at Oxford University, promoted the intensive investigation of microorganism as a source of novel bioactive agents.⁴ This also became the first time of natural products as true antibacterials rather than as external sterilants can be fixed in

time as the later stage of World War II, with the use of microbial derived secondary metabolites.³ This discovery was soon followed by numerous other antibacterials that gave physicians an enormously powerful weapon in their fight against infectious diseases. Microorganisms are a prolific source of structurally diverse bioactive metabolites and have yielded some of the most important products of pharmaceutical industry (Fig. 1.2). These include: antibacterial agents, such as the penicillins from *Penicillium* species, cephalosporins from *Cephalosporium acremonium*, aminoglycosides, tetracyclines, and other polyketides of many structural types from the *Actinomycetales*; immunosuppressive agents, such as the cyclosporins from *Trichoderma* and *Talypocladium* species, and rapamycin from *Streptomyces* species; cholesterol lowering agents, such as mevastatin (compactin) from *Penicillium* species and lovastatin from *Aspergillus* species; and anthelmintics and antiparasitic drugs, such as the ivermectins from *Streptomyces* species.⁵

Table 1.1 Approximate number of known synthetic compounds, natural, and microbial products.⁶

	Synthetic chemical compounds		Natural products				Microbial products	
Numbers	8-10 million		~500,000				~70,000	
Drugs	2,000-2,500		1,200-1,300				450-500	
Percentage	0.005		0.6				1.6	
	Natural Product	%	Animal derived	%	Plant derived	%	Microbial derived	%
Occurring bioactivities and drugs derived from natural products according to their origin								
Total numbers	~500,000	100	~100,000	~20	~350,000	~70	~70,000	~10
Bioactive	~60,000	~12	~5,000	~3	~25,000	~7	~33,000	47
Drugs	~1,300	0.03	100-150	0.001	600-1000	0.03	400-500	0.6

Natural products have turned out to be, by far, the most productive source of novel compound classes for biological studies and important source of new drugs discovery. Because it was developed by natural selection process, natural product possesses a unique and vast chemical diversity and developed for optimal

interactions with biological macromolecules.⁷ Table 1.1 shown number of known synthetic compounds, natural, and microbial product. Although, compound from natural products are less in number than synthetical products, natural products tend to be more bioactive than synthetic one. Therefore, in the present time, natural products still continue to play a significant role in drug discovery, and should be expanded.^{2,8-11}

1.2 Endophytic fungi

Endophytes have been attracting much attention in the field of natural products chemistry because of their sustainability to biosynthesized diverse structure and bioactive molecules.^{12,13} Endophytes are ubiquitous microorganisms that are found in all plant species.¹⁴ These microorganisms maintain a balance symbiotic relationship with their hosts, and this association is apparently asymptomatic and avirulent.¹⁵ The interaction between endophytes and its host is characterize by a finely tuned equilibrium between fungal virulence and plant defense. If this equilibrium changes by either a decrease in plant defense or an increase in fungal virulence, diseases will develop. Not only the endophyte synthesize metabolite must compete first with epiphytes and then with pathogens in order to colonize the host, then presumably also to regulate metabolism of the hosts in their balanced delicate association.¹⁶

Endophytic fungi were isolated from almost all parts of the plant, such as leaves, roots, stems, seeds, and fruits. Rational consider in choosing the potential plant host also become important. Specific climate, high secondary metabolite productivity, and several important aspects of the hosts, correlate to the metabolites production by endophytic fungi. Metabolites produced by endophytes are rich sources of diverse and pharmacologically active metabolites.^{5,16} Environmental factors (e.g., light, temperature, pH, and nutrients) play an important role in production of secondary metabolites by endophytes. These factors are associated with pathogenicity and fungal tolerance to stress including drought or heat stress.¹⁷

Revolutionary and creative techniques will utmost extent the search for bioactive fungal endophytes. Plants with peculiar biology, with medicinal and ethnobotanical backgrounds, growing in hotspots, and under endangered

categories, may be ideal for bioprospecting. Habitats that are not yet explored may also contain new fungal endophyte isolates with pharmaceutical value.¹⁸

Natural products obtained from endophytic fungi have been identified as continuous and prolific active agents sources that could have a profound effect on the advancement of drugs in modern medicine.^{16,19} Although there has been no clarity of the complex relationship between endophytic fungi and plants, their complex symbiotic relationship gives the powerful ability to produce new bioactive substances. Their huge biological diversity, coupled with their ability to biosynthesize bioactive metabolites, has given the motivation for investigations of endophytic fungi and bioactivity of isolate substances.¹⁵

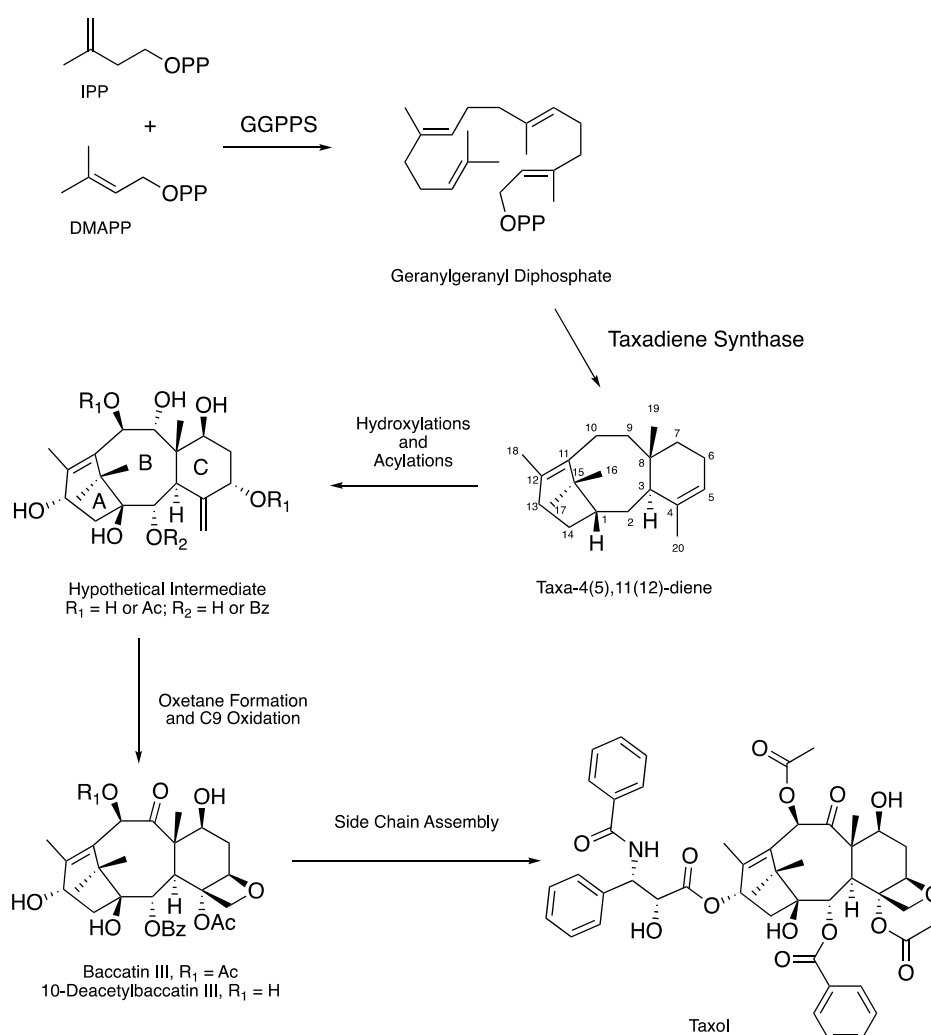


Figure 1.3 Outline of taxol biosynthesis.²⁰

In the history of secondary metabolites from endophytic fungi, the prominent and fascinating compound is paclitaxel (taxol). Taxol is a potent anti-tumor agent in breast and ovarian cancer. It is a highly polyfunctional polycyclic diterpenoid that belong to a class of taxanes. Fig 1.3 shown an outline of taxol biosynthesis. It was firstly discovered in plants isolated from the bark of the Pacific yew tree (*Taxus brevifolia*), but it took six trees of 100 years of age to treat one cancer patient.²¹ The efficacy and increased demand for taxol resulted in developing biotechnological approaches to prepare the drug. In the present day, taxol produced by semisynthetic approaches using 10-deacetyl-baccatin III, plant cell culture, and endophytic fungi.^{22–24} The recorded taxol producing fungi are including *Taxomyces adreanae*²², *Pestalotiopsis microspora*²⁵, *Tubercularia* sp.²⁶, and *Phyllosticta citricarpa*.²⁷

Endophytic fungi from several studies also have been reported to exhibit a large range of biological activities, not only limited to pharmaceutical but also in agricultural used. Yang et al., reported the isolation of trichothecrotocins A–C from potato endophytic fungus *Trichothecium crotocinigenum*. Trichothecrotocins C is a merosesquiterpenoid racemate, contained a new 6/6-5/5/5 fused ring system. These compounds showed antiphytopathogenic activities against potato diseases: *Phytophthora infestans* (late blight), *Alternaria solani* (early blight), *Rhizoctonia solani* (black scurf), and *Fusarium oxysporum* (blast).²⁸

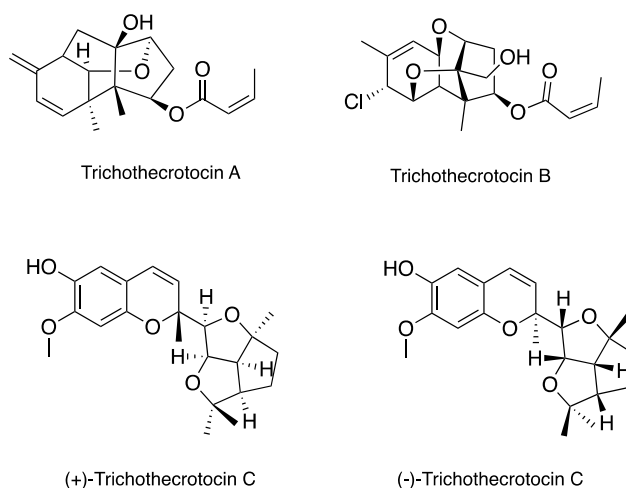


Figure 1.4 Structures of trichothecrotocins A–C from *T. crotocinigenum*.²⁸

Tang et al., also reported the isolation of isopenicins A–C. These compounds are new meroterpenoids possessing two types of unprecedented terpenoid-polyketides hybrid skeleton. They were isolated from the cultures of *Penicillium* sp. sh18. Isopenicins A was identified as a potent antitumor through the Wnt signaling pathway inhibition. The fungus is an endophyte isolated from *Isodon eriocalyx* var. *laxiflora*.²⁹

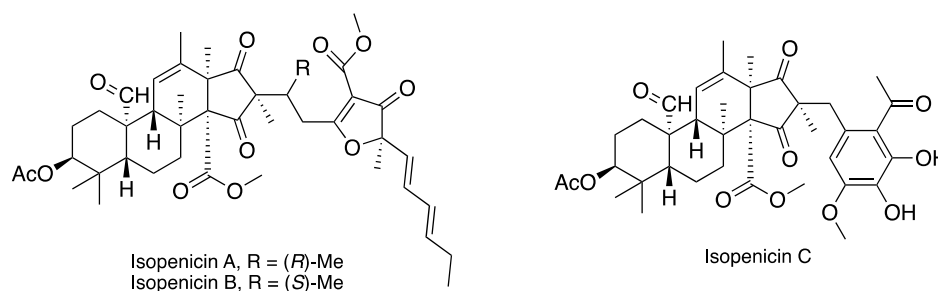


Figure 1.5 Structures of isopenicins A–C from *Penicillium* sp. sh18.²⁹

Cytorhizins A–D, four novel polyketide heterodimers, were isolated from the endophytic fungus *Cytospora rhizophorae* A761 derived from *Morinda officinalis*. These new compounds reported by Liu et al.³⁰, shared an unprecedented 6/6/5/6/8 or 6/6/5/6/7 pentacyclic ring system and fused as a fascinating cage-like skeleton, embodying by a polyoxygenated isopentyl unit and a highly structure combined benzophenone scaffold. These compounds showed cytotoxicity and antimicrobial activity.

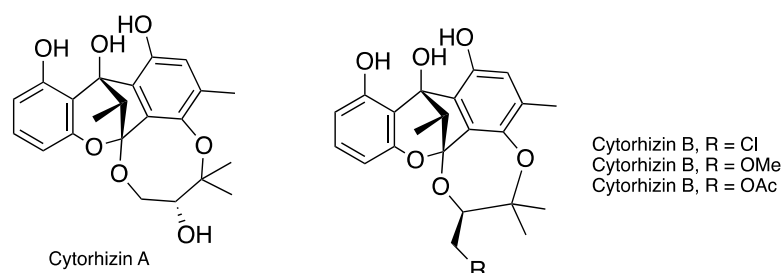


Figure 1.6 Structures of cytorhizins A–C from *C. rhizophorae* A761.

Overall, the utilization of endophytic fungi and the prospects for scientific discovery appear to be promising.³¹ Equipped with effective screening system, unique biological resources, and modern chemical separation science, many new products for medicine are likely to result. New bioactive drugs and new microorganisms are waiting to be discovered and to enhance the value of biodiversity.³²

1.3 Mount Merapi, a volcano in Java Island, Indonesia

The Indonesian tropical forest has a large diversity of plants due to its complex geological history, large number of islands, and tropical climate. Thus, the Indonesian tropical forest is a rich potential source for the isolation of endophytic fungi and their associated metabolites.³³ This biological diversity is reflected in a structural diversity representing a promising source of new bioactive compounds.

The country of Indonesia is made up of more than 17,000 islands, of which 922 are permanently inhabited. It is located in Southeast Asia, with a tropical climate, and contains wide diversity in plants and animals. The expanse of this beauty may disguise the frightening fact that Indonesia is located over seismic lines of the “Ring of Fire” that stretched around the Pacific from southeast Australia to the American Southwest (Fig. 1.7).³⁴

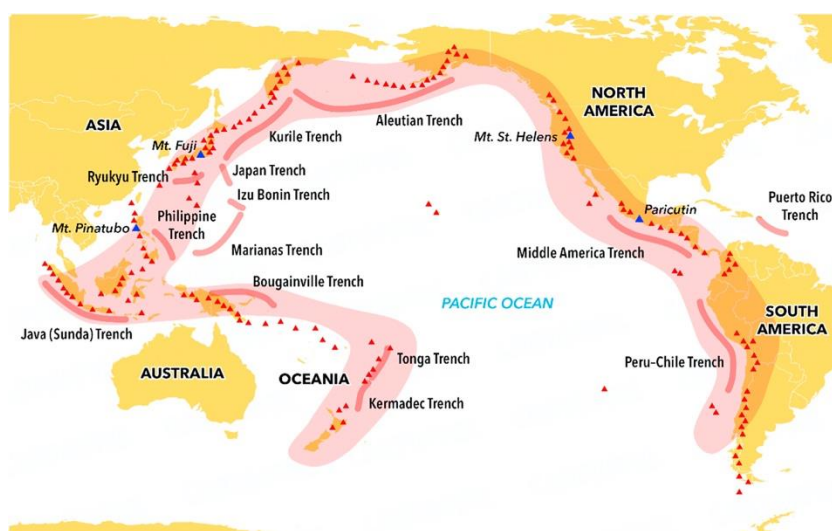


Figure 1.7 The Circum-Pacific “Ring of Fire”.³⁴

Merapi Volcano, located within heavily populated central Java and Yogyakarta, is one of the Earth's most active and feared volcanoes. Almost half of Merapi's nearly 80 reported historical eruptions are known to have been accompanied by *nuées ardentes* (burning cloud)—more than any other volcano. About a dozen of these *nuées* have caused fatalities.³⁵ Many eruptions of Merapi over the last 80 years have generated destructive and deadly pyroclastic density currents in association with lava dome effusion. The 2010 eruption of Merapi was the second most deadly in the historic record of this volcano, claiming over 380 lives.³⁶ A fast moving flow containing high-density mixture of hot lava blocks, pumice, ash, and volcanic gas, which reached temperature of 400-600 °C and speed of 130 Km/h, causing vegetation destruction.³⁷ Forest fire was often repeated following the eruption. The forest fire caused by an eruption were divided into three types: severe burnt forest, medium burnt forest, and light burnt forest. Fire can change the diversity, composition, and abundance of species in ecosystem.³⁸

Succession, after the disturbance of natural disaster, became important part of the ecological recovery. Ecological succession is the mechanism through which a biological community's structure evolves over time. Two different types of succession are distinguished, primary and secondary. Primary succession occurs in areas that are basically lifeless—regions where the soil is unable to sustain life due to factors such as lava flows. Secondary succession occurs in areas where a previously existing population has been removed; it is marked by small disruptions that do not eliminate all life and nutrients from the ecosystem.³⁹ Following the eruption in 2010, Merapi forest exhibited a high resilience for site recovery with the rapid re-colonization of plant species.⁴⁰ A recent eco-physiological approach suggests that the plant-associated microbial community may be the key factor for understanding the adaptation of plants to their habitat.⁴¹ These plant-associated microbial, including endophytic fungi, may also involve in the adaptation processes to suit the post-eruption condition. These microbial are unique genetic resources and can be utilized as new metabolites producer.

1.4 Objectives and overview of this study

In this study, endophytic fungi from Merapi volcano area were selected as sources to obtain new metabolites. A recent large eruption in 2010 caused many

changes to the environment, including plants and microorganisms, and it was assumed that during the post-eruption in this area, fungal endophytes were not investigated as metabolite sources. We explored new metabolite sources from the damaged area. The aims of this research were to obtain new compounds, characterize the physicochemical properties, and assess the potential bioactivity of isolated compounds. In chapter 2, the isolation and characterization of eight new metabolites, isolated from *N. pseudotrichia* 120-1NP, were described. In chapter 3 and 4, described the isolation, characterization, and biological activity of eight new compounds from *F. solani* B-18 and seven new compounds from *C. boninense* AM-12-2, respectively. Finally, in chapter 5 comprised a conclusion.

1.5 General experimental procedures

The optical rotations were measured using a Horiba SEPA-300 polarimeter (Horiba, Japan). IR and UV-vis spectra were respectively recorded with Horiba FT710 (Horiba, Japan) and Shimadzu UV-1800 spectrometer (Shimadzu, Japan). Mass spectra were obtained with a Synapt G2 (Water Corporation, USA) and JEOL HX110 mass spectrometer (JEOL, Japan). CD spectra were measured using a JASCO J-820 spectrometer (JASCO, Japan). NMR data were recorded on JEOL ECZ-600 spectrometer (JEOL, Japan) at 600 MHz for ^1H and 150 MHz for ^{13}C . Chemical shift are given on a δ (ppm) scale with TMS as an internal standard. ^1H , ^{13}C , COSY, HMQC, and HMBC spectra were recorded using standard JEOL pulse sequences. Column chromatography was performed on silica gel 60 (Kanto Chemical Co., Inc., Japan) or ODS (Fuji Silysia, Japan). Flash chromatography was performed using Büchi Flash Chromatography C-601 (Büchi, Switzerland) and packed column Biotage® SNAP Ultra (Biotage, Sweden) 10 g (25 μm). HPLC separations were carried out using Shimadzu LC-20AT and UV-vis detector SPD-20A (Shimadzu, Japan) on reverse phase-high performance liquid chromatography (RP-HPLC). Thin layer chromatography (TLC) was carried out on precoated silica gel 60 F₂₅₄ plates (Merck, Germany), and spot were detected by spraying with 10% vanillin in H_2SO_4 followed by heating, or by UV irradiation. Solvents and chemicals were purchased from Wako Chemicals Ltd. (Tokyo, Japan) or Kanto Chemical Co., Inc. (Tokyo, Japan), unless noted otherwise.

Chapter 2 Metabolites from *Nectria pseudotrichia* 120-1NP

2.1 Introduction

Strain 120-1NP was isolated from the inner tissue of *Gliricidia sepium*, which was subsequently identified as *Nectria pseudotrichia*. The *Nectria* genus is a saprophyte and considered as a phytopathogen that induced both stem-end rot of avocados⁴² and canker on trees.⁴³ However, this genus is also a rich source of interesting secondary metabolites with diverse structures and biological activities.^{43–45}

Separation of the extract derived from fungal culture of *N. pseudotrichia* 120-1NP led to the isolation of the following new compounds: two sesquiterpene-epoxycyclohexenones **1** and **2**, a sesquiterpene congener **3**, two new isocoumarins (**5–6**), a new naphthoquinones (**8**), and the new cleistanthane-type diterpene (**11**), along with four known compounds, 3,4-dimethyl-6,8-dihydroxyisocoumarin (**4**), nectriaquinone A (**7**), herbarin (**9**) and O-methylherbarin (**10**). In this chapter, we report the isolation, structure determination, and biological activity of these compounds.

2.2 Experimental

2.2.1 Fungal material and fermentation

The fungal strain 120-1NP was isolated from healthy stem of *Gliricidia sepium* collected in the Wanagama Forest (southern latitude 7°53'37", east longitude 110°32'49"), Yogyakarta, Indonesia. This strain was identified as *N. pseudotrichia* using DNA analysis of the 18S rRNA regions and was deposited in GenBank: LC317048. This fungus was deposited at our laboratory in the Faculty of Agriculture, Yamagata University. *N. pseudotrichia* 120-1NP was cultivated on sterilized brown rice (30 flask, each 120 g) at 25 °C for four weeks.

2.2.2 Extraction and isolation

The moldy media was extracted using methanol, and the methanol extract was concentrated. The resulting aqueous concentrate was partitioned into EtOAc. The separation of the EtOAc layer was guided by intense characteristic coloration with

vanillin-sulfuric acid solution, on TLC plates. The EtOAc layer (19.74 g) was chromatographed on a silica gel column using 10% stepwise of *n*-hexane-EtOAc (100:0-0:100), then a mixture of EtOAc-MeOH (50:50), and finally MeOH to give 13 fractions (Fr. 1-1 to 1-13). Fraction 1-5 further chromatographed on a silica gel column using 10% stepwise of CHCl₃-EtOAc (100:0-0:100) to afford 11 fractions (Fr. 1-5-1 to 1-5-11). Fraction 1-5-3 which was contained crude fraction of **3**, finally purified by an ODS column, using a mixture of MeOH-H₂O (90:10) to yielded **3** (84 mg). Fractions 1-8, 1-9, and 1-10 were combined and was chromatographed on a silica gel column, using 10% stepwise of CHCl₃-EtOAc (100:0-0:100) to afford crude fraction including **1** and **2**, which was purified by a flash chromatography, using mixture of CHCl₃-MeOH (150:1) to afford **2** (10 mg), and CHCl₃-MeOH (75:1) to afford **1** (53 mg). Fraction 1-5 (655 mg) was further chromatographed on a silica gel column, using 10% stepwise of CHCl₃-EtOAc (100:0-0:100, each 100 mL) to afford 11 fractions (Fr. 1-5-1 to 1-5-11). Fraction 1-5-3 which was contained amorphous powder was filtered and the residue was washed using MeOH to yielded **6** (37 mg). In each 1-6 and 1-7 fractions contained amorphous powder which then filtered, the residues were washed using MeOH to obtained **4** (15 mg) and **5** (28 mg), respectively. Fractions 1-8 to 1-10 were combined (4.32 g) and was chromatographed on a silica gel using 10% stepwise of CHCl₃-EtOAc (100:0-0:100, each 200 mL) to afford 11 fractions (Fr. 1-8-1 to 1-8-11). Fractions 1-8-5 to 1-8-7 were combined (503 mg) and was subjected on an ODS column, using 10% stepwise of H₂O and MeOH (100:0-0:100, each 50 mL) to afford 11 fractions (1-8-5-1 to 1-8-5-11). Fractions 1-8-5-5 to 1-8-5-7 were combined (184 mg) and then was subjected to a flash chromatography, using eluent hexane-EtOAc (1:1) to afford **7** (19 mg), **8** (59 mg), **9** (10 mg), and **10** (5 mg). Fraction 1-8-8 (41 mg) was purified using an ODS column with eluent system H₂O-MeOH (3:7) to afford **8** (28 mg).

2.2.3 Experimental X-ray of nectrianolin A (**1**)

Single crystal suitable for X-ray crystallography was obtained by recrystallization from a methanol solution. X-ray diffraction data were collected at 150 K on a Rigaku XtaLAB mini diffractometer with graphite monochromatic Mo K α radiation (λ = 0.71070 Å). The structure was solved by direct methods⁴⁶ and expanded using Fourier techniques. The non-hydrogen atoms were refined

anisotropically. Hydrogen atoms were refined using the riding model. The final Flack parameter⁴⁷ was -0.1(3). Crystallographic data of **1** has been deposited with Cambridge Crystallographic Data Center, deposition no. CCDC 1556508.

2.2.4 Chiral investigation of C-3'' of nectrianolin B (**2**)

A solution of **2** (0.5 mg) in 500 μ L MeOH was stirred with NaOMe (1.0 mg) at room temperature. The reaction monitored based on TLC analysis. After consumption of the starting material, **2**, in the reaction mixture was added with distilled water (100 μ L) and then was extracted using pentane (500 μ L). Pentane layer (10 μ L) was subjected to gas chromatography equipped with CycloSil-B capillary column. The signal was monitored with the 3-hydroxybutanoate ion ($[M-CH_3]^+$ $m/z = 103$) to afford the signal at 12.937 min. This signal was verified with a mixture of standard methyl (*S/R*)-3-hydroxybutanoate, which were appeared at 12.800 and 12.938 min, respectively, under same condition.

2.2.5 Preparation of the MTPA ester derivatives for **11**

To **11** (1.0 mg) in dry pyridine was added (*R*)-(-)- α -methoxy- α -(trifluoromethyl)phenylacetic chloride (MTPACl, 10 μ L). The mixture was stirred at room temperature for 24 h. Purification was performed using column chromatography on a silica gel using *n*-hexane: EtOAc (10% stepwise, each 4 mL) eluent system to afford the mono-(*S*)-MTPA ester (**11a**, 0.7 mg) and di-(*S*)-MTPA ester (**11c**, 0.3 mg). Compound **11** (1.0 mg) was treated with (*S*)-(+)- α -methoxy- α -(trifluoromethyl)phenylacetic chloride (MTPACl, 10 μ L) in the same procedure to afford the mono-(*R*)-MTPA ester (**11b**, 0.6 mg) and di-(*R*)-MTPA ester (**11d**, 0.4 mg).

11a: 1H -NMR (600 MHz, $CDCl_3$) δ_H 0.98 (3H, s, H-20), 1.32-1.68* (H-1, -2, -11, -12), 1.48 (3H, s, H-19), 2.11 (1H, t, $J = 7.8$ Hz, H-6a), 2.37 (1H, t, $J = 12.0$ Hz, H-6b), 2.17 (1H, dd, $J = 13.2, 6.0$ Hz, H-9), 2.61 (1H, d, $J = 8.4$ Hz, H-14), 3.47 (OMe of MTPA), 4.26 (1H, t, $J = 2.4$ Hz, H-3), 4.63 (1H, s, H-17a), 4.75 (1H, s, H-17b), 4.91 (1H, d, $J = 17.4$ Hz, H-16a), 5.07 (1H, d, $J = 10.2$ Hz, H-16b), 5.47 (1H, dd, $J = 11.4, 4.8$ Hz, H-7), 5.99 (1H, m, H-15), 7.40-7.54 (Ph of MTPA), an asterisk (*) indicates overlapped signals.

11b: ¹H-NMR (600 MHz, CDCl₃) δ_H 1.03 (3H, s, H-20), 1.35-1.71* (H-1, -2, -11, -12), 1.53 (3H, s, H-19), 2.13 (1H, t, *J* = 8.4 Hz, H-6a), 2.51 (1H, t, *J* = 12.0 Hz, H-6b), 2.24 (1H, dd, *J* = 12.6, 4.8 Hz, H-9), 2.54 (1H, d, *J* = 8.4 Hz, H-14), 3.56 (OMe of MTPA), 4.30 (1H, t, *J* = 3.0 Hz, H-3), 4.58 (1H, s, H-17a), 4.75 (1H, s, H-17b), 4.92 (1H, d, *J* = 17.4 Hz, H-16a), 5.08 (1H, d, *J* = 16.2 Hz, H-16b), 5.53 (1H, dd, *J* = 12.0, 4.8 Hz, H-7), 5.99 (1H, m, H-15), 7.39-7.58 (Ph of MTPA), an asterisk (*) indicates overlapped signals.

11c: ¹H-NMR (600 MHz, CDCl₃) δ_H 1.02 (3H, s, H-20), 1.28 (1H, td, *J* = 13.8, 3.6 Hz, H-1a), 1.56 (1H, qd, *J* = 7.8, 4.2 Hz, H-1b), 1.37 (1H, br d, *J* = 13.8 Hz, H-2a), 1.74 (1H, br d, *J* = 15.6 Hz, H-2b), 1.48 (1H, br t, *J* = 4.2 Hz, H-11a), 1.51 (1H, br d, *J* = 2.4 Hz, H-11b), 2.16 (1H, td, *J* = 13.8, 4.8 Hz, H-12a), 2.24 (1H, br d, *J* = 13.2 Hz, H-12b), 1.18 (3H, s, H-19), 1.98 (1H, dd, *J* = 12.6, 3.6 Hz, H-6a), 2.28 (1H, t, *J* = 9.0 Hz, H-6b), 2.10 (1H, dd, *J* = 13.2, 8.4 Hz, H-9), 2.62 (1H, d, *J* = 8.4 Hz, H-14), 3.56, 3.58 (OMe of MTPA), 5.64 (1H, t, *J* = 2.4 Hz, H-3), 4.64 (1H, s, H-17a), 4.76 (1H, s, H-17b), 4.94 (1H, d, *J* = 17.4 Hz, H-16a), 5.11 (1H, d, *J* = 11.4 Hz, H-16b), 5.47 (1H, dd, *J* = 11.4, 4.8 Hz, H-7), 5.97 (1H, m, H-15), 7.44-7.59 (Ph of MTPA).

11d: ¹H-NMR (600 MHz, CDCl₃) δ_H 0.97 (3H, s, H-20), 0.86 (1H, td, *J* = 12.0, 3.0 Hz, H-1a), 1.47 (1H, qd, *J* = 13.2, 5.4 Hz, H-1b), 1.19 (1H, br d, *J* = 13.8 Hz, H-2a), 1.64 (1H, br d, *J* = 16.2 Hz, H-2b), 1.38 (1H, br t, *J* = 4.2 Hz, H-11a), 1.41 (1H, br d, *J* = 2.4 Hz, H-11b), 2.09 (1H, td, *J* = 13.8, 4.8 Hz, H-12a), 2.17 (1H, br d, *J* = 12.0 Hz, H-12b), 1.34 (3H, s, H-19), 1.83 (1H, dd, *J* = 13.2, 3.6 Hz, H-6a), 2.40 (1H, t, *J* = 12.0 Hz, H-6b), 2.15 (1H, dd, *J* = 12.6, 4.8 Hz, H-9), 2.47 (1H, d, *J* = 8.4 Hz, H-14), 3.59, 3.61 (OMe of MTPA), 5.59 (1H, t, *J* = 3.0 Hz, H-3), 4.53 (1H, s, H-17a), 4.72 (1H, s, H-17b), 4.89 (1H, d, *J* = 12.0 Hz, H-16a), 5.10 (1H, d, *J* = 10.8 Hz, H-16b), 5.48 (1H, dd, *J* = 14.4, 9.6 Hz, H-7), 5.90 (1H, m, H-15), 7.39-7.50 (Ph of MTPA).

2.3 Antimicrobial assay

The antimicrobial activity was determined by the paper disk diffusion method (100 µg compound on 8 mm paper disk), using meat peptone agar for *Staphylococcus aureus* and *Pseudomonas aeruginosa*, peptone yeast agar for *Candida albicans*, and potato dextrose agar for *Aspergillus clavatus*. Compounds

which showed significant inhibition zone were apply to further experiment to determine the minimal inhibitory concentration (MIC). MIC is defined as the lowest concentration resulting in no visible growth after incubation. The MIC was determined by the agar dilution based on reported reference with slight modification.⁴⁸ Chloramphenicol and kanamycin were used for positive control against *S. aureus* and *P. aeruginosa* (each 1 µg/mL), respectively.

2.4 Phytotoxic assay

The phytotoxicity procedure was the same as published reference⁴⁸ using lettuce seeds (*Lactuca sativa* L.). The negative control was using only distilled water and the positive control was using 2,4-dichlorophenoxyacetic acid (2,4-D) with $IC_{50} = 0.594 \mu\text{g/mL}$. The elongation of the roots and shoots was measured and compared with those of the negative control.

2.5 Cell culture and cytotoxicity assay

HL60 cells (RCB0041, RIKEN BioResource Center, Tsukuba, Japan) and Hela cells (RCB0007) were grown in RPMI 1640 medium supplemented with 10% heat-inactivated FBS (BioWest, Canada) and penicillin (50 units/ml)-streptomycin (50 µg/ml) (Gibco Corp., Carlsbad, USA) in a humidified atmosphere at 37°C under 5% CO₂. The cytotoxicities of the compounds were examined by MTT assay. Positive control camptothecin was used as positive control for HL60 and doxorubicin for HeLa with $IC_{50} = 23.6 \text{ nM}$ and $1.9 \mu\text{M}$ respectively.

2.6 Physicochemical properties

2.6.1 Nectrianolin A (1)

Colorless crystal; $[\alpha]_D^{25} -30.7$ (*c* 0.1, MeOH); UV (MeOH) λ_{max} (log ϵ) 220 (3.96) nm; CD ($3.7 \times 10^{-5} \text{ M}$, MeOH) λ_{max} ($\Delta\epsilon$) 248 (-4.2), 333 (-2.2); IR (KBr) ν_{max} 3332, 2935, 1677, 1249, 1045, 732 cm^{-1} ; ¹H NMR (600 MHz, pyridine-*d*₅) and ¹³C NMR (150 MHz, pyridine-*d*₅) data, see Table 2.1; HRESITOFMS (positive-ion mode) *m/z* 399.2142 ([M + Na]⁺ calcd. for C₂₂H₃₂NaO₅, 399.2147).

2.6.2 Nectrianolin B (2)

Yellow oil; $[\alpha]_D^{25}$ -43.2 (c 0.1, MeOH); UV (MeOH) λ_{\max} (log ϵ) 219 (4.97) nm; CD (3.7×10^{-5} M, MeOH) λ_{\max} ($\Delta\epsilon$) 248 (-4.2), 340 (-1.9); IR (KBr) ν_{\max} 3444, 2962, 1677, 1407, 1110, 740 cm^{-1} ; ^1H NMR (600 MHz, pyridine- d_5) and ^{13}C NMR (150 MHz, pyridine- d_5) data, see Table 2.1; HRESITOFMS (positive-ion mode) m/z 485.2509 ($[\text{M} + \text{Na}]^+$ calcd. for $\text{C}_{26}\text{H}_{38}\text{NaO}_7$, 485.2515).

2.6.3 Nectrianolin C (3)

Yellow oil; $[\alpha]_D^{25}$ +23.3 (c 0.1, MeOH); UV (MeOH) λ_{\max} (log ϵ) 222 (2.87) nm; IR (KBr) ν_{\max} 3421, 2923, 1635, 1380, 1091, 798 cm^{-1} ; ^1H NMR (600 MHz, pyridine- d_5) and ^{13}C NMR (150 MHz, pyridine- d_5) data, see Table 2.1; HRESITOFMS (positive-ion mode) m/z 245.1876 ($[\text{M} + \text{Na}]^+$ calcd. for $\text{C}_{15}\text{H}_{26}\text{NaO}$, 245.1875).

2.6.4 6,8-Dihydroxy-3,4,7-trimethylisocoumarin (5)

White amorphous powder; mp 195-198 $^{\circ}\text{C}$; UV (MeOH) λ_{\max} (log ϵ) 328 (3.4), 277 (3.5) nm; IR (KBr) ν_{\max} 3436, 1635, 1396, 1018 cm^{-1} ; ^1H -NMR (600 MHz, pyridine- d_5) and ^{13}C -NMR (150 MHz, pyridine- d_5) data, see Table 2.2; HRESITOFMS (positive-ion mode) m/z 243.0628 ($[\text{M} + \text{Na}]^+$, calcd. for $\text{C}_{12}\text{H}_{12}\text{NaO}_4$, 243.0633).

2.6.5 8-Hydroxy-6-methoxy-3,4,7-trimethylisocoumarin (6)

White amorphous powder; mp 172-175 $^{\circ}\text{C}$; UV (MeOH) λ_{\max} (log ϵ) 333 (3.8), 279 (3.9) nm; IR (KBr) ν_{\max} 3421, 1646, 1137, 1018 cm^{-1} ; ^1H -NMR (600 MHz, CDCl_3) and ^{13}C -NMR (150 MHz, CDCl_3) data, see Table 2.2; HRESITOFMS (positive-ion mode) m/z 257.0784 ($[\text{M} + \text{Na}]^+$, calcd. for $\text{C}_{13}\text{H}_{14}\text{NaO}_4$, 257.0789).

2.6.6 Nectriaquinone A (7)

Yellow amorphous powder; mp 161-162 $^{\circ}\text{C}$; UV (MeOH) λ_{\max} (log ϵ) 404 (3.4), 265 (4.1), 214 (4.1) nm; IR (KBr) ν_{\max} 1697, 1650, 1519, 1160 cm^{-1} ; ^1H -NMR (600 MHz, CDCl_3) and ^{13}C -NMR (150 MHz, CDCl_3) data, see Table 2.3; HRESITOFMS (positive ion mode) m/z 311.0895 ($[\text{M} + \text{Na}]^+$, calcd for $\text{C}_{16}\text{H}_{17}\text{NaO}_5$, 311.0895).

2.6.7 Nectriaquinone B (8)

Yellow amorphous powder; mp 132-136 °C; $[\alpha]_D^{20}$ +110.0 (c 0.01, CH₂Cl₂), +72.0 (c 0.1, CH₂Cl₂); UV (MeOH) λ_{\max} (log ϵ) 402 (3.2), 266 (4.1), 219 (4.1) nm; IR (KBr) ν_{\max} 3421, 1697, 1650, 1519, 1018 cm⁻¹; ¹H-NMR (600 MHz, CDCl₃) and ¹³C-NMR (150 MHz, CDCl₃) data, see Table 2.3; HRESITOFMS (positive ion mode) m/z 313.1056 ([M + Na]⁺, calcd for C₁₆H₁₈NaO₅, 313.1052).

2.6.8 Zythiostromic acid C (11)

Colorless oil; $[\alpha]_D^{20}$ +168.0 (c 0.1, MeOH); UV (MeOH) λ_{\max} (log ϵ) 211 (4.0) nm; IR (KBr) ν_{\max} 3432, 1631, 1396, 1025 cm⁻¹; ¹H-NMR (600 MHz, CD₃OD) and ¹³C-NMR (150 MHz, CD₃OD) data, see Table 2.4; HRESITOFMS (positive ion mode) m/z 389.1938 ([M + Na]⁺, calcd for C₂₀H₃₀NaO₆, 389.1940).

2.7 Results and Discussion

The structures of the known compounds, 3,4-dimethyl-6,8-dihydroxyisocoumarin (**4**), herbarin (**9**) and O-methylherbarin (**10**), were assigned by comparing their physicochemical properties and spectral data with those reported in the literatures^{49–52} (Fig. 2.1).

Compound **1** was obtained as a colorless crystal. Its molecular formula was determined to be C₂₂H₃₂O₅ through a combination of HRESITOFMS (m/z 399.2142 [M + Na]⁺) and NMR data. The molecular formula of **1** revealed seven degrees of unsaturation. The IR absorptions at 3332 and 1677 cm⁻¹ suggested the presence of hydroxyl and α,β -unsaturated carbonyl groups. The ¹³C NMR results (Table 2.1) along with the HMQC data of **1** revealed the presence of 22 carbon resonances and confirmed the presence of four methyls, five methylenes, seven methines, one ketone carbonyl, and five quaternary carbons. The ¹H NMR spectral data (Table 2.1) showed proton resonances, which include a doublet methyl at δ_H 0.68 (3H, d, J = 6.9 Hz, H-14), two singlet methyls at δ_H 0.70 (3H, s, H-15) and 1.50 (3H, s, H-13), an aliphatic methine at δ_H 1.53 (1H, m, H-5), two methylenes at δ_H 1.29 (2H, m, H₂-4), 1.85 (1H, m, H-3a), and 1.89 (1H, m, H-3b), and an olefinic methine at δ_H 5.36 (1H, s, H-2). The double bond position was assigned by HMBC correlations from the olefinic methyl (H-13) to two sp² carbons at δ_C 139.4 (C-1) and 124.5 (C-2) and to the quaternary carbon at δ_C 40.4 (C-6), consistent with the presence of a

substituted cyclohexene ring. Additional HMBC correlations from H-2, H-4, H-5, H-14, and H-15 to C-6 confirmed that the structure of **1** contained a 1,5,6-trimethylcyclohexene moiety (Fig. 2.2). The presence of a 3-methyl-2-penten-1-ol moiety was clarified using HMBC correlations from Me-12 to C-8, C-9 and C-10, and from H-11 to C-9 and C-10.

The HMBC correlation from H-7 to C-6 indicated that the pent-2-en-1-ol was located at C-6. Further analysis of the HMBC of **1** revealed the correlations from H-2' to C-6', H-4' to C-2' along with C-5' and H-7' to C-3' and C-2'. These data suggested the presence of an oxygenated cyclohexenone skeleton as well as hydroxymethyl and hydroxyl moieties. The presence of an epoxy group at C-5' and C-6' was deduced from the chemical shift of the ^{13}C NMR signals at these positions. The presence of this epoxy group was also supported by the ^1H NMR data acquired in CD_3OD since H-5' appeared at the epoxy region (δ_{H} 3.73 d, $J = 1.2$ Hz), compared to H-4', which appeared at the hydroxyl region (δ_{H} 4.47 s). The HMBC correlations from H-11 to C-5' and C-6' indicated a link between C-11 and C-6' of the cyclohexenone moiety (Fig. 2.2).

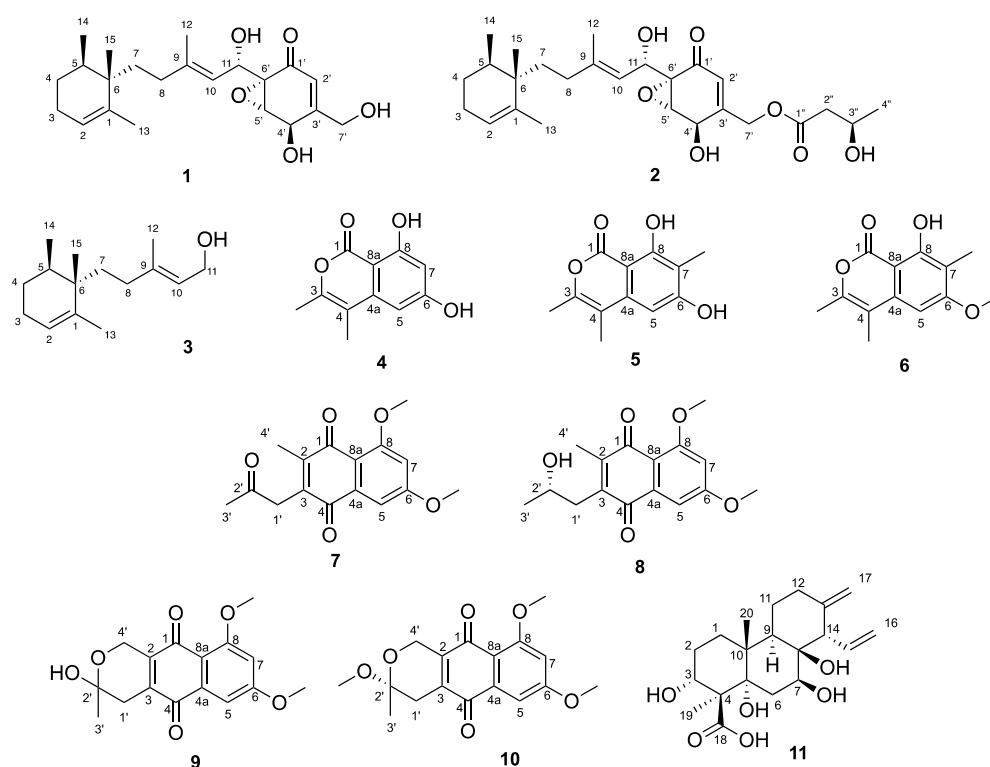


Figure 2.1 Structures of **1–11**.

Table 2.1 ^{13}C NMR (150 MHz) and ^1H NMR (600 MHz) spectral data of **1–3** in pyridine- d_5 .

Pos.	1		2		3	
	δ_{C} , type	δ_{H} (J in Hz)	δ_{C} , type	δ_{H} (J in Hz)	δ_{C} , type	δ_{H} (J in Hz)
1	139.4, C		139.5, C		137.5, C	
2	124.5, CH	5.36, s	124.5, CH	5.37, s	125.7, CH	5.69, m
3	25.7, CH ₂	1.85, m 1.89, m	25.7, CH ₂	1.85, m 1.89, m	25.8, CH ₂	1.82, m 1.88, m
4	27.1, CH ₂	1.29, m	27.1, CH ₂	1.29, m	27.2, CH ₂	1.31, m
5	33.3, CH	1.53, m	33.3, CH	1.53, m	33.4, CH	1.62, m
6	40.4, C		40.5, C		40.5, C	
7	34.8, CH ₂	1.36, td (5.5, 13.1) 1.42, td (3.4, 13.1)	34.8, CH ₂	1.37, m 1.42, m	35.1, CH ₂	1.41, m 1.46, m
8	34.6, CH ₂	1.56, m 1.81, m	34.7, CH ₂	1.58, m 1.82, m	34.3, CH ₂	1.88, m 1.91, m
9	141.2, C		141.2, C		139.6, C	
10	124.1, CH	5.68, d (8.9)	123.9, CH	5.66, d (9.6)	124.5 CH	5.39, br s
11	63.4, CH ^a	5.63, d (8.9)	63.5, CH	5.61, d (8.9)	58.9, CH ₂	4.39, d (6.9)
12	17.2, CH ₃	1.92, s	17.3, CH ₃	1.93, s	16.6, CH ₃	1.67, s
13	19.2, CH ₃	1.50, s	19.2, CH ₃	1.51, s	19.3, CH ₃	1.52, s
14	15.8, CH ₃	0.68, d (6.9)	15.9, CH ₃	0.68, d (6.2)	15.9, CH ₃	0.73, d (6.1)
15	20.9, CH ₃	0.70, s	20.9, CH ₃	0.71, s	21.1, CH ₃	0.76, s
1'	194.6, C		194.1, C			
2'	121.1, CH	6.78, s	122.6, CH	6.49, s		
3'	162.3, C		154.9, C			
4'	63.4, CH ^a	5.11, s	64.3, CH	5.13, s		
5'	60.4, CH	4.58, s	60.4, CH	5.09, s		
6'	61.7, C		61.6, C			
7'	63.4, CH ₂	4.64, d (17.2) 5.02, d (17.2)	63.4, CH ₂	5.12, d (16.8) 5.38, d (16.8)		
1''			171.5, C			
2''			44.7, CH ₂	2.61, dd (4.8, 15.1) 2.71, dd (8.2, 15.1)		
3''			63.3, CH	4.55, m		
4''			24.0, CH ₃	1.33, d (6.2)		

^a Overlapped signals.

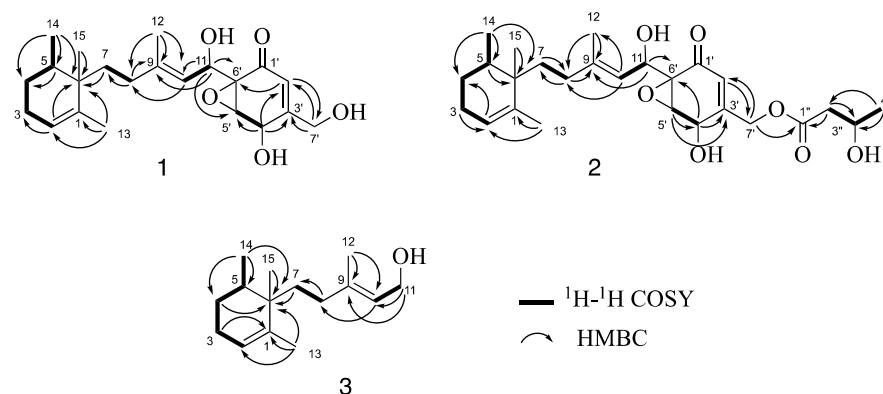


Figure 2.2 ^1H - ^1H COSY and key HMBC correlations of **1**–**3**.

The relative configuration of the cyclohexene ring in **1** was determined on the basis of ^{13}C NMR shifts compared to the reported compounds and 1D NOE (Fig. 2.3). The ^{13}C NMR shifts of C-5, C-6, C-14, and C-15 were similar with those of stelliosphaerol A isolated from *Stelliosphaera formicum*⁵³ [δ_{C} 34.6 (C-5), 41.6 (C-6), 16.3 (C-14), and 21.5 (C-15)]. These carbons have a *cis* orientation that is slightly different from the *trans* orientation in subersin⁵⁴ [δ_{C} 37.8 (C-5), 39.5 (C-6), 16.0 (C-14), and 26.6 (C-15)] and oculatolide⁵⁵ [δ_{C} 37.7 (C-5), 39.5 (C-6), 15.9 (C-14), and δ_{C} 26.4 (C-15)]. The NOEs data showed correlations from Me-14 to H-4, Me-14 to H₂-7, and Me-15 to H-4, but not from Me-15 to H-5. These data showed that the Me-15 has a pseudo-axial orientation along with the Me-14 and C-7 have a pseudo-equatorial orientation. Further, NOE correlation between H-12 and H-11 indicated an *E*-form double bond at C-9 and C-10. The *trans* orientation for both the epoxide and C-4'-OH groups were assigned on the basis of their H-4' and H-5' 3J coupling constant of 0 Hz, and further confirmed by CD data comparison.

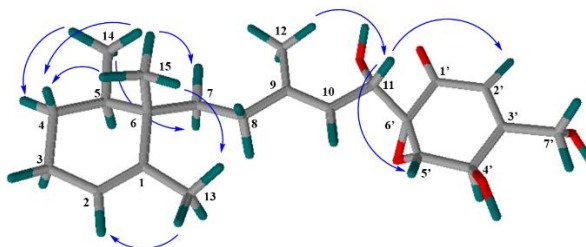


Figure 2.3 Key NOE correlations of **1**.

The absolute configuration of epoxycyclohexenone was deduced by circular dichroism (CD) analysis. The CD spectrum of **1** generated negative cotton effects at 240 nm (-4.2) and 340 nm (-2.2). The CD data was compared with that of 13-hydroxylmacrophorin A (4'*R*, 5'*R*, 6'*R*) isolated from *Microdiplodia* sp. TT-12⁵⁶ [CD (MeOH) $\Delta\epsilon$: 240 (-4.6), 334 (+2.86)]. This comparison suggested that the C-4'-OH in **1** was β -oriented, identical to that observed in 13-hydroxylmacrophorin A (4'*R*). In contrast, the epoxide at C-5' and C-6' in **1** was α -oriented (5'*S*, 6'*S*), which is opposite of that observed in 13-hydroxylmacrophorin A. This was supported by a similar relationship between the CD spectra of neomacrophorin III isolated from *Trichoderma* sp. 1212-03⁵⁷ [ECD (MeOH) $\Delta\epsilon$: 243 (-6.1), 339 (-3.2)] and myrothecol B isolated from *Myrothecium fungus*⁵⁸ [CD (MeOH) $\Delta\epsilon$: 249 (-5.5), 334 (-3.8)], where the C-4'-OH and epoxide at C-5' and C-6' were *trans* oriented (4'*R*, 5'*S*, 6'*S*). Furthermore, single crystal was obtained from a methanol solution of **1** and was suitable for X-ray crystallography. Final refinement of the diffraction data resulted in a small Flack parameter -0.1(3), allowing the assignment of the absolute configuration of **1** (Fig. 2.4).

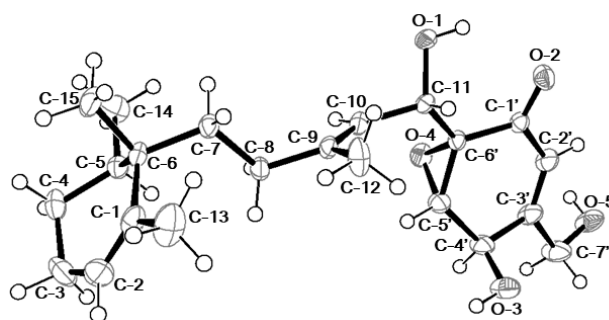


Figure 2.4 ORTEP drawing of **1**, showing 50% probability ellipsoids.

Compound **2** was isolated utilizing a less polar eluent system than **1**, which indicated that **2** is a less polar compound compared to **1**. The HRESITOFMS data of **2** showed a sodium adduct ion at m/z 485.2509 $[M + Na]^+$, suggesting the molecular formula $C_{26}H_{38}O_7$ with eight degrees of unsaturation. The molecular formula of **2** was 86 units larger than the molecular formula of **1**. The 1H and ^{13}C NMR spectral data (Table 2.1) of **2** closely resembled those of **1** except for several additional resonances at δ_C 171.5 (C-1"), 44.7 (C-2"), 63.3 (C-3"), 24.0 (C-4"), δ_H

2.61 (dd, $J = 4.8, 15.1$ Hz, H-2a"), 2.71 (dd, $J = 8.2, 15.1$ Hz, H-2b"), 4.55 (m, H-3"), and 1.33 (d, $J = 6.2$ Hz, H-4"), which indicated characteristic signals for a 3-hydroxybutanoate moieties. In the HMBC analysis of **2**, correlations from H-7' to C-1" indicated that the butanoate moiety was connected to C-7' (Fig. 2.2). Compound **2** exhibited identical ^{13}C NMR chemical shifts (Table 1) and CD data [CD (MeOH) $\Delta\epsilon$: 248 (-4.2), 340 (-1.9)] to those of **1**. These data indicated that **1** and **2** have the same configuration of the cyclohexene (C-5, C-6 and C-11) and epoxycyclohexenone (C-4', C-5' and C-6') moieties.

The absolute configuration at C-3" of **2** was determined by alkaline methanolysis. The resulting product was compared to the authentic standards by chiral GC-MS. Injection of the pentane extract of hydroxylate into GC-MS with a CycloSil-B capillary column was monitored by the 3-hydroxybutanoate ion ($[\text{M} - \text{CH}_3]^+$, $m/z = 103$) generating a signal at 12.937 min. This signal was verified with a mixture of standard methyl (*S/R*)-3-hydroxybutanoate that appeared at 12.800 and 12.938 min, respectively, under the same conditions. The configuration of C-3" was then determined to be the (*R*)-form. The structure of **2** was finally determined as shown in Fig. 2.1.

The molecular formula of **3** was assigned as $\text{C}_{15}\text{H}_{26}\text{O}$ by HRESITOFMS analysis (m/z 245.1876 $[\text{M} + \text{Na}]^+$) in combination with NMR data, which indicated only three degrees of unsaturation. In the NMR data of **3**, characteristic upfield signals at δ_{C} 19.3 (C-13), 15.9 (H-14), 21.1 (C-15), δ_{H} 1.52 (H-13), 0.73 (H-14), and 0.76 (H-15) revealed the presence of a 1,5,6-trimethyl-cyclohexene moiety. Furthermore, signals at δ_{C} 35.1 (C-7), 34.3 (C-8), 139.6 (C-9), 124.5 (C-10), 58.9 (C-11), δ_{H} 1.41 (H-7a), 1.46 (H-7b), 1.88 (H-8a), 1.91 (H-8b), 5.39 (H-10), and 4.39 (H-11) revealed the presence of a 2-methylbutene moiety. Intensive HMBC analysis confirmed that the planar structure of **3** has the same sesquiterpene part of **1**. The critical difference between **1** and **3** was the absence of the epoxycyclohexenone group and the appearance of a new oxygenated methylene at C-11 in compound **3**. The absence of the epoxycyclohexenone group in **3** was also supported by the finding that **3** lacked the IR absorbance at ν_{max} 1677 cm^{-1} that was present in **1** and **2**. The relative configuration of **3** was determined to be identical to **1** on the basis similar ^{13}C NMR chemical shifts shown in Table 2.1. The structure of **3** was elucidated and is shown in Fig. 2.1.

Table 2.2 ¹³C NMR (150 MHz) and ¹H NMR (600 MHz) spectral data for **5** and **6**.

Pos.	5 (pyridine- <i>d</i> ₅)		6 (CDCl ₃)	
	δ _C , type	δ _H , mult. (<i>J</i> in Hz)	δ _C , type	δ _H , mult. (<i>J</i> in Hz)
1	166.8, C		166.5, C	
3	149.0, C		149.3, C	
4	108.7, C		108.7, C	
4a	138.0, C		138.2, C	
5	100.1, CH	6.64, s	94.6, CH	6.34, s
6	165.1, C		164.6, C	
7	110.8, C		111.9, C	
8	161.9, C		160.4, C	
8a	99.0, C		100.1, C	
4-Me	11.9, CH ₃	1.82, s	12.6, CH ₃	2.11, s
3-Me	16.7, CH ₃	2.02, s	17.3, CH ₃	2.29, s
7-Me	8.5, CH ₃	2.53, s	7.9, CH ₃	2.14, s
6-OMe			55.8, O-CH ₃	3.93, s

Compound **5** was isolated as a white amorphous powder. Its molecular formula was determined to be C₁₂H₁₂O₄ by combination of HRESITOFMS (*m/z* 243.0628 [M + Na]⁺) and NMR data (Table 2.2), indicating seven degrees of unsaturation and 14 mass units more than the molecular formula of **5**. Its UV spectrum exhibited absorption maxima at 277 and 328 nm, indicating the presence of an α,β-unsaturated carbonyl group. The IR spectrum showed the absorption bands of hydroxyl (3436 cm⁻¹) and ester carbonyl (1635 cm⁻¹) groups. Comparison of the 1D NMR data of **5** with those of **4**, suggested that they have similar structures. The main difference was the replacement of one of the meta-coupled proton resonances with an additional signal of methyl group (δ_H 2.53, s, 7-Me, 3H) in **5**, indicating the presence of a pentasubstituted benzene ring. The HMBC correlations from 7-Me to C-6, C-7, and C-8 suggested that the methyl group was attached to C-7 (Fig. 2.5). Hence, the structure of **5** was established as 6,8-dihydroxy-3,4,7-trimethylisocoumarin (Fig. 2.1).

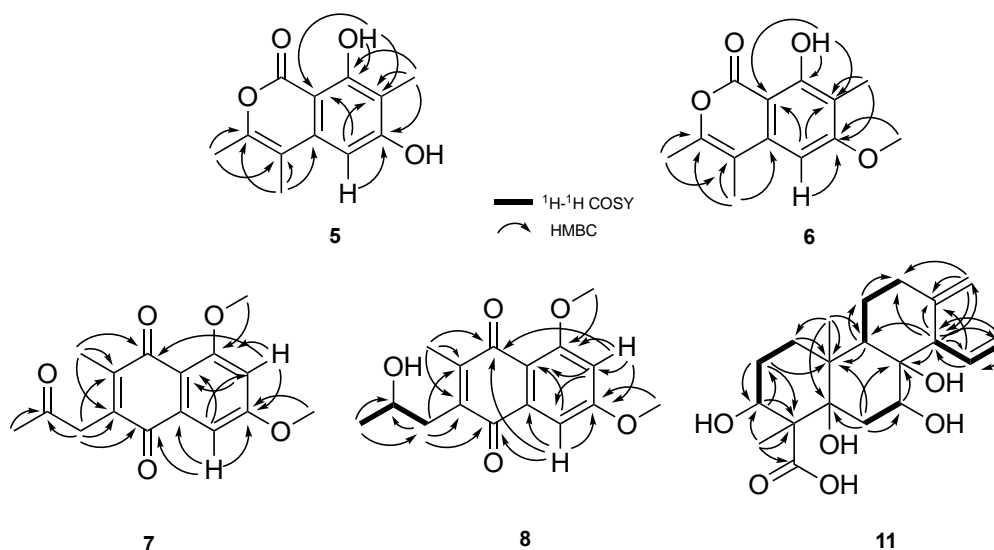


Figure 2.5 ^1H - ^1H COSY and key HMBC correlations observed for **5-8** and **11**.

The close similarity of NMR data suggested that the structure of **6** was similar to those of **4** and **5** (Table 2.2). Its molecular formula, $\text{C}_{13}\text{H}_{14}\text{O}_4$ (m/z 257.0784 $[\text{M} + \text{Na}]^+$), was 14 mass units more than that of **5**. The UV spectrum (absorption maxima at 279 and 328 nm) and IR (hydroxyl and ester carbonyl at 3421 and 1646 cm^{-1}) spectrum of **6** were also similar to those of **1** and **2**. The main difference between **6** and **5** was the presence of an additional methoxy signal at δ_{C} 55.8 and δ_{H} 3.93 (s, 6-OMe, 3H) which was attached to C-6 on the basis of the HMBC correlation from 6-OMe to C-6 (Fig. 2.5). Hence, the structure of **6** was established as 8-hydroxy-6-methoxy-3,4,7-trimethylisocoumarin (Fig. 2.1).

Compound **7** was isolated as a yellow amorphous powder, and its molecular formula of **7** was determined to be $\text{C}_{16}\text{H}_{16}\text{O}_5$ by combination of HRESITOFMS (m/z 311.0895 $[\text{M} + \text{Na}]^+$) and NMR data, indicating nine degrees of unsaturation. The UV spectrum of **7** exhibited absorption maxima at 214, 265, and 404 nm, indicating the presence of a naphthoquinone core.⁵⁹ This finding was also supported by the IR spectrum, which showed absorption bands at 1697 (carbonyl), 1650 (carbonyl), and 1519 (unsaturated carbon) cm^{-1} . The ^{13}C -NMR and DEPT data of **7** confirmed the presence of 16 carbons, including two methyls carbons, two methoxy carbons, one methylene, two sp^2 methines, four sp^2 quaternary carbons, two oxygenated sp^2 quaternary carbons, and three ketone carbonyls (Table 2.3). The ^1H NMR together with HMQC data of **7** showed seven

proton resonances, corresponding to two methyl groups, two methoxy groups, a methylene proton, and two meta-coupled aromatic doublet protons. The HMBC correlations from H-7 to C-1, C-6, C-8, and C-8a, and from H-5 to C-4, C-4a, C-6, C-7, and C-8a, revealed the presence of 1,4-naphthoquinone core; moreover, the HMBC correlations from 6-MeO to C-6 and from 8-MeO to C-8 indicated that the two methoxy groups were attached to C-6 and C-8, respectively, and those from H-3' to C-2' and from H-1' to C-2', C-2, C-3, and C-4 indicated the presence of an 2-oxopropyl moiety attached to C-3. The last methyl group was found to be attached to C-2 on the basis of HMBC correlation from H-4' to C-1, C-2, and C-3 (Fig. 2.5). Hence, the structure of **7** was established as 3-(2-oxopropyl)-6,8-methoxy-2-methyl-1,4-naphthoquinone (Fig. 2.1), which was previously reported as an intermediate in the synthesis of dehydroherbarin.⁶⁰ The physicochemical and spectral data of the reported synthetic compound are similar to those observed for **7**. However, to the best of our knowledge, this is the first report of **7** as a natural product, which named nectriaquinone A.

Table 2.3 ¹³C NMR (150 MHz) and ¹H NMR (600 MHz) spectral data for **7–8** in CDCl₃.

Pos.	7		8	
	δ _c , type	δ _H , mult. (J in Hz)	δ _c , type	δ _H , mult. (J in Hz)
1	182.6, C		183.2, C	
2	147.7, C		147.5, C	
3	137.4, C		141.2, C	
4	184.1, C		185.6, C	
4a	135.4, C		135.7, C	
5	102.8, CH	7.22, d (2.1)	103.1, CH	7.02, d (2.1)
6	164.1, C		164.2, C	
7	103.8, CH	6.70, d (2.8)	103.5, CH	6.49, d (2.1)
8	161.5, C		161.4, C	
8a	114.4, C		114.2, C	
1'	41.4, CH ₂	3.73, s	36.9, CH ₂	a 2.68, dd (13.2, 8.4); b 2.72, dd (13.2, 4.2)
2'	203.5, C		67.5, CH	4.04, m
3'	29.9, CH ₃	2.28, s	23.9, CH ₃	1.27, d (6.2)
4'	13.3, CH ₃	2.08, s	13.6, CH ₃	2.10, s
8-OMe	55.6, O-CH ₃	3.92, s	55.2, O-CH ₃	3.82, s
6-OMe	56.2, O-CH ₃	3.95, s	56.3, O-CH ₃	3.84, s

Compound **8** was obtained as a yellow amorphous powder, and its molecular formula was established to be C₁₆H₁₈O₅ by HRESITOFMS (*m/z* 313.1056 [M +

Na]⁺), indicating eight degrees of unsaturation. The UV and IR spectrum of **5** were similar to those of **7**, suggesting the presence of a 1,4-naphthoquinone core, with the only difference being the hydroxyl absorption band at 3431 cm⁻¹ observed in the IR spectrum of **8**. A comparison of the NMR data also revealed structural difference between **7** and **8** (Table 2.3). The NMR spectrum of **8** exhibited signals for an oxygenated methine, a doublet methyl, and only two carbonyl resonances, suggesting that the ketone group at C-2' in **7** was reduced to an alcohol group in **8**. The configuration at C-2' of **8** was assigned as (*S*) by comparison of its specific rotation ([α]_D²⁰ +110 (c 0.01, CH₂Cl₂)) with that of the closely related compound 3-(2-(*R*)-hydroxypropyl)-8-methoxy-1,4-naphthoquinone⁶¹ with opposite specific rotation ([α]_D²⁰ -25.3, c 0.01, CH₂Cl₂). Based on these evidences, the structure of **8** was established as 3-(2-(*S*)-hydroxypropyl)-6,8-dimethoxy-2-methyl-1,4-naphthoquinone (Fig. 2.1), and named nectriaquinone B.

Table 2.4 ¹³C NMR (150 MHz) and ¹H (600 MHz) spectral data for **11** in CD₃OD.

Pos.	11	
	δ_C , type	δ_H , mult. (<i>J</i> in Hz)
1	27.1, CH ₂	a 1.28, m; b 1.61, m
2	25.8, CH ₂	a 1.58, m; b 2.26, m
3	72.3, CH	4.08, t (3.5)
4	49.0, C	
5	80.2, C	
6	33.8, CH ₂	a 1.90, dd (11.7, 4.8); b 2.36, t (11.7)
7	66.9, CH	4.04, dd (11.7, 4.8)
8	75.6, C	
9	42.0, CH	2.03, dd (12.4, 3.4)
10	42.5, C	
11	22.1, CH ₂	a 1.54, br t (4.2) b 1.56, br d (3.0)
12	31.2, CH ₂	a 2.21, br d (4.2) b 2.22, br d (3.6)
13	148.9, C	
14	57.9, CH	3.05, d (8.9)
15	137.3, CH	6.03, ddd (17.3, 10.4, 9.0)
16	115.7, CH ₂	a 4.99, dd (10.3, 2.0) b 5.10, dd (17.9, 3.4)
17	109.2, CH ₂	a 4.67, d (2.0) b 4.69, d (2.0)
18	177.7, C	
19	19.2, CH ₃	1.40, s
20	16.5, CH ₃	1.00, s

Compound **11** was isolated as a colorless oil, and its molecular formula was determined to be $C_{20}H_{30}O_6$ by HRESITOFMS (m/z 389.1938 $[M + Na]^+$), indicating six degrees of unsaturation. The IR spectrum of **11** showed absorption bands at 3432 and 1631 cm^{-1} , suggesting the presence of hydroxyl and carbonyl group, respectively. The extensive analysis of 1H -NMR and ^{13}C -NMR for **11** (Table 2.4) revealed closely similar to those of $3\alpha,5\alpha,8\beta$ -trihydroxycleistanth-13(17),15-dien-18-oic acid, a cleistanthane-type diterpene previously isolated from *Albatrellus confluens*.⁶² The distinct differences were the presence of an oxygenated methine (δ_C 66.9, C-7) in **8** instead of the methylene in $3\alpha,5\alpha,8\beta$ -trihydroxycleistanth-13(17),15-dien-18-oic acid (δ_C 33.8, C-7), which suggested that **11** is a 7-hydroxy derivative of $3\alpha,5\alpha,8\beta$ -trihydroxycleistanth-13(17),15-dien-18-oic acid. The HMBC correlation from H-7 to C-8, and from H-6 to C-5, C-7, C-8, and C-10 supported the above conclusion.

Next, the relative configuration of **11** was assigned on the basis of coupling constants and NOE experiments (Fig. 2.6 (a)). In the 1H NMR spectrum, H-7 appeared as a doublet of doublets ($J = 11.7, 4.8$ Hz) indicating the axial-axial and axial-equatorial coupling interaction, suggested that the hydroxyl group was in the equatorial position. This was confirmed by NOE experiments. Irradiation at δ_H 4.04 (H-7) and 2.03 (H-9) enhanced the signals of H-6a/H-9/H-15 and H-7, respectively, which indicated the α -axial orientation of H-7 and H-9; moreover, irradiation of methyl singlet at δ_H 1.00 (H-20) resulted in an NOE enhancement of H-6b signal, whereas irradiation of the methyl singlet at δ_H 1.40 (H-19) enhanced the signals of H-3/H-6a, indicating the β -axial and α -axial orientations of the carboxyl group C-18 and the hydroxyl at C-3, respectively. In addition, the absolute configuration of secondary alcohols at C-3 and C-7 were determined using modified Mosher's ester method. In the preparation of MTPA ester for **11**, the mono-MTPA ester products (**11a** and **11b**) were obtained in the higher ratio than those of di-MTPA ester products (**11c** and **11d**), indicated that methyl group next to 3-OH give steric effect of the esterification and the reactions were more selective to 7-OH. Based on $\Delta\delta$ ($\delta_S - \delta_R$) values of both mono- and di-MTPA esters (Fig. 2.6 (b) and (c)) the absolute configuration of C-3 and C-7 were determined to be (*R*) and (*S*), respectively. The anomalous behavior value at H-9 in both mono- and di-MTPA ester were resulted by its position was in a different plane to MTPA ester at C-7 and located at a long

distance from MTPA ester at C-3 to give shielding/deshielding effects.⁶³ Hence, the structure of **11** was assigned as 3 α ,5 α ,7 β ,8 β -tetrahydroxycycloleistanth-13(17),15-dien-18-oic acid and named zythiostromic acid C (Fig. 2.1).

We propose that the biosynthetic pathway of **3** derived from a farnesyl pyrophosphate, which is different from the biosynthetic pathway of **1** and **2** that are derived from a farnesyl pyrophosphate and a gentysil alcohol. Compounds **1** and **2** have a rearranged monocyclo-farnesyl skeleton (which is uncommon to sesquiterpene-epoxycyclohexane conjugates) instead of a bicyclo-farnesyl skeleton which is present in macrophorins⁶⁴, neomacrophorins⁵⁷, myrothecols⁵⁸, and craterellins.⁶⁵

Compounds **1**, **2**, and **3** were evaluated for their in vitro cytotoxicity against HL60 and HeLa cell lines by the MTT method using a published protocol.⁶⁶ Compounds **1**, **2**, and **3** exhibited cytotoxic activity against the HL60 cell lines with IC₅₀ values of 1.7, 1.5 and 10.1 μ M, respectively. Additionally, compound **1**, **2**, and **3** exhibited cytotoxicity against the HeLa cell lines with IC₅₀ values of 34.7, 16.6 and 52.1 μ M, respectively.

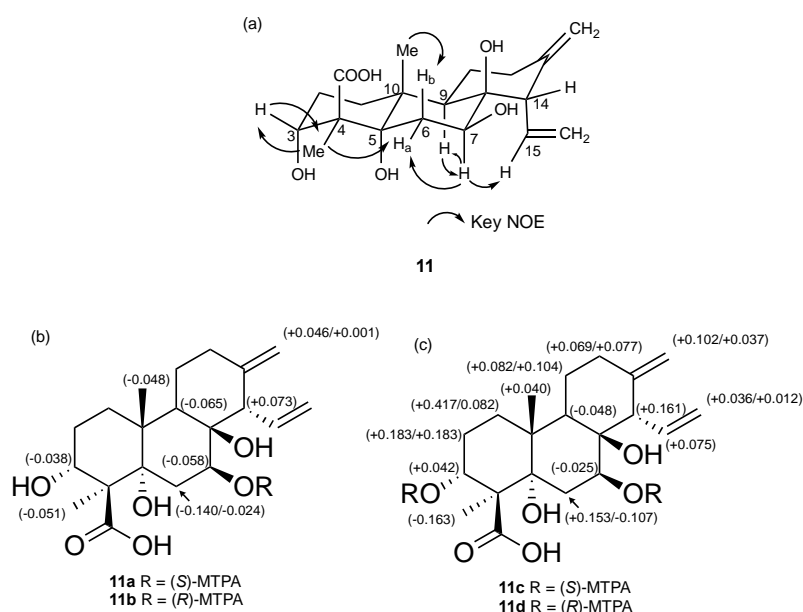


Figure 2.6 (a) Key NOE correlations observed for **11**, (b) chemical shift differences for mono-(*S*)-MTPA ester (**11a**) and mono-(*R*)-MTPA ester (**11b**) and (c) chemical shift differences for di-(*S*)-MTPA ester (**11c**) and di-(*R*)-MTPA ester (**11d**) (in ppm).

Isocoumarins, 1,4-naphthoquinones, and cleistanthane-type diterpene have been reported to have a wide range of pharmacological activities including antimicrobial and anticancer.^{67–69} Thus, **4–11** were evaluated for their antimicrobial activity against *S. aureus*, *P. aeruginosa*, *C. albicans*, and *A. clavatus*, phytotoxicity, and in vitro cytotoxicity. Unlike the other compounds, **8** and **9** exhibited antibacterial activity against *S. aureus* and *P. aeruginosa* with MIC values ($\mu\text{g/mL}$) of >50 and 6.25, and of >50 and 3.125, respectively. The phytotoxicity was tested using lettuce seeds; notably, only **9** induced significant seedling growth inhibition compared to control (Fig. 2.7). Moreover, **7–10** exhibited cytotoxicity against human promyelocytic leukemia HL60 cells with IC_{50} values (μM) of 11.9, 1.33, 1.93, and 11.6, respectively. Compounds **9** and **10** previously reported to cytotoxic against Jurkat, Colo-320, Neuro-2A, and L-1210, also exhibited antibacterial properties.⁷⁰ The results of these biological study, suggest that the 1,4-naphthoquinone pharmacophore is associated with strong cytotoxic activity compared to those of isocoumarins and diterpene, due to its ability to generate reactive metabolites and interfere with cellular enzymes that are critical for cell growth and apoptosis.⁷¹ Moreover, naphthoquinone pharmacophore can disrupt crucial metabolic and signaling pathways by the oxidation or arylation of nucleophilic sites in enzymes and signaling proteins.⁷² The higher cytotoxicity of **8** and **9** compared to that of the related compounds **7** and **10** was attributed to their increased cell membrane permeability due to the presence of the hydroxyl group.

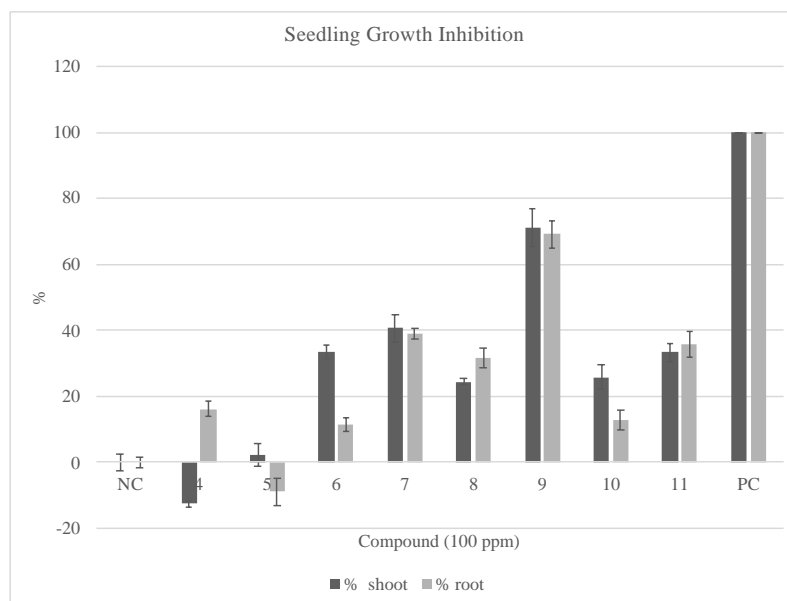


Figure 2.7 Seedling growth inhibition of **4-11** using lettuce (*Lactuca sativa* L.) seeds. NC (negative control); PC (positive control).

Chapter 3 Metabolites from *Fusarium solani* B-18

3.1 Introduction

Strain B-18 was obtained from the inner tissues of unidentified forest litter and subsequently identified as *Fusarium solani*. *Fusarium* species have been widely used in the biotechnological production of food and cosmetic additives, biofuels, and enzymes.⁷³ This species is also a rich source of diverse structures and biologically active metabolites.^{74–78} Purification of the extract derived from the brown rice culture of fungal strain *F. solani* B-18 led to the identification of four new compounds, fusaspirols A-D (**12–15**), which are structurally related to oxaspirol A (**1**) isolated from *Rhodotorula glutinis* T-110.⁷⁹ In this chapter, we report the isolation and structure determination of these compounds, including absolute configurations of secondary alcohols in **12** and **15**. All isolated compounds were also tested for activity in osteoclastic differentiation using murine macrophage derived RAW264.7 cells.

TLC analysis of crude extracts from *F. solani* B-18 indicated the presence of additional metabolites; however, we could not identify these metabolites due to the small quantities present. We therefore re-fermented the fungus on a larger scale using the same brown-rice fermentation method. Separation of its EtOAc extract led to the isolation of four new compounds, designated as fusopoltides B–E (**20–23**), along with four known compounds (**16–19**). To the best of our knowledge, this is the first report of (-)-lanyulactone (**18**) from a fungal source.

3.2 Material and methods

3.2.1 Fungal material and fermentation

The fungal strain B-18 was isolated from inner tissue of the unidentified forest litters collected in the Mount Merapi area (southern latitude 7°35'28", east longitude 110°27'3"), Sleman, Yogyakarta, Indonesia. This strain was identified as *F. solani* using DNA analysis of the 18S rRNA regions and deposited in DNA Database of Japan (DDBJ) with the accession number of LC426035. This fungus was deposited at our laboratory in the Faculty of Agriculture, Yamagata University. *F. solani* B-18 was cultivated on sterilized brown rice (120 g in five flasks) at 25 °C for four weeks.

The scale-up fermentation was done also using the same cultivation method on sterilized brown rice (120 g in ten flasks) at 25 °C for four weeks.

3.2.2 Extraction and isolation

The moldy media were extracted using MeOH, and the MeOH extract was concentrated. The resulting aqueous concentrate was partitioned into EtOAc. The purification of the EtOAc layer was guided by intense characteristic purple coloration with vanillin-sulfuric acid solution on TLC plates. The EtOAc layer (15.9 g) was chromatographed on a silica gel column using 10% stepwise of *n*-hexane-EtOAc (100:0-0:100, each 300 mL), then a mixture of EtOAc-MeOH (50:50, 300 mL), and finally MeOH (300 mL) to give 13 fractions (Fr. 1-1 to 1-13). Fraction 1-6 (2.16 g) was further chromatographed on a silica gel column using 10% stepwise of CHCl₃-EtOAc (100:0-0:100, each 150 mL) to afford 11 fractions (Fr. 1-6-1 to 1-6-11). Fraction 1-6-3 (1.37 g) was further subjected on an ODS column using 10% stepwise of H₂O and MeOH (100:0-0:100, each 50 mL) to afford 11 fractions (1-6-3-1 to 1-6-3-11). Fraction 1-6-3-6 (82 mg) was subjected on preparative RP-HPLC using gradient solvent system (MeOH: H₂O, 40%-100% MeOH 20 min, 100% MeOH 5 min, 100%-40% MeOH 5 min, flow rate 1 mL/min) followed by freeze drying to afford **12** (24 mg) and **13** (8 mg). Fraction 1-7 (5.75 g) was further chromatographed on a silica gel column using 10% stepwise of CHCl₃-EtOAc (100:0-0:100, each 120 mL) to afford 11 fractions (Fr. 1-7-1 to 1-7-11). Fraction 1-7-3 (1.58 g) was further subjected on an ODS column using 10% stepwise of H₂O and MeOH (100:0-0:100, each 50 mL) to afford 11 fractions (1-7-3-1 to 1-7-3-11). Fraction 1-7-3-7 and 1-7-3-8 were combined (956 mg) and was subjected to a flash chromatography using eluent CHCl₃-MeCN (75:1), further purification has done by preparative RP-HPLC using gradient solvent system (MeOH: H₂O, 40%-100% MeOH 20 min, 100% MeOH 5 min, 100%-40% MeOH 5 min, flow rate 1 mL/min) to afford **14** (2 mg). Fraction 1-8 and 1-9 were combined (525 mg) and was further chromatographed on a silica gel column using 10% stepwise of CHCl₃-EtOAc (100:0-0:100, each 100 mL) to afford 11 fractions (Fr. 1-8-1 to 1-8-11). Fraction 1-8-7, 1-8-8, and 1-8-9 were combined (54 mg) and was subjected on an ODS column using 10% stepwise of H₂O and MeOH (100:0-0:100, each 50 mL) to afford 11 fractions (1-8-7-1 to 1-8-7-11). Fraction 1-8-7-7 was identified as **15** (24 mg).

The moldy media from scale-up fermentation were extracted using MeOH, and the MeOH extract was concentrated. The resulting aqueous concentrate was partitioned into EtOAc. The separation of the EtOAc layer was guided by intense characteristic coloration with vanillin-sulfuric acid solution on TLC plates. The EtOAc layer (26.747 g) was chromatographed on a silica gel column using 10% stepwise of *n*-hexane-EtOAc (100:0-0:100, each 700 mL), then a mixture of EtOAc-MeOH (50:50, 700 mL), and finally MeOH (700 mL) to give 13 fractions (Fr. 1-1 to 1-13). Fractions 1-10 to 1-12 (2.594 g) were combined and re-chromatographed on a silica gel column using 10% stepwise of CHCl₃-EtOAc (100:0-0:100, each 200 mL) to afford 11 fractions (Fr. 1-10-1 to 1-10-11). Fractions 1-10-3 and 1-10-4 were combined (497 mg) and subjected on ODS column using 10% stepwise of H₂O and MeOH (100:0-0:100, each 70 mL) to afford 11 fractions (1-10-3-1 to 1-10-3-11). Fraction 1-10-3-4 was identified as **19** (137 mg). Fractions 1-10-3-5 and 1-10-3-6 (72 mg) were combined and subjected on a silica gel column using 10% stepwise *n*-hexane-EtOAc (100:0-0:100, each 30 mL) to afford 11 fractions (1-10-3-5-1 to 1-10-3-5-11). Fraction 1-10-3-5-7 and 1-10-3-5-8 were combined and subjected to RP-HPLC using Mightysil column and gradient system (MeOH:H₂O, 20-100 20 min, 100-20% 2 min, 20% 3 min) to afford **16** (6 mg), **17** (1 mg), **18** (4 mg), and **23** (1 mg). Fractions 1-10-6 to 1-10-8 were combined (872 mg) and subjected on ODS column using 10% stepwise of H₂O and MeOH (100:0-0:100, each 70 mL) to afford 11 fractions (1-10-6-1 to 1-10-6-11). Fraction 1-10-6-4 was subjected to RP-HPLC using Mightysil column and gradient system (MeOH: H₂O, 20-100 20 min, 100-20% 2 min, 20% 3 min) to afford **20** (11 mg, 0.041% yield), **21** (4 mg), and **22** (13 mg).

3.2.3 Preparation of acetyl derivatives

To **12** (5 mg), **13** (1 mg), and **14** (1 mg) each in pyridine (0.5 mL) was added with acetic anhydride (1 mL), each mixture was stirred at room temperature for 24 h, to afford the triacetate **12a** (4, 0.7, and 0.5 mg, respectively). To **15** (6 mg) was treated in the same procedure to afford the triacetate **15a** (5 mg).

4,9-di-*O*-acetylfusaspirol A (**12a**): Brown oil; $[\alpha]_D^{20}$ +350.6 (*c* 3.8, CHCl₃); UV (CHCl₃) λ_{\max} (log ϵ) 259 (4.21), 284 (4.17) nm; IR (KBr) ν_{\max} 1751, 1654 cm⁻¹; ¹H-NMR (600 MHz, CDCl₃) and ¹³C-NMR (150 MHz, CDCl₃) data, see Table 3.2;

HRESITOFMS (positive ion mode) m/z 427.1378 ($[M + Na]^+$, calcd. for $C_{21}H_{24}NaO_8$, 427.1369).

4,9,10-tri-*O*-acetylfusaspireol D (**15a**): Brown oil; $[\alpha]_D^{20}$ -71.5 (c 0.2, $CHCl_3$); UV (MeOH) λ_{max} (log ϵ) 254 (3.73), 279 (3.67) nm; IR (KBr) ν_{max} 1747, 1635 cm^{-1} ; 1H -NMR (600 MHz, $CDCl_3$) and ^{13}C -NMR (150 MHz, $CDCl_3$) data, see Table 3.2; HRESITOFMS (positive ion mode) m/z 427.1369 ($[M + Na]^+$, calcd. for $C_{21}H_{24}NaO_8$, 427.1369).

3.2.4 Preparation of MTPA ester derivatives for **12**

To protect one of the secondary alcohols in **12**, to **12** (10 mg, 0.031 mmol) in dry pyridine, pivaloyl chloride (3.75 mg, 0.031 mmol) was added, the mixture was stirred at 10 °C for 24 h. Purification was performed by column chromatography (*n*-hexane: EtOAc) to afford the 9-*O*-pivaloyl derivative of **12** (**12b**, 3.5 mg). To **12b** (1.0 mg) in dry pyridine was added (*R*)-(-)-MTPACl (10 μ L), the mixture was stirred at room temperature for 24 h. Purification by column chromatography was performed on a silica gel column (*n*-hexane: EtOAc) to afford the (*S*)-MTPA ester (**12c**, 0.7 mg). Compound **1b** (1.0 mg) was treated with (*S*)-(+)-MTPACl (10 μ L) in the same procedure to afford the (*R*)-MTPA ester (**12d**, 0.9 mg).

12b: 1H -NMR (600 MHz, $CDCl_3$) δ_H 1.17 (9H, s, Me of pivaloyl), 1.71 (3H, d, J = 7.2 Hz, H-16), 2.15 (3H, s, Me of 10-OAc), 3.24 (1H, dd, J = 9.6, 2.4 Hz, H-6), 3.34 (1H, d, J = 7.2, 4-OH), 4.66 (1H, t, J = 2.4 Hz, H-11a), 4.86 (1H, t, J = 2.4 Hz, H-11b), 4.81 (1H, br, H-4), 5.48 (1H, m, H-9), 5.52 (1H, dd, J = 15.0, 9.6 Hz, H-12), 5.53 (1H, d, J = 4.8 Hz, H-10), 5.65 (1H, dd, J = 15.0, 7.2 Hz, H-15), 5.61 (1H, dt, J = 10.2, 2.4 Hz, H-7), 5.74 (1H, dq, J = 10.2, 2.4 Hz, H-8), 5.94 (1H, ddd, J = 15.0, 10.2, 1.2 Hz, H-14), 6.04 (1H, dd, J = 15.0, 10.2 Hz, H-13).

12c: 1H -NMR (600 MHz, $CDCl_3$) δ_H 1.15 (9H, s, Me of pivaloyl), 1.66 (3H, d, J = 7.2 Hz, H-16), 2.04 (3H, s, Me of 10-OAc), 2.97 (1H, d, J = 9.0 Hz, H-6), 3.41 (OMe of MTPA), 4.34 (1H, dd, J = 3.0, 1.8 Hz, H-11a), 4.76 (1H, dd, J = 3.0, 1.8 Hz, H-11b), 5.42 (1H, m, H-9), 5.25 (1H, dd, J = 15.0, 9.0 Hz, H-12), 5.26 (1H, d, J = 4.8 Hz, H-10), 5.52 (1H, dq, J = 15.0, 7.2 Hz, H-15), 5.58 (2H, s, overlapped signals of H-7 and H-8), 5.78 (1H, ddd, J = 15.0, 10.2, 1.8 Hz, H-14), 5.85 (1H, dd, J = 15.0, 10.2 Hz, H-13), 6.04 (1H, t, J = 1.8 Hz, H-4), 7.40, 7.46, 7.61 (Ph of MTPA).

12d: $^1\text{H-NMR}$ (600 MHz, CDCl_3) δ_{H} 1.14 (9H, s, Me of pivaloyl), 1.68 (3H, d, J = 6.6 Hz, H-16), 2.03 (3H, s, Me of 10-OAc), 2.71 (1H, dd, J = 9.0, 2.4 Hz, H-6), 3.56 (OMe of MTPA), 4.47 (1H, dd, J = 3.0, 2.4 Hz, H-11a), 4.84 (1H, dd, J = 3.0, 2.4 Hz, H-11b), 5.39 (1H, m, H-9), 5.22 (1H, dd, J = 15.0, 9.0 Hz, H-12), 5.18 (1H, d, J = 5.4 Hz, H-10), 5.65 (1H, dd, J = 15.0, 6.6 Hz, H-15), 5.48 (1H, dt, J = 10.2, 1.8 Hz, H-7), 5.54 (1H, dq, J = 10.2, 3.0 Hz, H-8), 5.82 (1H, ddd, J = 15.0, 10.2, 1.2 Hz, H-14), 5.76 (1H, dd, J = 15.0, 10.2 Hz, H-13), 6.01 (1H, t, J = 2.4 Hz, H-4), 7.38, 7.47, 7.61 (Ph of MTPA).

3.2.5 Preparation of MTPA ester derivatives for 15

Using the same procedure as that described to **12b**, **15** (1.0 and 1.0 mg) was treated with (*R*)-(-)-MTPACl and (*S*)-(+)-MTPACl to respectively afford the (*S*)-MTPA ester **15b** (0.8 mg) and the (*R*)-MTPA ester **15d** (0.7 mg).

15b: $^1\text{H-NMR}$ (600 MHz, CD_3OD) δ_{H} 1.69 (3H, d, J = 7.2 Hz, H-16), 3.42 (1H, d, J = 7.8 Hz, H-6), 3.53 (OMe of MTPA), 3.81 (1H, d, J = 7.8 Hz, H-10), 4.51 (1H, t, J = 2.4 Hz, H-11a), 5.21 (1H, t, J = 2.4 Hz, H-4), 5.39 (1H, dd, J = 15.0, 7.8 Hz, H-12), 5.60 (1H, dq, J = 15.0, 7.2 Hz, H-15), 5.63 (1H, d, J = 10.8 Hz, H-7), 5.69 (1H, dt, J = 10.8, 3.0 Hz, H-8), 5.88 (1H, ddd, J = 15.0, 10.8, 1.2 Hz, H-14), 6.06 (1H, dd, J = 15.0, 10.8 Hz, H-13), 6.17 (1H, m, H-9), 7.41, 7.53, 8.52 (Ph of MTPA), H-11b signal was overlapped with solvent.

15c: $^1\text{H-NMR}$ (600 MHz, CD_3OD) δ_{H} 1.68 (3H, d, J = 6.6 Hz, H-16), 3.42 (1H, d, J = 7.8 Hz, H-6), 3.58 (OMe of MTPA), 3.82 (1H, d, J = 6.0 Hz, H-10), 4.52 (1H, t, J = 2.4 Hz, H-11a), 5.24 (1H, t, J = 2.4 Hz, H-4), 5.38 (1H, dd, J = 15.0, 7.8 Hz, H-12), 5.59 (1H, dq, J = 15.0, 6.6 Hz, H-15), 5.58 (2H, m, overlapped signals of H-7 and H-8), 5.88 (1H, ddd, J = 15.0, 10.8, 1.2 Hz, H-14), 6.05 (1H, dd, J = 15.0, 10.8 Hz, H-13), 6.15 (1H, m, H-9), 7.39, 7.48, 8.52 (Ph of MTPA), H-11b signal was overlapped with solvent.

3.2.6 Preparation of MTPA ester derivatives for 20

Using the same procedure as that described to **12b**, **20** (1.0 and 1.0 mg) was treated with (*R*)-(-)-MTPACl and (*S*)-(+)-MTPACl to respectively afford the (*S*)-MTPA ester (**20a**, 0.7 mg) and the (*R*)-MTPA ester (**20b**, 0.8 mg).

20a: $^1\text{H-NMR}$ (600 MHz, CDCl_3) δ_{H} 4.83 (dq, $J = 6.6, 1.8$ Hz, H-3), 5.51 (d, $J = 1.8$ Hz, H-4), 4.37 (d, $J = 9.0$ Hz, H-6), 3.04 (t, $J = 9.0$ Hz, H-7), 2.12 (m, H-9a), 2.21 (m, H-9b), 1.97 (m, H-10a), 2.06 (m, H-10b), 3.67 (t, $J = 7.2$ Hz, H-11), 1.42 (d, $J = 6.6$ Hz, H-13), 3.41 (s, H-14), 3.87 (s, OMe of MTPA), 7.58-8.84 (Ph of MTPA). HRESITOFMS (positive ion mode) m/z 469.1510 ($[\text{M} + \text{H}]^+$, calcd. for $\text{C}_{23}\text{H}_{24}\text{F}_3\text{O}_7$, 469.1474).

20b: $^1\text{H-NMR}$ (600 MHz, CDCl_3) δ_{H} 4.75 (dq, $J = 7.2, 1.8$ Hz, H-3), 5.52 (d, $J = 1.8$ Hz, H-4), 4.58 (d, $J = 9.0$ Hz, H-6), 3.12 (t, $J = 9.0$ Hz, H-7), 2.14 (m, H-9a), 2.24 (m, H-9b), 1.98 (m, H-10a), 2.10 (m, H-10b), 3.73 (t, $J = 7.8$ Hz, H-11), 1.39 (d, $J = 7.2$ Hz, H-13), 3.48 (s, H-14), 3.88 (s, OMe of MTPA), 7.56-8.90 (Ph of MTPA). HRESITOFMS (positive ion mode) m/z 469.1504 ($[\text{M} + \text{H}]^+$, calcd. for $\text{C}_{23}\text{H}_{24}\text{F}_3\text{O}_7$, 469.1474).

3.2.7 Preparation of MTPA ester derivatives for 22

Using the same procedure as that described to **12b**, **22** (1.0 and 1.0 mg) was treated with (*R*)-(-)-MTPACl and (*S*)-(+)-MTPACl to respectively afford the (*S*)-MTPA ester **22b** (0.8 mg) and the (*R*)-MTPA ester **22c** (0.7 mg).

22b: $^1\text{H-NMR}$ (600 MHz, CDCl_3) δ_{H} 5.48 (m, H-3), 5.10 (s, H-4), 4.49 (d, $J = 7.8$ Hz, H-6), 3.34 (t, $J = 7.8$ Hz, H-7), 2.16 (m, H-9a), 2.23 (m, H-9b), 1.86 (m, H-10a), 2.01 (m, H-10b), 3.66 (t, $J = 8.4$ Hz, H-11), 1.36 (d, $J = 7.2$ Hz, H-13), 3.43 (s, H-14), 3.44 (s, OMe of MTPA), 7.56-8.89 (Ph of MTPA). HRESITOFMS (positive ion mode) m/z 469.1508 ($[\text{M} + \text{H}]^+$, calcd. for $\text{C}_{23}\text{H}_{24}\text{F}_3\text{O}_7$, 469.1474).

22c: $^1\text{H-NMR}$ (600 MHz, CDCl_3) δ_{H} 5.53 (m, H-3), 5.07 (s, H-4), 4.51 (d, $J = 7.8$ Hz, H-6), 3.35 (t, $J = 7.8$ Hz, H-7), 2.19 (m, H-9a), 2.23 (m, H-9b), 1.88 (m, H-10a), 2.02 (m, H-10b), 3.78 (t, $J = 8.4$ Hz, H-11), 1.42 (d, $J = 6.6$ Hz, H-13), 3.46 (s, H-14), 3.45 (s, OMe of MTPA), 7.56-8.89 (Ph of MTPA). HRESITOFMS (positive ion mode) m/z 491.1292 ($[\text{M} + \text{Na}]^+$, calcd. for $\text{C}_{23}\text{H}_{23}\text{F}_3\text{O}_7\text{Na}$, 491.1294).

3.2.8 Osteoclastic differentiation assay

Murine macrophage-like cell line RAW264.7 was induced osteoclastic differentiation in α -MEM medium containing 10% fetal bovine serum (FBS), 2 mM L-glutamine, 100 units/mL penicillin, 100 $\mu\text{g/mL}$ streptomycin, and 100 ng/mL soluble RANKL (sRANKL, *Oriental Yeast*, Japan) in the presence of 0.1% DMSO

(control), 1 μ M of each compound, or 1 μ M of kenpaullone as a positive control. After 4 days incubation at 37 °C, cells were fixed with 10% glutaraldehyde for 15 min at 37 °C, and subsequently incubated for 10 min at 37 °C in TRAP buffer, which consisted of 0.1 M sodium acetate, 0.1 M acetic acid, 10 mg/ml naphthol AS-MX phosphate (*Sigma-Aldrich*, Japan), 0.1% Triton X-100 (*Sigma-Aldrich*, Japan), 0.3 M potassium tartrate (*Sigma-Aldrich*, Japan), and 0.3 mg/mL Fast Red Violet LB Salt (*Sigma-Aldrich*, Japan). TRAP-positive dark-red cells with more than three nuclei were counted as multinucleated osteoclasts under light microscope.

3.2.9 ECD calculations for 21–23

The initial conformational search for **21–23** were performed in the GMMX program (GMMX Gaussian Software) using the MMFF94 force field.⁸⁰ Conformations were kept in a 3.5 kcal mol⁻¹ window. The force field minimum energy conformers suitably obtained were subsequently optimized by applying the density functional theory (DFT) with the B3LYP/6-31G (d) level, in gas phase, implemented in the Gaussian 16 software package. Harmonic vibrational frequencies were also performed to confirm no imaginary frequencies of the finally optimized conformers. These predominant conformers were subjected to theoretical calculation of ECD by utilizing time-dependent density functional theory (TDDFT) calculations at the B3LYP/6-311G+(d) level in gas phase. The energies, oscillator strengths, and rotational strengths of each conformers were carried out with Gaussian 09⁸¹ software package. Theoretical calculations of ECD spectra for each conformer were then approximated by the Gaussian distribution with a half-bandwidth σ of 0.3 eV. The final ECD spectrum of the individual conformers was summed up on the basis of Boltzmann-weighted population contribution by the SpecDisv 1.64.

3.3 Physicochemical properties

3.3.1 Fusaspirol A (12)

Reddish oil; $[\alpha]_D^{20}$ -128.8 (*c* 0.2, CHCl₃); UV (MeOH) λ_{\max} (log ϵ) 248 (3.71), 287 (2.94) nm; IR (KBr) ν_{\max} 3482, 1731, 1650 cm⁻¹; ¹H-NMR (600 MHz, CDCl₃) and ¹³C-NMR (150 MHz, CDCl₃) data, see Table 3.1; HRESITOFMS (positive ion mode) *m/z* 343.1160 ([M + Na]⁺, calcd. for C₁₇H₂₀NaO₆, 343.1158).

3.3.2 Fusaspirol B (13)

Yellow oil; $[\alpha]_D^{20}$ -179.0 (*c* 0.6, CHCl₃); UV (MeOH) λ_{\max} (log ϵ) 255 (3.25), 277 (2.88) nm; IR (KBr) ν_{\max} 3421, 1793, 1635 cm⁻¹; ¹H-NMR (600 MHz, CDCl₃) and ¹³C-NMR (150 MHz, CDCl₃) data, see Table 3.1; HRESITOFMS (positive ion mode) *m/z* 343.1153 ([M + Na]⁺, calcd. for C₁₇H₂₀NaO₆, 343.1158).

3.3.3 Fusaspirol C (14)

Reddish oil; $[\alpha]_D^{20}$ -77.5 (*c* 0.04, MeOH); UV (MeOH) λ_{\max} (log ϵ) 245 (3.49) nm; IR (KBr) ν_{\max} 3421, 1731, 1650 cm⁻¹; ¹H-NMR (600 MHz, CD₃OD) and ¹³C-NMR (150 MHz, CD₃OD) data, see Table 3.1; HRESITOFMS (negative ion mode) *m/z* 277.1067 ([M - H]⁻, calcd. for C₁₅H₁₇O₅, 277.1076).

3.3.4 Fusaspirol D (15)

Pale-yellow oil; $[\alpha]_D^{20}$ -134.4 (*c* 0.5, MeOH); UV (MeOH) λ_{\max} (log ϵ) 245 (3.49) nm; IR (KBr) ν_{\max} 3394, 1731, 1650 cm⁻¹; ¹H-NMR (600 MHz, CD₃OD) and ¹³C-NMR (150 MHz, CD₃OD) data, see Table 3.1; HRESITOFMS (negative ion mode) *m/z* 277.1077 ([M - H]⁻, calcd. for C₁₅H₁₇O₅, 277.1076).

3.3.5 (-)-Lanyulactone (18)

Yellowish oil; $[\alpha]_D^{24}$ -32 (*c* 0.085, MeOH); UV (MeOH) λ_{\max} (log ϵ) 265 (4.32) nm; IR (KBr) ν_{\max} 1770, 1650 cm⁻¹; ¹H-NMR (600 MHz, CDCl₃) and ¹³C-NMR (150 MHz, CDCl₃), see Table 3.3. HRESITOFMS (positive ion mode) *m/z* 203.0682 ([M + Na]⁺, calcd. for C₁₀H₁₂O₃Na, 203.0684).

3.3.6 Fusopoltide B (20)

Yellowish oil; $[\alpha]_D^{20}$ +281 (*c* 0.15, MeOH); UV (MeOH) λ_{\max} (log ϵ) 211 (4.07) nm; IR (KBr) ν_{\max} 3448, 1720, 1639 cm⁻¹; ¹H-NMR (600 MHz, CDCl₃) and ¹³C-NMR (150 MHz, CDCl₃) data, see Table 3.4; HRESITOFMS (positive ion mode) *m/z* 253.1078 ([M + H]⁺, calcd. for C₁₃H₁₇O₅, 253.1076).

3.3.7 Fusopoltide C (21)

White solid; $[\alpha]_D^{22}$ -27 (*c* 0.13, MeOH); UV (MeOH) λ_{\max} (log ϵ) 212 (2.75) nm; IR (KBr) ν_{\max} 3448, 1731, 1635 cm^{-1} ; ^1H -NMR (600 MHz, CDCl_3) and ^{13}C -NMR (150 MHz, CDCl_3) data, see Table 3.4; HRESITOFMS (positive ion mode) m/z 293.1002 ($[\text{M} + \text{Na}]^+$, calcd. for $\text{C}_{13}\text{H}_{18}\text{O}_6\text{Na}$, 293.1001).

3.3.8 Fusopoltide D (22)

Yellowish oil; $[\alpha]_D^{22}$ +272 (*c* 0.1, MeOH); UV (MeOH) λ_{\max} (log ϵ) 216 (4.11) nm; IR (KBr) ν_{\max} 3432, 1735, 1650 cm^{-1} ; ^1H -NMR (600 MHz, CDCl_3) and ^{13}C -NMR (150 MHz, CDCl_3) data, see Table 3.5; HRESITOFMS (positive ion mode) m/z 275.0895 ($[\text{M} + \text{Na}]^+$, calcd. for $\text{C}_{13}\text{H}_{16}\text{O}_5\text{Na}$, 275.0895).

3.3.9 Fusopoltide E (23)

Yellowish oil; $[\alpha]_D^{22}$ +112 (*c* 0.1, MeOH); UV (MeOH) λ_{\max} (log ϵ) 216 (3.78), 223 (3.84) nm; IR (KBr) ν_{\max} 3444, 1747, 1650 cm^{-1} ; ^1H -NMR (600 MHz, CDCl_3) and ^{13}C -NMR (150 MHz, CDCl_3) data, see Table 3.5; HRESITOFMS (positive ion mode) m/z 275.0894 ($[\text{M} + \text{Na}]^+$, calcd. for $\text{C}_{13}\text{H}_{16}\text{O}_5\text{Na}$, 275.0895).

3.4 Results and Discussion

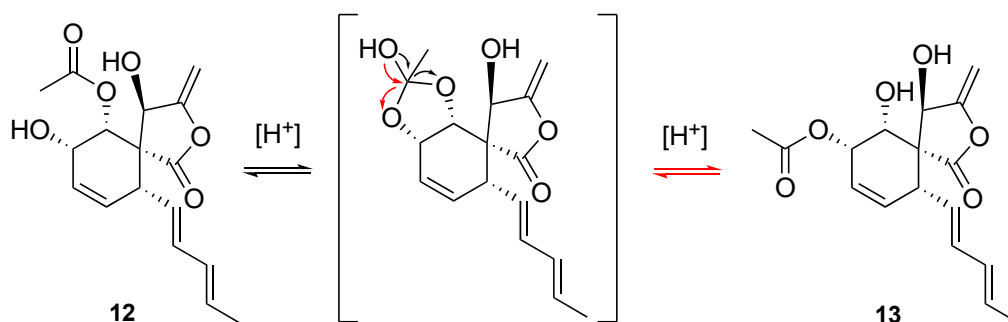
Compounds **12** and **13** displayed two peaks in RP-HPLC (MeOH- H_2O), and retention times of 16.6 and 14.7 min were observed, respectively. However, upon attempting isolation, these two isomers were found to be interchangeable because the reinjection of each isomer resulted in the appearance of two peaks, suggesting an equilibrium of **12** and **13** in aqueous MeOH. The separation was completed successfully by RP-HPLC followed by freeze drying.

Compound **12** was isolated as a reddish oil. Its molecular formula was determined to be $\text{C}_{17}\text{H}_{20}\text{O}_6$, based on the combination of HRESITOFMS (m/z 343.1160 $[\text{M} + \text{Na}]^+$) and NMR data. Its molecular formula indicated eight degrees of unsaturation. The ^{13}C NMR (Table 3.1) spectrum confirmed the presence of 17 carbons, including two methyls [δ_{C} 18.2 (C-16) and 20.9 (10-OAc)], an exocyclic methylene (δ_{C} 89.7, C-11), ten methines [δ_{C} 40.5 (C-6), 62.8 (C-9), 69.8 (C-4), 71.0 (C-10), 126.0 (C-12), 128.3 (C-7), 128.4 (C-8), 130.4 (C-14), 132.5 (C-15), 136.0

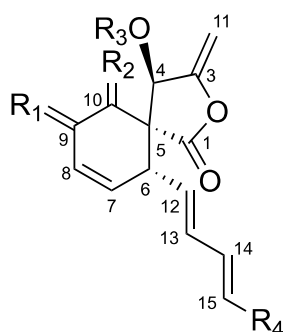
(C-13)], two quaternary carbons [δ_{C} 54.2 (C-5) and 156.8 (C-3)], and two carbonyls [δ_{C} 170.7 (10-OAc) and 173.9 (C-1)]. The ^1H NMR (Table 3.1) and HMQC data indicated the presence of two methyl groups [δ_{H} 1.72 (dd, $J = 7.2, 1.8$ Hz, H-16) and 2.15 (s, 10-OAc)], an exocyclic methylene group [δ_{H} 4.63 (t, $J = 2.4$ Hz, H-11a) and 4.81 (t, $J = 2.4$ Hz, H-11b)], seven methine protons [δ_{H} 5.97 (dq, $J = 10.2, 2.4$ Hz, H-8), 5.55 (dt, $J = 10.2, 1.2$ Hz, H-7), 3.55 (dd, $J = 9.0, 1.2$ Hz, H-6), 5.38 (dd, $J = 15.0, 9.0$ Hz, H-12), 6.16 (dd, $J = 15.0, 10.2$ Hz, H-13), 5.68 (dq, $J = 15.0, 7.2$ Hz, H-15), and 5.93 (ddd, $J = 15.0, 10.2, 1.8$ Hz, H-14)], and three oxygenated methine protons [δ_{H} 4.94 (dt, $J = 7.2, 2.4$ Hz, H-4), 4.38 (m, H-9), 5.02 (d, $J = 5.4$ Hz, H-10)]. COSY data showed the spin system from H-16/H-15/H-14/H-13/H-12/H-6/H-7/H-8/H-9/H-10, as well as HMBC correlations from H-13 to C-6 and from H-6 to C-12, indicated the presence of a penta-1,3-dienyl moiety attached at C-6. Further HMBC correlations from H-4 to C-3 and C-10, from H-10 to C-1, C-4, C-5, C-6, and C-9, and from H-11 to C-3 and C-4 suggested that **12** has a spiro-cyclohexene with a γ -methyldiene-butanolide ring, along with three oxygen attachments at C-4, C-9, and C-10. Additionally, the acetyl group (δ_{C} 170.7 and 20.9) in **12** was placed at C-10 based on the HMBC correlation from H-10 to 10-OAc (Fig. 3.2). The remaining two oxygenated carbons, C-4 and C-9, were designated to each hydroxyl group. These data suggested that the structure of **12** closely resembled that of **1**.⁸² However, a comparison of their ^1H and ^{13}C NMR data showed that the alkyl side-chain at C-6 in **12** has two fewer carbons than **1**, with the addition of acetyl group at C-10.

Compound **12** contains four chiral centers (C-4, C-6, C-9, and C-10), along with C-5 as a spiro center. The relative configuration of **12** was determined according to NOESY experiment (Fig. 3.3). The NOESY correlations between H-9/H-10 and H-6/H-10, suggested that H-6 and H-10 were in a pseudo-axial position, whereas H-9 was in a pseudo-equatorial position. This data suggesting that the cyclohexene ring in **12** has pseudoboat conformation. Moreover, the NOESY correlations between H-12/H-14 and H-14/H-16 suggested the *E,E*-geometry of the double bonds of the side chain in **12**. Further stereochemistry study was done utilizing the equilibrium between **12** and **13**, which was observed by the intramolecular acetyl migration. This kind of equilibrium was previously reported between salvinorins D and E⁸³, which stereochemically occurs between the 10-pseudo-axial and 9-

pseudo-equatorial orientation of the O-acetyl and hydroxyl group functionality in these kinds of compounds. The migration of the O-acetyl group, from C-9 to C-10 and vice versa, was facilitated by a 9,10-dioxolane intermediate in acidic condition (Scheme 3.1).



Scheme 3.1 Intramolecular conversion of **12** and **13** through acetyl migration.



	R ₁	R ₂	R ₃	R ₄
12	α-OH, β-H	α-OAc, β-H	H	CH ₃
12a	α-OAc, β-H	α-OAc, β-H	Ac	CH ₃
13	α-OAc, β-H	α-OH, β-H	H	CH ₃
14	α-OH, β-H	α-OH, β-H	H	CH ₃
15	α-H, β-OH	α-OH, β-H	H	CH ₃
15a	α-H, β-OAc	α-OAc, β-H	Ac	CH ₃
I	α-H, β-OH	α-OH, β-H	H	CH ₂ CH ₂ CH ₃
II	α-H, β-OAc	α-OAc, β-H	Ac	CH ₂ CH ₂ CH ₃

Figure 3.1 Structures of **12-15**, **12a**, **15a**, and **I-II**.

Table 3.1 ¹³C NMR (150 MHz) and ¹H NMR (600 MHz) spectral data for **12-15**.

Pos.	12 (CDCl ₃)		13 (CDCl ₃)		14 (CDCl ₃)		15 (CD ₃ OD)	
	δ _C , type	δ _H , mult. (<i>J</i> in Hz)	δ _C , type	δ _H , mult. (<i>J</i> in Hz)	δ _C , type	δ _H , mult. (<i>J</i> in Hz)	δ _C , type	δ _H , mult. (<i>J</i> in Hz)
1	173.9, C		173.3, C		175.2, C		174.1, C	
3	156.8, C		155.9, C		157.8, C		160.5, C	
4	69.8, CH	4.94, dt (7.2, 2.4)	72.0, CH	4.93, br	69.8, CH	5.45, dt (7.2, 2.4)	69.6, CH	5.27, t (2.4)
5	54.2, C		54.1, C		57.0, C		60.0, C	
6	40.5, CH	3.55, dd (9.0, 1.2)	38.6, CH	3.14, dd (9.6, 3.0)	40.1, CH	3.44, dd (9.0, 1.8)	40.5, CH	3.59, dd (7.8, 2.4)
7	128.3, CH	5.55, dt (10.2, 1.2)	131.3, CH	5.76, dt (10.2, 3.0)	127.4, CH	5.60, dt (10.2, 1.8)	128.5, CH	5.41, dt (10.8, 2.4)
8	128.4, CH	5.97, dq (10.2, 2.4)	123.4, CH	5.70, dq (10.2, 2.4)	130.2, CH	5.94, dq (10.2, 3.0)	130.6, CH	5.65, dt (10.8, 2.4)
9	62.8, CH	4.38, m	68.1, CH	5.40, m	64.6, CH	4.16, m	71.4, CH	4.70, m
10	71.0, CH	5.02, d (5.4)	69.2, CH	4.29, d (4.2)	67.9, CH	3.82, br	74.1, CH	3.56, d (7.8)
11	89.7, CH ₂	4.63 t (2.4) 4.81, t (2.4)	90.7, CH ₂	4.73, t (2.4) 4.95, t (2.4)	89.2, CH ₂	4.61, t (2.4) 4.79, t (2.4)	87.4, CH ₂	4.58, t (2.4) 4.88, t (2.4)
12	126.0, CH	5.38, dd (15.0, 9.0)	128.2, CH	5.55, dd (14.4, 9.6)	126.6, CH	5.37, dd (15.0, 9.0)	128.7, CH	5.38, dd (15.0, 7.8)
13	136.0, CH	6.16, dd (15.0, 10.2)	134.1, CH	6.03, dd (14.4, 10.8)	135.5, CH	6.15, dd (15.0, 10.2)	135.5, CH	6.06, dd (15.0, 10.2)
14	130.4, CH	5.93, ddd (15.0, 10.2, 1.8)	130.8, CH	5.66, ddd (14.4, 10.2, 1.8)	131.2, CH	6.06, ddd (15.0, 10.2, 1.8)	132.4, CH	5.88, ddd (15.0, 10.2, 1.8)
15	132.5, CH	5.68, dq (15.0, 7.2)	130.6, CH	5.96, dq (14.4, 7.2)	130.4, CH	5.92, dq (15.0, 7.2)	130.1, CH	5.58, dq (15.0, 7.2)
16	18.2, CH ₃	1.72, dd (7.2, 1.8)	18.2, CH ₃	1.70, dd (7.2, 1.8)	18.2, CH ₃	1.72, dd (7.2, 1.8)	18.2, CH ₃	1.66, dd (7.2, 1.8)
9-OAc			171.6, C; 21.3, CH ₃	2.16, s				
10-OAc	170.7, C; 20.9, CH ₃	2.15, s						
4-OH		2.70, d (7.2)		2.99, br		2.43, d (7.2)		
9-OH		4.01, d (12.6)				3.88, d (12.6)		
10-OH				3.66, br		3.39, br		

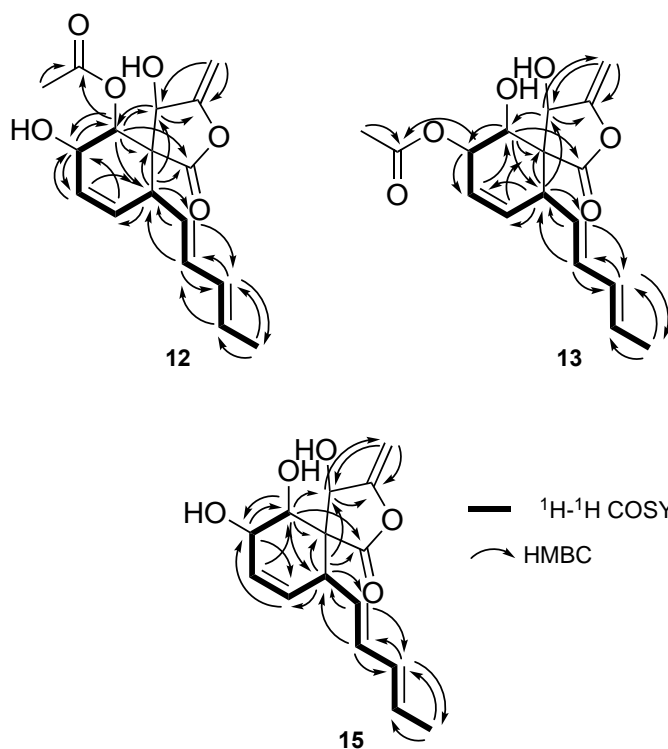


Figure 3.2 ^1H - ^1H COSY and key HMBC correlations observed for **12**, **13**, and **15**.

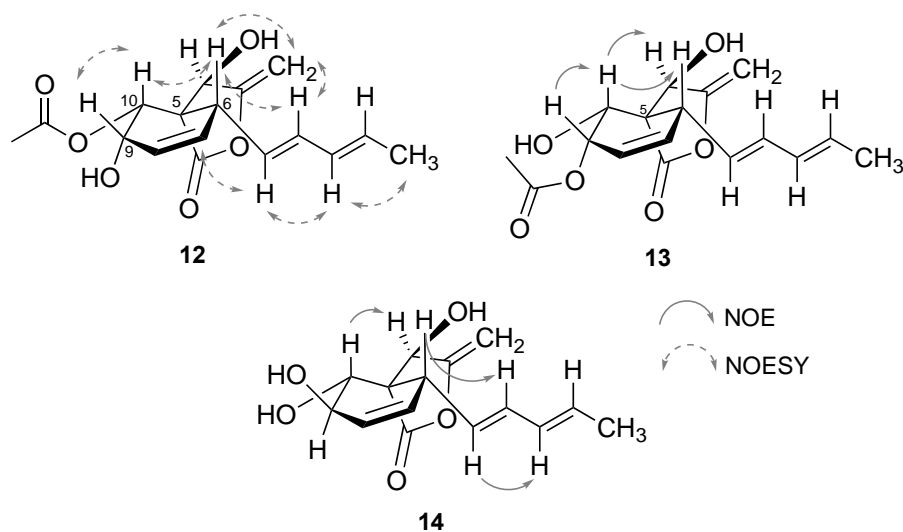


Figure 3.3 Key NOE correlations observed for **12**, **13**, and **15**.

The absolute configuration of the secondary alcohol in **12** was finally determined using the modified Mosher's ester method.⁶³ The direct treatment of **12** with (*R*)- and (*S*)- α -methoxy-(trifluoromethyl)-phenylacetic chloride [(*R*)- and

(*S*)-MTPACl] yielded di-(*S*)- and di-(*R*)-MTPA ester and took place at 9-OH and 4-OH, respectively. The analysis of $\Delta\delta_H$ ($\delta_S - \delta_R$) indicated anomalous values and did not provide specific conclusions. Thus, **12** was first treated using pivaloyl chloride in a 1:1 mol ratio to protect one of the secondary alcohols in **12**. This treatment was successful to protect the secondary alcohol at C-9 to yield 9-O-pivaloyl-**12** (**12b**). Subsequently, **12b** was treated with (*R*)- and (*S*)-MTPACl to give mono-(*S*)- (**12c**) and mono-(*R*)-MTPA (**12d**) esters, respectively, which took place at 4-OH. The analysis of $\Delta\delta_H$ ($\delta_S - \delta_R$) suggested that the absolute configuration of C-4 was (*4R*) (Fig. 3.4). Hence, the structure of **12** was established as shown in Fig. 3.1 and was named fusaspirol A.

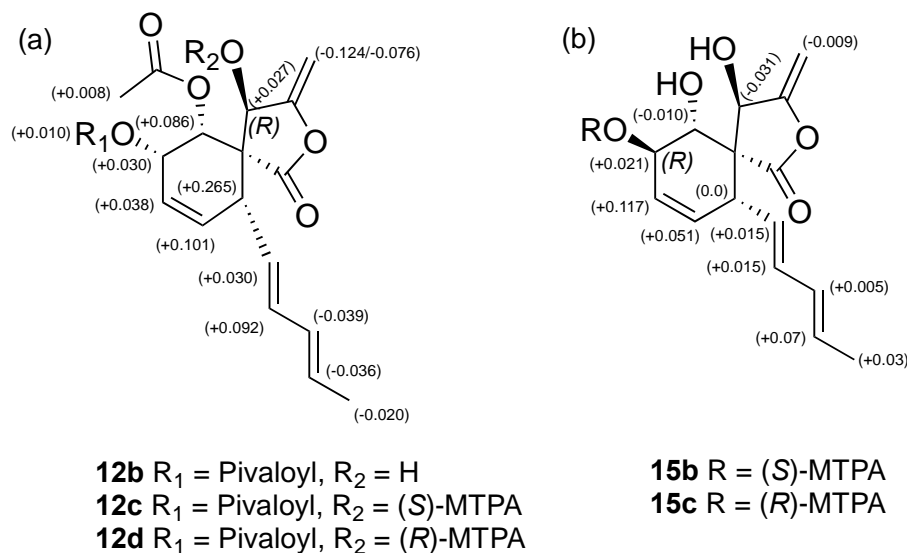


Figure 3.4 Chemical shift differences for (a) (*S*)-MTPA ester (**12c**) and (*R*)-MTPA ester (**12d**) of **12b** and (b) chemical shift differences for (*S*)-MTPA ester (**15b**) and (*R*)-MTPA ester (**15c**) of **15** (in ppm).

Compound **13** was isolated as a yellow oil. Based on previous discussion, **13** was found as the regioisomer of **12**, this deduction was supported by HRESITOFMS data that showed the same molecular formula ($C_{17}H_{20}NaO_6$, m/z 343.1153 [$M + Na$] $^+$). The main difference between **12** and **13** was the attachment of the acetyl group (δ_C 171.6 and 21.3) in **13**. The HMBC (Fig. 3.2) correlation from H-9 to 9-OAc confirmed the attachment of the acetyl group at C-9. The

configuration of **13** was identical to **12** based on similar NMR data (Table 3.1) and NOE correlations (Fig. 3.3). Hence, the structure of **13** was established as shown in Fig. 3.1 and was named fusaspirol B.

Compound **14** was isolated as a reddish oil. Its molecular formula ($C_{15}H_{18}O_5$) has 42 fewer mass units than **12** and **13**. Extensive NMR data analyses (Table 3.1), revealed that **14** has a similar planar structure as **12**. The main difference was an unobservable acetyl group in **14**, suggesting that **14** was a biosynthetically deacetyl form of **12/13**. The multiplicity of H-10 (δ_H 3.82, br) in **14** was too unclear to determine its relative configuration. This ambiguity was resolved by the preparation of the acetyl derivatives of **12** and **14** to afford **12a** and **14a**, respectively. The NMR data comparison of the triacetyl derivative **14a** to that of **12a** (Table 3.2) showed a superimposed relationship. Hence, the structure of **14** was determined as shown in Fig. 3.1 and was named fusaspirol C.

Table 3.2 ^{13}C NMR (150 MHz) and 1H NMR (600 MHz) spectral data for **12a** and **15a** (in $CDCl_3$).

Pos.	12a		15a	
	δ_C , type	δ_H , mult. (J in Hz)	δ_C , type	δ_H , mult. (J in Hz)
1	169.0, C		169.6, C	
3	152.6, C		152.7, C	
4	72.1, CH	5.87, t (1.8)	69.6, CH	5.89, t (1.8)
5	51.5, C		55.8, C	
6	41.0, CH	3.22, dd (9.0, 1.2)	41.1, CH	3.40, m
7	132.8, CH	5.77, m	125.8, CH	5.68, m*
8	122.9, CH	5.75, m	128.9, CH	5.55, dt (10.8, 2.4)
9	63.9, CH	5.46, m	71.4, CH	6.04, dq (7.8, 2.4)
10	69.8, CH	5.39, d (4.8)	71.3, CH	5.39, d (7.8)
11	91.0, CH ₂	4.55, dd (3.0, 1.8) 4.82, dd (3.0, 1.8)	90.3, CH ₂	4.12, dd (3.0, 1.8) 4.80 dd (3.0, 1.8)
12	127.1, CH	5.55, dd (15.0, 9.0)	124.8, CH	5.42, dd (14.4, 7.2)
13	134.5, CH	6.06, dd (15.0, 10.2)	135.9, CH	6.12, dd (14.4, 10.2)
14	130.8, CH	5.65, ddd (15.0, 10.2, 1.2)	130.5, CH	5.94, ddd (15.0, 10.2, 1.2)
15	130.6 (CH)	5.97, dq (15.0, 6.0)	131.3, CH	5.68, m*
16	18.2 (CH ₃)	1.71, d (6.0)	18.3, CH ₃	1.73, d (6.0)
4-OH				
4-OAc	170.0, C; 21.2, CH ₃	2.09, s	170.7, C; 20.7, CH ₃	2.01, s
9-OAc	170.6, C; 20.6, CH ₃	2.02, s	169.6, C; 21.1, CH ₃	2.20, s
10-OAc	169.6, C; 20.9, CH ₃	2.03, s	169.9 C; 20.8, CH ₃	2.08, s

*) Overlapped signals designated by HMQC.

Compound **15** was isolated as a pale-yellow oil. Its molecular formula was the same as **14** ($C_{15}H_{17}O_5$, m/z 277.1077 $[M - H]^+$). The NMR data (Table 3.1) comparison of **15** and **14** revealed that they had the same planar structure. The relative configurations of **15** were assigned by coupling constant values and NOE experiments (Fig. 3.3). The *E,E*-geometry of the double bonds in the side chain were established according to large coupling constants ($^3J_{12-13} = 15.0$ Hz and $^3J_{14-15} = 15.0$ Hz). In NOE experiment, irradiation of H-10 of **15** caused only enhancements of the signal of H-4, suggesting that H-10 and H-4 were cofacial and H-10 and H-9 were anti-facial (Fig. 3.3). Furthermore, the acetyl derivative 4,9,10-tri-*O*-acetyl-**15** (**15a**) was prepared from **15** to give conclusive information about the configuration of the chiral centers. The comparison of the coupling constant of **15a** ($J_{9-10} = 7.8$ Hz) and **II** ($J_{9-10} = 8.0$ Hz) suggesting that both C-9 and C-10 in these compounds have the same configurations. Accordingly, the cyclohexene ring in **15a** has pseudoboat conformation as in **II** (Fig. 3.5). Finally, the absolute configuration of the secondary alcohol in **15** was determined using the modified Mosher's ester method. The treatment of **15** with (*R*)- and (*S*)-MTPACl, gave mono-(*S*)- (**15b**) and mono-(*R*)-MTPA (**15c**) ester, respectively, which took place at 9-OH. The analysis of chemical shift differences [$\Delta\delta_H$ ($\delta_S - \delta_R$)] of both esters suggested that the absolute configuration of C-9 was (9*R*) (Fig. 3.4). Therefore, the structure of **15** was established as shown in Fig. 3.1 and was named fusaspirol D.

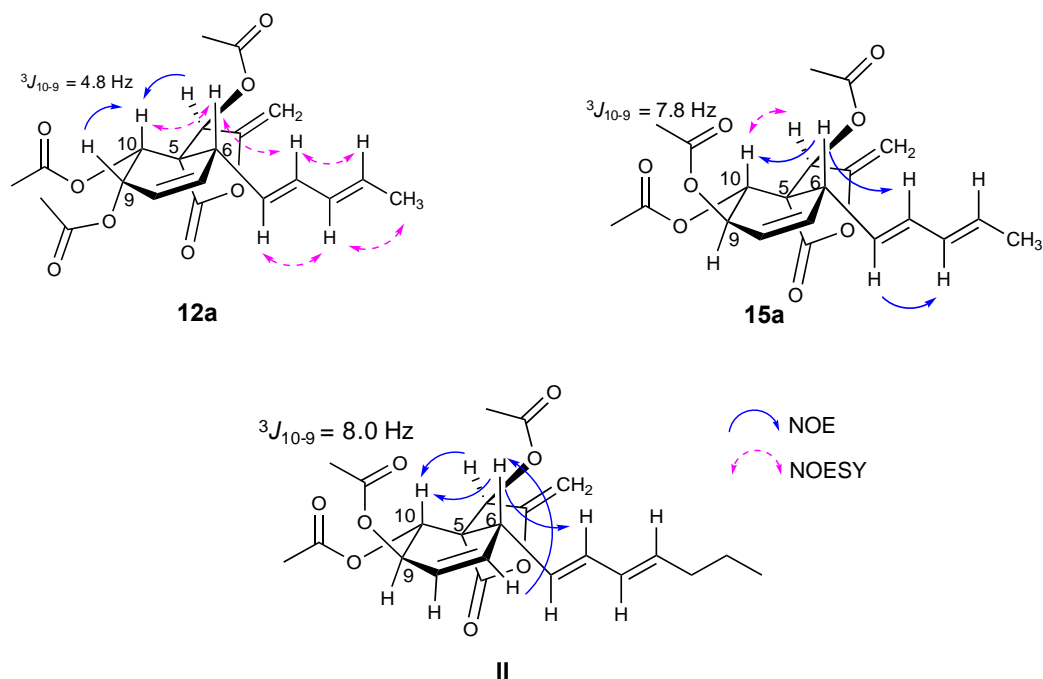


Figure 3.5 The key NOE correlations and coupling constant values (J_{10-9}) of **12a**, **15a**, and **II**.

Oxaspirol analogues have been reported to possess various biological activities, including p97 inhibitory⁸², cytotoxic⁸⁴, TNF- α promoter⁸⁵, and antimicrobial activities.^{86,87} Since all isolated compounds and its derivatives did not show cytotoxicity against murine macrophage derived RAW264.7 cells, all compounds were tested for osteoclastic differentiation activity using the same cells. After four days of the osteoclastic induction, mature osteoclasts of multinucleated-TRAP (tartrate-resistant acid phosphatase)-positive cells were counted. As shown in Fig. 3.6, **12** and **12a** significantly increased the number of mature osteoclasts at the comparable levels to the positive control of kenpaullone⁸⁸, compared to the negative control (DMSO), suggesting that **12** and **12a** activated a signaling pathway in osteoclastic differentiation (Fig. 3.7). Osteoporosis is characterized by the reduction of bone strength, progressive loss of bone density, and deterioration of bone micro-architecture.⁸⁹ The imbalance between osteoblast-mediated bone formation and osteoclast-mediated absorption is associated with metabolic bone diseases, such as osteoporosis. In the case of osteoporosis, the osteoclasts are unable to function properly, which affects resorption of bones. As a result of the

reduction of bone resorption, excess bones are formed, but they are fragile.⁹⁰ This study showed that **12** and **12a** stimulated differentiation in osteoblasts. Thus, further investigation and optimization of these compounds may allow for new approaches to osteoporosis.

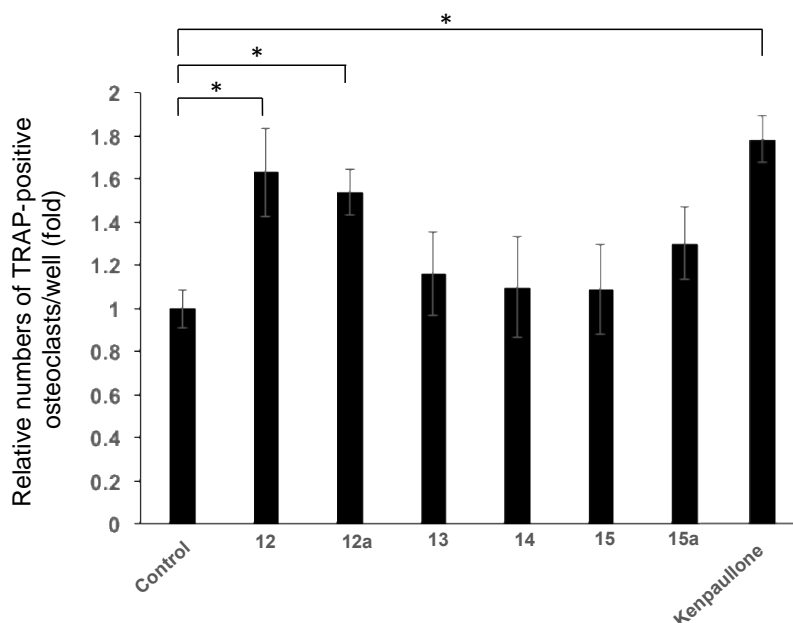


Figure 3.6 The effect of isolated compounds and its derivatives on osteoclastic differentiation. RAW264.7 cells were induced osteoclastic differentiation in the presence of 1 μ M of each compound, 0.1% DMSO (solvent), or 1 μ M kenpaulone as a positive control. After 4 days, TRAP-positive multinucleated cells in each well were counted. The data represent mean values (\pm S.D., $n=4$) and were analyzed by ANOVA and Tukey-Kramer's multiple-comparison tests (* $P<0.01$).

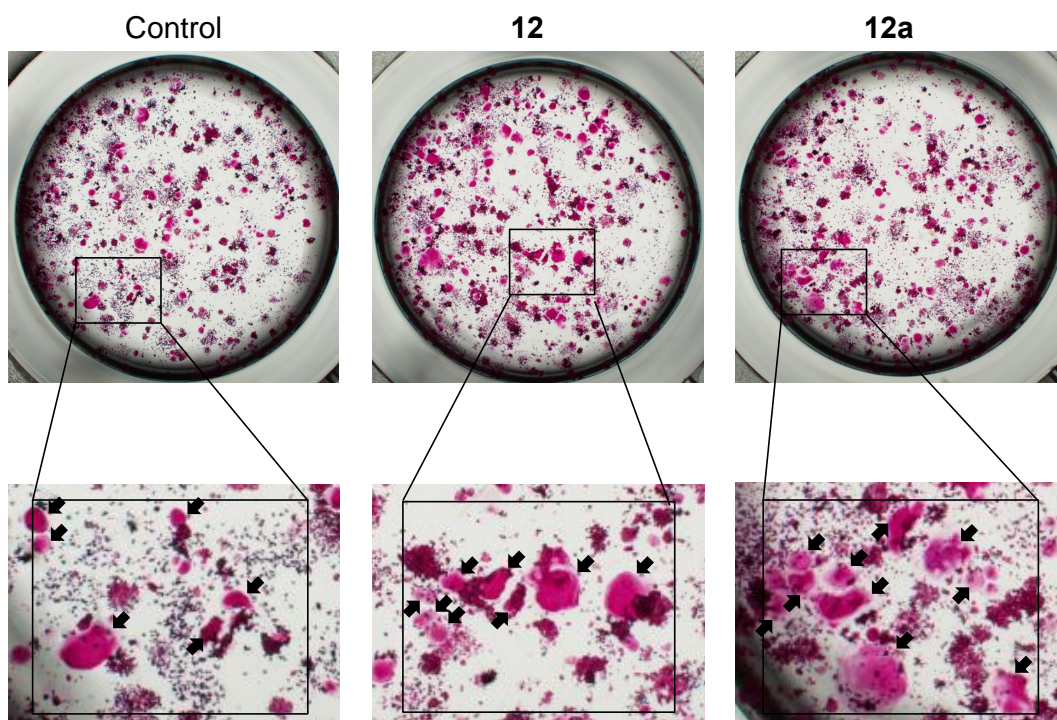


Figure 3.7 Typical images of TRAP-stained mature osteoclasts. The images show TRAP-stained multinucleated cells in 96-well plate in the presence of 1 μ M of 0.1% DMSO (control), **12**, and **12a**. The black square in each well was magnified to show the TRAP-stained mature osteoclasts, which are in magenta color as shown by black arrows.

The structures of the three known compounds, from scale-up fermentation, were assigned by comparing their spectral data and were found to be identical to the previously reported compounds, two known dihydronaphthalenones (**16–17**) from *Fusarium* sp. BCC14842⁹¹, and fusopoltide A (**19**) from *F. solani* KY051566⁹² (Fig. 3.8).

Compound **18** was isolated as a yellowish oil. Its molecular formula was assigned as $C_{10}H_{12}O_3$ through a combination of HRESITOFMS and NMR data. The extensive analyses of 1D and 2D NMR data (Fig. 3.9) suggested that **19** has the same structure as a known compound, lanyulactone. Lanyulactone has been frequently isolated from several species of Sichuan pepper (*Zanthoxylum* spp.).^{93–98} However, to the best of our knowledge, this is the first report of **18** being isolated from a fungal culture and the configuration at C-7 is remaining undiscussed in the

previous studies. The NOE experiment did not give any certain conclusion, because of the flexible bond of C-6–C-7. Since there is no report for the specific rotation of this compound, the configuration at C-7 was therefore determined on the basis of a comparison between its specific rotation ($[\alpha]_D^{24}$ -32) and the related synthetic compound, (*R*)-5-allyldihydrofuran-2(3*H*)-one ($[\alpha]_D^{20}$ -17)⁹⁹, to be 7*R*. Therefore, **18** was designated as (-)-lanyulactone (Fig. 3.8).

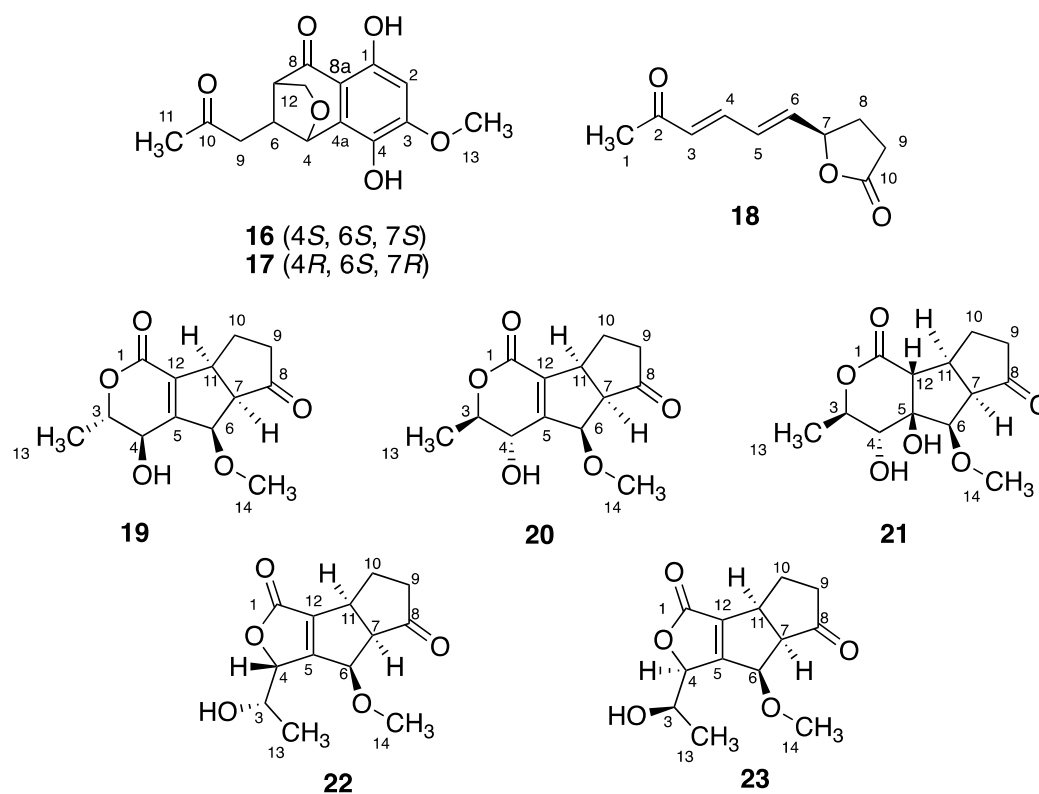


Figure 3.8 Structures of **16–23**.

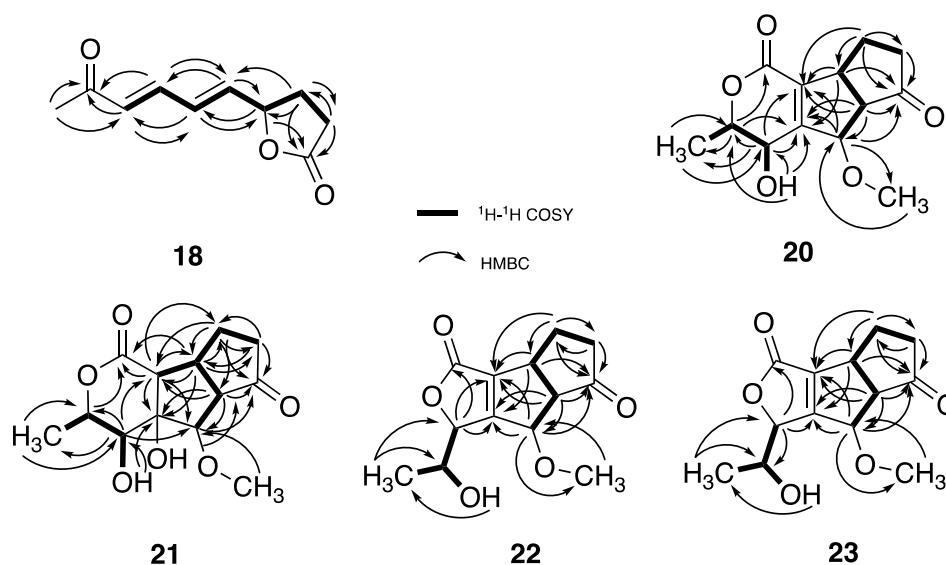


Figure 3.9 ^1H – ^1H COSY and key HMBC correlations observed for **18** and **20–23**.

Table 3.3 ^{13}C NMR (150 MHz) and ^1H NMR (600 MHz) spectral data for **18**.

Pos.	18 (CDCl_3)	
	δ_{C} , type	δ_{H} , mult. (J in Hz)
1	27.7, CH_3	2.29, s
2	198.3, C	
3	132.1, CH	6.19, d (15.0)
4	140.9, CH	7.08, dd (16.2, 10.4)
5	129.9, CH	6.43, dd (15.6, 10.4)
6	138.7, CH	6.12, dd (15.0, 5.4)
7	79.0, CH	5.06, q (6.6)
8	28.4, CH_2	2.03, m 2.56, m*
9	28.2, CH_2	2.43, m 2.56, m*
10	176.4, C	

*) overlapped signals were resolved using HMQC.

Compound **20** was isolated as a yellowish oil. Its molecular formula was assigned as $\text{C}_{13}\text{H}_{16}\text{O}_5$ (six degrees of unsaturation) through a combination of HRESITOFMS and NMR data. The ^1H NMR data for **20** (Table 3.4) showed a methyl group at δ_{H} 1.45 (d, J = 6.0 Hz, H-13); a methoxy group at δ_{H} 3.56 (s, H-14); two methylene protons at δ_{H} 2.01 (m, H-10a), 2.19 (m, H-10b), 2.22 (m, H-9a), and 2.29 (m, H-9b); two methine protons at δ_{H} 3.14 (td, J = 9.0, 1.8 Hz, H-7) and

3.68 (t, $J = 8.4$ Hz, H-11); and also three oxygenated methine protons at δ_{H} 4.36 (t, $J = 6.0$ Hz, H-4), 4.51 (quint, $J = 6.0$ Hz, H-3), and 4.86 (d, $J = 9.0$ Hz, H-6). The ^{13}C NMR data of **20** confirmed the presence of 13 carbons, including a methyl carbon, a methoxy carbon, two methylene carbons, five methine carbons, two olefinic quaternary carbons, an ester carbonyl, and a ketone carbonyl (Table 3.4). Three unsaturation degrees were attributed to the presence of two carbonyl groups and one olefinic bond, therefore, to fulfill three more unsaturation degrees, **20** must contain three rings in its structure. The ^1H - ^1H COSY of **20** showed a spin system of H-6/H-7/H-11/H-10/H-9 along with HMBC correlations from H-6, H-7, H-9, H-10, H-11 to C-8, H-7 to C-5, and H-11 to C-12, to construct the pentalenone moiety (Fig. 3.9). Furthermore, the ^1H - ^1H COSY cross-peak of H-3/H-4, along with the key HMBC correlations from H-3 to C-1 and C-5, and from H-4 to C-3, C-5, and C-12, suggested the structure of **20** contains a pentaleno[1,2-*c*]pyran ring. Finally, the methyl group (Me-13) and the methoxy group (H-14) were attached at C-3 and C-6 based on the ^1H - ^1H COSY cross-peak of H-13/H-3 and the HMBC correlation from H-14 to C-6, respectively. The last hydroxyl group was determined to be attached at C-4 based on the ^1H - ^1H COSY cross-peak of H-4/4-OH and HMBC correlations from 4-OH to C-3, C-4, and C-5.

The planar structure of **20** was previously reported as its co-isolated metabolite, fusopoltide A (**19**).⁹² Extensive comparison of their NOE (Fig. 3.10) data showed only distinct differences in the correlation of H-4 and H-6, which was present in **19** but unobservable in **20**, indicating that they have a different configuration in C-4. The coupling constants between H-3 and H-4 in **19** (J_{3-4} 6.5 Hz) and **20** (J_{3-4} 6.0 Hz) were similar in values, indicating their dihedral angle must be the same and suggested the opposite configuration of methyl and hydroxyl group. Furthermore, Diff-NOE irradiation at δ_{H} 3.14 (H-7) and 4.86 (H-6) enhanced the signal of H-11 and H-7, respectively, indicating a *cis*-configuration at H-7–H-11 and the co-facial orientation of H-6 and H-7, identical to that observed in **19**. Thus, **20** was designated as a diastereomers of **19** at C-3 and C-4. Furthermore, the absolute configuration of **20** was finally determined using the modified Mosher's ester method. Based on $\Delta\delta$ ($\delta_{\text{S}} - \delta_{\text{R}}$) values (Fig. 3.11) the absolute configuration of C-4 in **20** was determined to be 4*S*, supporting the deduction of its relative configuration. Hence, the structure of **20** was assigned as shown in Fig. 3.8 and was named fusopoltide B.

Table 3.4 ^{13}C NMR (150 MHz) and ^1H NMR (600 MHz) spectral data for **20** and **21** (in CDCl_3).

Pos.	20		21	
	δ_{C} , type	δ_{H} , mult. (J in Hz)	δ_{C} , type	δ_{H} , mult. (J in Hz)
1	162.2, C		174.7, C	
3	80.6, CH	4.51, quint (6.0)	66.6, CH	3.82, m
4	66.1, CH	4.36, t (6.0)	85.5, CH	4.04, d (9.6)
5	156.9, C		84.6, C	
6	84.9, CH	4.86, d (9.0)	83.6, CH	4.09, d (7.8)
7	51.5, CH	3.14, td (9.0, 1.8)	50.9, CH	2.94, t (7.8)
8	214.8, C		216.3, C	
9	38.2, CH_2	2.22, m 2.29, m	37.4, CH_2	2.23, m 2.71, qd (12.0, 9.0)
10	24.2, CH_2	2.01, m 2.19, m	28.1, CH_2	2.03, dd (13.8, 9.0) 2.17, m
11	45.2, CH	3.68, t (8.4)	39.2, CH	3.12, td (7.8, 2.4)
12	130.9, C		56.6, CH	2.91, d (2.4)
13	18.5, CH_3	1.45, d (6.0)	20.3, CH_3	1.34, d (6.0)
14	60.2, OCH_3	3.56, s	58.8, OCH_3	3.73, s
4-OH		2.63, d (6.0)		3.44, d (4.2)
5-OH				2.97, s

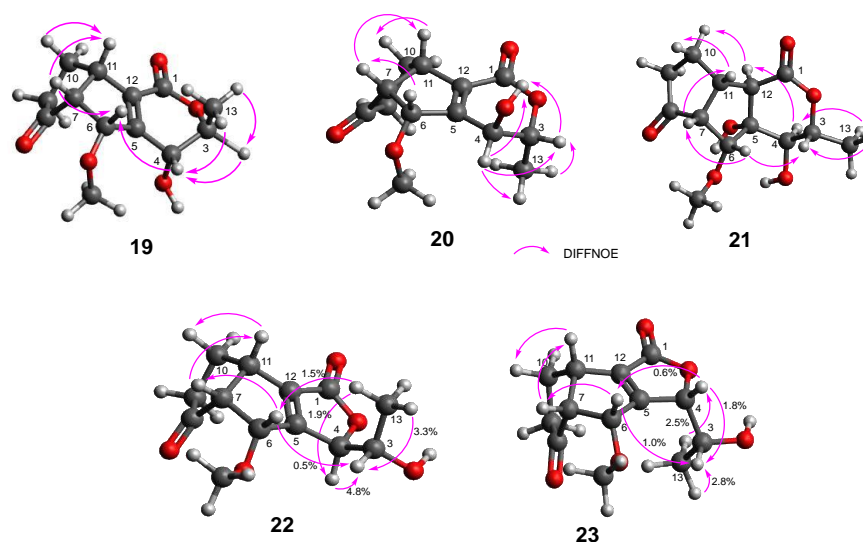


Figure 3.10 Key NOE correlations observed for **19–23**.

Compound **21** was isolated as a colorless solid, and its molecular formula was established to be $C_{13}H_{18}O_6$ by HRESITOFMS, indicating five degrees of unsaturation. With the additional 18 units of mass and the decrease in one degree of unsaturation, it was assumed that **21** was the hydrated form of **20**. The comparison of 1H and ^{13}C NMR data of **21** and **20** revealed differences in the olefinic carbons; in **20**, δ_C 156.9 (C-5) and 130.9 (C-12) were shifted to δ_C 84.6 (C-5) and 56.6 (C-12) in **21**, respectively, supporting the above discussion. The 1H - 1H COSY cross-peak (Fig. 3.9) of H-11/H-12, along with key HMBC from H-12 to C-1, C-5, and C-6 confirmed that the structure of **21** contained a decahydro-pentaleno[1,2-*c*]pyran ring as well as substitutions of a hydrogen at C-12 and a hydroxyl group at C-5. The attachments of a methyl group at C-3 and a methoxy group at C-6 in **21** were assigned the same as **20** based on the 1H - 1H COSY cross-peak H-3/H-13 and the HMBC correlation from H-14 to C-6. The last hydroxyl group was attached at C-4 to fulfill the molecular formula and supported by the 1H - 1H COSY cross-peak H-4/4-OH and HMBC correlations from OH-4 to C-4 and C-5.

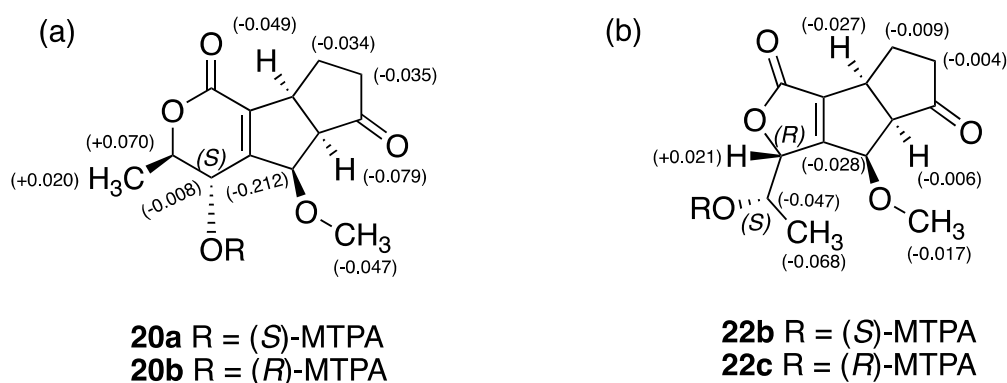


Figure 3.11 Chemical shift differences for (a) (*S*)-MTPA ester (**20a**) and (*R*)-MTPA ester (**20b**) of **20**, and (b) chemical shift differences for (*S*)-MTPA ester (**22b**) and (*R*)-MTPA ester (**22c**) of **22** (in ppm).

The relative configuration of **21** was determined by NOE experiments (Fig. 3.10). Irradiation at δ_H 4.09 (H-6), 2.94 (H-7), and 4.04 (H-4) enhanced the signals of H-3/H-7, H-11, and H-12, respectively, suggesting co-facial orientation between

H-6, H-3, and H-7, between H-7 and H-11, and between H-4 and H-12, as well as a rigid *cis*-configuration between H-7 and H-11, and between H-12 and OH-5. The absolute configuration of chiral centers in **21** were clarified by comparison with the experimental ECD curve and the calculated ECD curve, using TDDFT. The initial MMFF94 minimum conformers of **21**, derived from its relative configuration, were DFT optimized at the B3LYP/6-31G(d) level using Gaussian 09 software (Fig. 3.12). The ECD calculations were conducted using the TDDFT method at the B3LYP/6-311G+(d) level in the gas phase. The good agreement of this comparison was successfully determined the absolute configuration of **21** to be 3*R*,4*R*,5*R*,6*R*,7*R*,11*S*,12*R* (Fig. 3.13) and **21** was thus named as fusopoltide C.

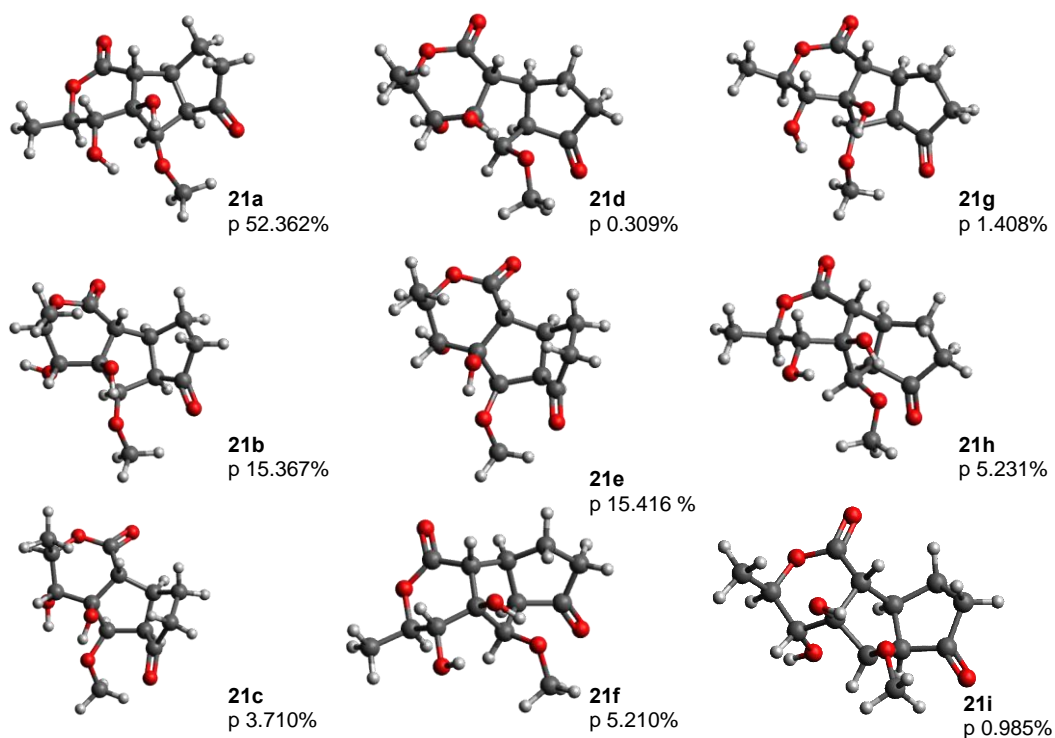


Figure 3.12 Populations and B3LYP/611G+(d) optimized lowest energy 3D conformers of **21**.

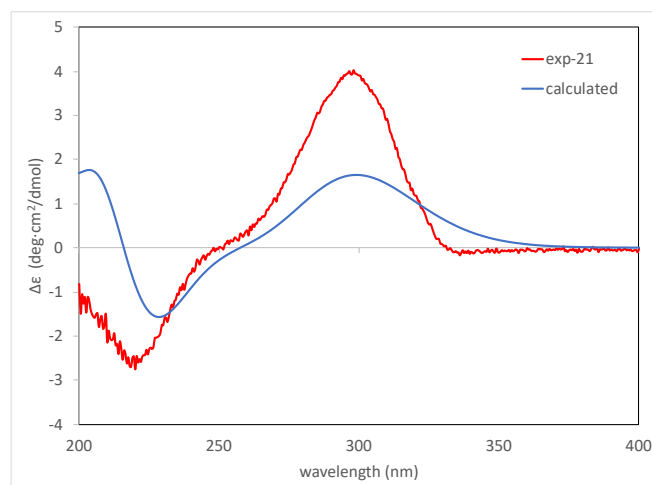


Figure 3.13 Experimental and calculated ECD spectra of **21**.

The close similarity of NMR data between **20** (Table 3.4) and **22** (Table 3.5) suggested they have similar structures. The molecular formula of **22** was also the same as that of **20** ($C_{13}H_{16}O_5$, m/z 275.0895 $[M + Na]^+$, calcd. for $C_{13}H_{16}O_5Na$, 275.0895). The significant differences between **20** and **22** were notably that by ^{13}C NMR, δ_c 80.6 (C-3), 66.1 (C-4), and 156.9 (C-5) in **20** were shifted to δ_c 67.3 (C-3), 82.8 (C-4), and 171.6 (C-5) in **22**, corresponding to a different lactone ring arrangement. This deduction was supported by the key HMBC correlation from H-4 to C-1 (Fig. 3.9), which indicated that a five-membered lactone ring is present in the structure of **22**, rather than a six-membered lactone ring. Thus, the structure of **22** was confirmed to be a pentaleno[1,2-*c*]furan ring. The attachments of 2-hydroxy-ethyl group at C-4 and a methoxy group at C-6 were determined based on the 1H - 1H COSY spin system between H-4/H-3/H-13 and the HMBC correlation from H-14 to C-6, respectively.

Next, the relative configuration of **22** was also determined using NOE experiments (Fig. 3.10). The irradiation at δ_H 3.52 (H-7) enhanced signal of H-11, indicating a *cis*-configuration between H-7 and H-11. Furthermore, irradiation at δ_H 4.87 (H-6) only enhanced signals of H-3 and H-7, suggesting these all protons are co-facial while the configuration between H-6 and H-4 is anti-facial. The flexible rotating bond at C-3 was deduced to be $3S^*$ configuration, based on NOE enhancement percentages between H-13 and H-6/H-4/H-3 (Fig. 3.9). The absolute configurations at C-4, C-6, C-7, and C-11 in **22** were determined by comparison of the experimental ECD curve and the calculated ECD curve with the truncated

model (4*S*,6*R*,7*R*,11*S*)-**22a**, using TDDFT at the B3LYP/6-311G+(d) level. Both curves showed the good agreement (Fig. 3.14). Finally, the absolute configuration of C-3 was determined using the modified Mosher's ester (Fig. 3.11) to be 3*S*. Thus, the absolute configuration of **22** was determined as 3*S*,4*R*,6*R*,7*R*,11*S* (Fig. 3.8), and the compound was named fusopoltide D.

Table 3.5 ¹³C NMR (150 MHz) and ¹H NMR (600 MHz) spectral data for **22** and **23** (in CDCl₃).

Pos.	22	δ_{H} , mult. (<i>J</i> in Hz)	23	δ_{H} , mult. (<i>J</i> in Hz)
	δ_{C} , type		δ_{C} , type	
1	167.9, C		167.2, C	
3	67.3, CH	4.15, m	68.7, CH	3.61, m
4	82.8, CH	4.97, d (4.8)	83.9, CH	4.64, dd (8.4, 1.8)
5	171.6, C		171.1, C	
6	82.5, CH	4.87, d (8.4)	82.1, CH	4.90, dt (8.4, 1.8)
7	57.9, CH	3.52, t (8.4)	57.4, CH	3.54, t (8.4)
8	214.1, C		213.2, C	
9	38.2, CH ₂	1.98, m	37.8, CH ₂	2.22, m
		2.21, m		2.26, m
10	23.1, CH ₂	2.28, m	22.8, CH ₂	1.97, m
		2.29, m		2.25, m
11	40.1, CH	3.64, td (8.4, 1.2)	40.0, CH	3.68, td (8.4, 2.4)
12	140.3, C		140.8, C	
13	18.5, CH ₃	1.32, d (6.0)	19.5, CH ₃	1.38, d (6.0)
14	59.9, OCH ₃	3.53, s	60.1, OCH ₃	3.62, s
3-OH		2.13, d (4.8)		4.03, d (3.6)

Compound **23** was isolated as a yellowish oil. Extensive analyses of its 1D/2D NMR data showed that **23** has the same planar structure as **22** (Fig. 3.9), supported by the same molecular formula from HRESITOFMS (C₁₃H₁₆O₅). A distinct difference was observed in the ¹H NMR chemical shifts (Table 3.3) as well as the coupling constants, (³*J*_{H4-H3}) at δ_{H} 4.15 (m, H-3) and 4.97 (d, *J* = 4.8 Hz, H-4) in **7**, which were shifted to δ_{H} 3.61 (m, H-3) and 4.64 (dd, *J* = 8.4, 1.8 Hz, H-4), respectively, in **23**, indicating a different configuration in both positions. Long-range W-coupling was also observed between H-6 and H-4 (⁴*J*_{H4-H6} = 1.8 Hz) indicated both protons are co-facial; this deduction was also supported by NOE correlations from H-4 to H-6 (Fig. 3.10). The flexible rotating bond at C-3 was deduced to be 3*R*^{*} configuration, based on NOE enhancement percentages between H-13 and

H-4/H-3; unlike in **22**, no NOE correlation between H-13 and H-6 was observable in **8** (Fig. 3.10). The good agreement of the experimental ECD curve and the calculated ECD curve with the truncated model (4*R*,6*R*,7*R*,11*S*)-**23a** (Fig. 3.14) suggested that the absolute configuration of **23** is (4*S*,6*R*,7*R*,11*S*). The absolute configuration at C-3 is remains undetermined due to it only being present in trace quantities. From its relative configuration and biosynthetic pathway (Scheme 3.2), the configuration at C-3 was assumed to be (*R*)-form, as described later. Accordingly, **23** is a C-3 and C-4 diastereomer of **7** (Fig. 3.8) and was named fusopoltide E.

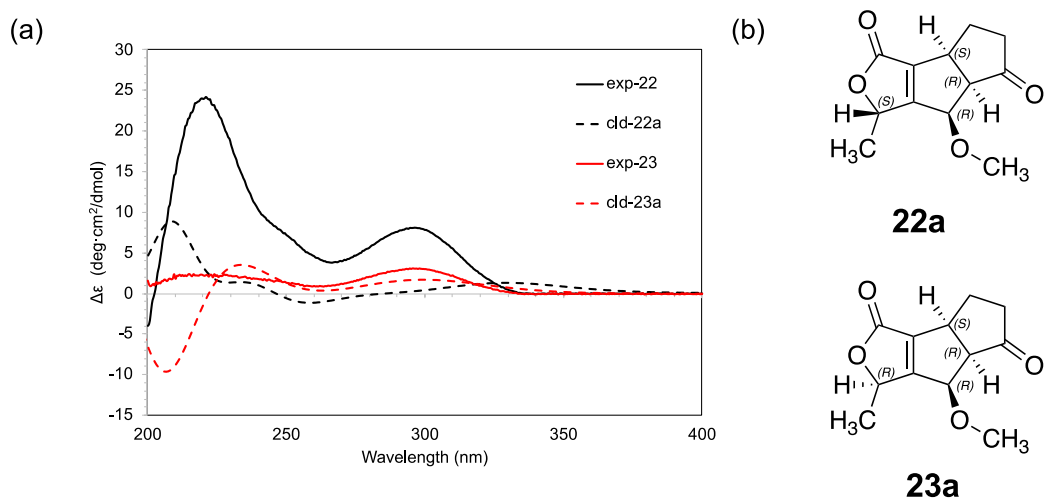
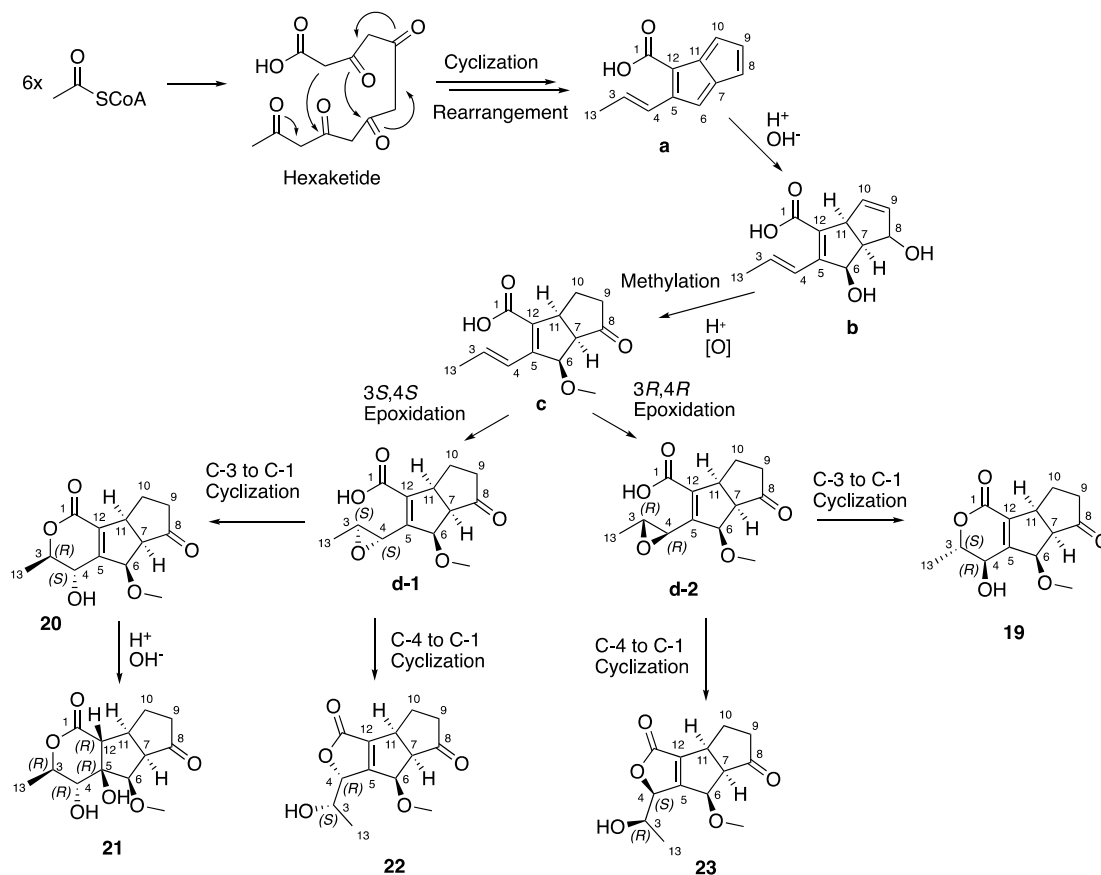


Figure 3.14 (a) experimental and calculated ECD spectra of **22**, **22a**, **23** and **23a**, and (b) structures of truncated model of **22a** and **23a**.

Compound **19**, as previously reported by Zhang's group⁹², is the first example of a polyketide bearing a unique pentaleno[1,2-*c*]pyran ring system; this was followed by Dai's group, who isolated a C-4 epimer of **19**, pysarone A.¹⁰⁰ Here, we reported the isolation of a new C-3 and C-4 diastereomer (**20**) of **19**, and three new derivatives which are bearing unique decahydro-pentaleno[1,2-*c*]pyran (**21**) and pentaleno[1,2-*c*]furan (**22**, **23**) ring systems. The diversity of their stereochemistry can be explained by the proposed biosynthetic pathway shown in Scheme 3.2. It is possible that **19–23** are biosynthesized from a hexaketide precursor¹⁰¹, followed by cyclization, rearrangement, oxidation, and methylation, to formed the key

intermediate, **c**. These processes initiated the same configuration in the positions C-6, C-7, and C-11 of **19–23**. Next, two different types of epoxidation of intermediate **c** resulted in **d-1** (3*S*,4*S*) and **d-2** (3*R*,4*R*), followed by two different types of cyclization resulting in the formation of pyran (**19**, **20**) and furan (**22**, **23**) ring systems. The hydration reaction of the double bond (C-5 and C-12) in **20** was finally resulted the formation of **21**.

None of **16–23** exhibited any growth inhibition (100 µg/disk) when tested against *S. aureus* NBRC 13276, *P. aeruginosa* ATCC 15442, *C. albicans* ATCC 2019, or *A. clavatus* F318a. Similarly, none of **16–23** were cytotoxic towards HL60 cells line.



Scheme 3.2 The proposed biosynthetic pathway of compounds **19–23**.

Chapter 4 Metabolites from *Colletotrichum boninense* AM-12-2

4.1 Introduction

Fungal strain AM-12-2 was isolated from inner tissue of *Acacia mangium*, and subsequently identified as *Colletotrichum boninense*. *Colletotrichum* species have been known as anthracnose pathogen and endophyte of diverse range host plants.¹⁰² This species is also a rich source of various active metabolites with unique structures, including hybrid peptide-polyketide¹⁰³, glycosylated cyclic lipodepsipeptides¹⁰⁴, and diterpenoids.¹⁰⁵

Separation of the EtOAc extract derived from the brown rice culture of fungal strain *C. boninense* AM-12-2, led to the identification of seven new compounds, including colletofurans A–E (**26–30**). These compounds are first example of natural product featured with 1-octyl-1,3-dihydroisobenzofuran core. We evaluate the bioactivity of this new core, against important agricultural pest, aphids.

4.2 Material and methods

4.2.1 Fungal material and fermentation

The fungal strain AM-12-2 was isolated from inner tissue of *Acacia mangium* collected in the Merapi Mt. area (southern latitude 7°35'16", east longitude 110°27'28"), Yogyakarta, Indonesia. This strain was identified as *C. boninense* using DNA analysis of the 18S rRNA regions, GenBank: LC511737. This fungus was deposited at our laboratory in the Faculty of Agriculture, Yamagata University. *C. boninense* AM-12-2 was cultivated on sterilized brown rice (120 g in 22 flasks) at 25 °C for four weeks.

4.2.2 Extraction and isolation

The moldy media were extracted using MeOH, and the MeOH extract was concentrated. The resulting aqueous concentrate was partitioned into EtOAc. The separation of the EtOAc layer was guided by intense characteristic coloration with vanillin-sulfuric acid solution on TLC plates. The EtOAc layer (29.59 g) was chromatographed on a silica gel column using 10% stepwise of *n*-hexane-EtOAc (100:0-0:100), then a mixture of EtOAc-MeOH (50:50), and finally MeOH to give 13 fractions (Fr. 1-1 to 1-13). Fractions 1-10 and 1-11 (3.279 g) were combined

and re-chromatographed on a silica gel column using 10% stepwise of CHCl₃-EtOAc (100:0-0:100) to afford 11 fractions (Fr. 1-10-1 to 1-10-11). Fractions 1-10-8 and 1-10-11 were combined (2.375 g) and subjected on an ODS column using 10% stepwise of H₂O and MeOH (100:0-0:100) to afford 11 fractions (1-10-8-1 to 1-10-8-11). Fractions 1-10-8-7 and 1-10-8-8 were combined (0.982 mg) and was subjected to flash column chromatography (isocratic, CHCl₃-MeOH;150:3) to obtained fraction 1-10-8-7-1 (135 mg). This fraction was further subjected to RP-HPLC using Develosil C30-UG-5 column (*Nomura Chemical*, Tokyo) and using isocratic solvent system (MeOH-H₂O, 7:3, 3 mL/min) to afford **27** (*t_R* 9.4 min, 20 mg), **28** (*t_R* 8.7 min, 23 mg), **29** (*t_R* 11.5 min, 10 mg), and **30** (*t_R* 10.3 min, 9 mg). Fractions 1-6 and 1-7 were combined and a powder was present in the mixture, the powder was then filtered to afford residue 1-6a (56 mg) and filtrate 1-6b (2,777 g). The residue 1-6a was then applied to RP-HPLC (Develosil, gradient system MeOH-H₂O, 20 min 20-100%, 5 min 100-20%, 1 mL/min) to afford **24** (*t_R* 10 min, 5 mg) and **25** (*t_R* 15 min, 7 mg). The filtrate 1-6b was subjected to a silica gel column using 10% stepwise of CHCl₃-EtOAc (100:0-0:100, each 50 mL) to afford 11 fractions (Fr. 1-6b-1 to 1-6b-11). Fractions 1-6b-4 to 1-6b-6 were combined (1.316 g) and subjected on ODS using 10% stepwise of H₂O and MeOH (100:0-0:100, each 60 mL) to afford 11 fractions (1-6b-4-1 to 1-6b-4-11). Fractions 1-6b-4-7 and 1-6b-4-8 were combined (283 mg) and was subjected to a silica gel column using 10% stepwise of CHCl₃-EtOAc (100:0-0:100, each 40 mL) to afford 11 fractions (Fr. 1-6b-4-7-1 to 1-6b-4-7-11). Fractions 1-6b-4-7-6 and 1-6b-4-7-7 were combined (259 mg) and was subjected to a flash chromatography (isocratic, CHCl₃-MeOH, 150:3) to obtained fraction 1-6b-4-7-6-1. This fraction was then subjected to RP-HPLC (Develosil, gradient system MeOH-H₂O, 15 min 70-80%, 1 min 80-70%, 1 mL/min) to afford **26** (*t_R* 7.9 min, 8 mg).

4.2.3 Preparation of MTPA ester derivatives for **26**

To **26** (1.0 mg) in dry pyridine were added (*R*)-(-)-MTPACl (10 μL), the mixture was stirred at room temperature for 24 h. Purification by column chromatography was performed on a silica gel column (*n*-hexane: EtOAc) to afford the (*S*)-MTPA ester (**26a**, 0.7 mg). Compound **26** (1.0 mg) was treated with (*S*)-(+)-MTPACl (10 μL) in the same procedure to afford the (*R*)-MTPA ester (**26b**, 0.8 mg).

26a: $^1\text{H-NMR}$ (600 MHz, CDCl_3) δ_{H} 6.91 (d, $J = 7.8$ Hz, H-4), 6.99 (t, $J = 7.8$ Hz, H-5), 7.30 (d, $J = 7.8$ Hz, H-6), 4.13 (d, ($J = 13.2$ Hz, H-9a), 4.75 (d, $J = 13.2$ Hz, H-9b), 5.62 (d, $J = 7.2$ Hz, H-10), 4.29 (t, $J = 6.0$ Hz, H-11), 5.34 (dd, $J = 7.2$, 1.8 Hz, H-12), 1.72 (m, H-13), 1.42 (m, H-14), 1.30-1.31 (m, H-15 and H-16, overlapped), 0.86 (t, $J = 6.0$ Hz, H-17), 3.50 (s, OMe of MTPA), 3.60 (s, OMe of MTPA), 7.26-7.52 (Ph of MTPA).

26b: $^1\text{H-NMR}$ (600 MHz, CDCl_3) δ_{H} 7.16 (d, $J = 8.4$ Hz, H-4), 7.43 (t, $J = 8.4$ Hz, H-5), 7.28 (d, $J = 8.4$ Hz, H-6), 4.66 (d, $J = 13.2$ Hz, H-9a), 4.95 (d, $J = 13.2$ Hz, H-9b), 5.65 (d, $J = 6.0$ Hz, H-10), 4.18 (t, $J = 5.4$ Hz, H-11), 5.27 (dd, $J = 6.6$, 3.6 Hz, H-12), 1.63 (q, $J = 7.8$ Hz, H-13), 1.28 (m, H-14), 1.22-1.23 (m, H-15 and H-16, overlapped), 0.82 (t, $J = 6.6$ Hz, H-17), 3.53 (s, OMe of MTPA), 3.61 (s, OMe of MTPA), 7.25-7.48 (Ph of MTPA).

4.2.4 Preparation of MTPA ester derivatives for **27**

To **27** (1 mg) in dichloromethane (1 mL) were added 4,4-dimethylaminopyridine (16 mg), N,N' -dicyclohexylcarbodiimide (16 mg), and (*S*)-MTPA (24 mg). The mixture was kept for 2 hours at room temperature and was then dried under vacuum to yield crude product. The crude product was subjected to RP-HPLC (Develosil, isocratic MeOH- H_2O , 9:1, 3 mL/min) to afford (*S*)-MTPA ester (**27a**, 0.5 mg). Using the same procedure, **27** was treated with (*R*)-MTPA to afford (*R*)-MTPA ester (**27b**, 0.6 mg).

27a: $^1\text{H-NMR}$ (600 MHz, CDCl_3) δ_{H} 6.91 (d, $J = 7.2$ Hz, H-4), 7.21 (t, $J = 7.2$ Hz, H-5), 6.83 (d, $J = 7.8$ Hz, H-6), 4.83 (s, H-9), 3.22 (d, $J = 1.8$ Hz, H-10), 3.14 (dd, $J = 6.6$, 1.8 Hz, H-11), 4.93 (q, $J = 6.6$ Hz, H-12), 1.63 (m, H-13), 1.37 (m, H-14), 1.27 (m, H-15 and H-16, overlapped), 0.86 (t, $J = 7.2$ Hz, H-17), 3.01 (s, H-18), 4.24 (dd, $J = 10.2$, 7.2 Hz, H-20a), 4.36 (dd, $J = 10.2$, 2.4 Hz, H-20b), 5.38 (dd, $J = 7.8$, 2.4 Hz, H-21), 1.27 (s, H-23), 1.22 (s, H-24), 3.52 (s, OMe of MTPA), 3.54 (s, OMe of MTPA), 7.28-7.54 (Ph of MTPA).

27b: $^1\text{H-NMR}$ (600 MHz, CDCl_3) δ_{H} 6.95 (d, $J = 7.2$ Hz, H-4), 7.31 (t, $J = 7.8$ Hz, H-5), 6.78 (d, $J = 7.8$ Hz, H-6), 4.84 (d, $J = 13.2$ Hz, H-9a), 4.95 (d, $J = 13.2$ Hz, H-9b), 3.34 (d, $J = 1.2$ Hz, H-10), 3.19 (dd, $J = 7.2$, 1.8 Hz, H-11), 4.86 (q, $J = 6.6$ Hz, H-12), 1.59 (m, H-13), 1.31 (m, H-14), 1.19 (m, H-15 and H-16, overlapped), 0.83 (t, $J = 6.6$ Hz, H-17), 3.00 (s, H-18), 4.14 (dd, $J = 10.2$, 7.8 Hz, H-20a), 4.28 (dd, J

= 10.2, 3.6 Hz, H-20b), 5.32 (dd, J = 7.8, 3.6 Hz, H-21), 1.28 (s, H-23), 1.23 (s, H-24), 3.48 (s, OMe of MTPA), 3.56 (s, OMe of MTPA), 7.34-7.53 (Ph of MTPA).

4.2.5 Preparation of MTPA ester derivatives for **28**

Using the same procedure as that described for **27**, **28** (1.0 mg and 1.0 mg) was treated with (*S*)-MTPA and (*R*)-(MTPA) to respectively afford (*S*)-MTPA ester (**28a**, 0.8 mg) and (*R*)-MTPA (**28b**, 0.6 mg).

28a: $^1\text{H-NMR}$ (600 MHz, CDCl_3) δ_{H} 6.91 (d, J = 7.2 Hz, H-4), 7.20 (t, J = 7.2 Hz, H-5), 6.81 (d, J = 7.2 Hz, H-6), 4.81 (s, H-9), 3.22 (d, J = 1.8 Hz, H-10), 2.99 (dd, J = 9.0, 7.8 Hz, H-11), 4.92 (q, J = 7.2 Hz, H-12), 1.69 (m, H-13), 1.38 (m, H-14), 1.28 (m, H-15 and H-16, overlapped), 0.85 (t, J = 7.2 Hz, H-17), 3.13 (dd, J = 7.2, 2.4 Hz, H-18a), 3.32 (dd, J = 9.0, 7.2 Hz, H-18b), 1.10 (t, J = 7.2, H-19), 4.25 (dd, J = 10.2, 7.2 Hz, H-20a), 4.36 (dd, J = 10.2, 2.4 Hz, H-20b), 5.38 (dd, J = 8.4, 2.4 Hz, H-21), 1.26 (s, H-23), 1.22 (s, H-24), 3.52 (s, OMe of MTPA), 3.53 (s, OMe of MTPA), 7.27-7.40, (Ph of MTPA).

28b: $^1\text{H-NMR}$ (600 MHz, CDCl_3) δ_{H} 6.94 (d, J = 7.8 Hz, H-4), 7.27 (t, J = 7.8 Hz, H-5), 6.88 (d, J = 7.8 Hz, H-6), 4.78 (d, J = 13.2 Hz, H-9a), 4.96 (d, J = 13.2 Hz, H-9b), 3.23 (d, J = 1.8 Hz, H-10), 3.03 (dd, J = 9.0, 6.6 Hz, H-11), 4.79 (q, J = 6.6 Hz, H-12), 1.41 (m, H-13), 1.25 (m, H-14), 1.12 (m, H-15 and H-16, overlapped), 0.77 (t, J = 6.6 Hz, H-17), 3.20 (dd, J = 7.8, 2.4 Hz, H-18a), 3.36 (dd, J = 9.0, 7.8 Hz, H-18b), 1.08 (t, J = 7.2 Hz, H-19), 3.92 (dd, J = 10.8, 7.2 Hz, H-20a), 4.08 (dd, J = 10.8, 2.4 Hz, H-20b), 5.48 (dd, J = 7.8, 3.0 Hz, H-21), 1.67 (s, H-23), 1.24 (s, H-24), 3.35 (s, OMe of MTPA), 3.47 (s, OMe of MTPA), 7.29-7.53 (Ph of MTPA).

4.2.6 NMR calculation for **26**

The initial conformational search for **26** were performed in the GMMX program (GMMX Gaussian Software) using the MMFF94 force field.⁸⁰ Conformations were kept in a 3.5 kcal mol⁻¹ window. The force field minimum energy conformers suitably obtained were subsequently optimized by applying the density functional theory (DFT) with the B3LYP/6-31G (d) level, in gas phase, implemented in the Gaussian 16 software package. Harmonic vibrational frequencies were also performed to confirm no imaginary frequencies of the finally optimized conformers. Magnetic shielding tensors from the B3LYP/6-31G(d)-optimized structures were

calculated with the gauge-invariant atomic orbital (GIAO) method using ω B97XD/631G(d) level of theory. Solvation modeling in chloroform for NMR computation was achieved using the integral equation formalism of the polarizable continuum method (IEF-PCM). Isotropic shielding values obtained from the computation were referenced to the carbon isotropic shielding values of tetramethylsilane (TMS) computed at the same level of theory. The ^{13}C NMR values were Boltzmann-weighted according to its relative Gibbs energy. All quantum mechanical NMR calculations were carried out using the Gaussian 16 program.

4.2.7 Preparation of X-ray crystalline sponge for **27–30**

Preparation of the crystalline sponge complex with **27**: a single crystal of the porous complex $[(\text{ZnI}_2)_2(\text{tpt})_3 \cdot x(\text{solvent})]_n$ (crystalline sponge **31**, tpt = 1,3,5-tris(4-pyridyl)triazine)¹⁰⁶, submerged in, cyclohexane (45 μL) in a small vial, was treated with cyclohexane solution (10 μL) of **27** (1 $\mu\text{g}/\mu\text{L}$, 10 μg) for 2 d at 50 $^\circ\text{C}$ and 9 d at 4 $^\circ\text{C}$ for the uptake of **27** into the pores of **31**.

X-ray crystal structure analysis: all crystal structures were solved using the program *SHELXT* ver. 2014/5 and refined using the program *SHELXL* ver. 2014/7. All non-hydrogen atoms were refined anisotropically. All hydrogen atoms were generated using the proper HFIX command and refined isotropically using the riding model. The solvent cyclohexane molecules suggested in the electron density map were refined using some restraints (DFIX, DANG, SIMU, and ISOR), because the corresponding electron densities were obscured due to their thermal motion and disorder. Short intermolecular interactions were detected by the HTAB command. Using the same procedure as that described for **27**, **28–30** were treated using the same method for the determination of the absolute configuration. The details procedures of X-ray crystalline sponge in this chapter, will be described/published elsewhere.

4.2.8 Insecticidal assay

The insecticidal activities of **26–30** against *Aphis gossypii* (Glover) and *Myzus persicae* (Sulzer), were evaluated by feeding chamber assay.¹⁰⁷ The assay was done in an air-conditioned room at 25 ± 2 $^\circ\text{C}$. Each tested sample was dissolved

in methanol at a concentration of 1000 µg/mL and diluted with distilled water containing 0.1% Tween-80 to obtain a required concentration. For comparative purposes, the positive control (milbemectin) and negative control (distilled water containing 0.1% Tween-80) were tested under the same conditions. Each experiment used 10 of *A. gossypii* or *M. persicae*, placed in the plastic tube (3.5×1 cm) using fine paintbrush, then a single sheet of Parafilm was stretched across open end of the tube. The Parafilm then was pressed using a gloved finger to make a depression. The test solution (20 µL) was pipetted onto the surface of the first Parafilm. The second Parafilm was stretched and carefully laid over the liquid. The second parafilm was then wrapped onto the sides of the tube, trapping the liquid between the two sheets. The mortalities were evaluated 24 h after treatment in two independent replicates. The LC₅₀ values were obtained using probit model on the SPSS program (version 23). The insects were provided by Sumika Techno Service Co., Ltd. (Japan).

4.3 Physicochemical properties

4.3.1 3-(3-hydroxy-2-(hydroxymethyl)phenyl)propanoic acid (24)

White powder; UV (MeOH) λ_{\max} (log ϵ) 216 (4.46), 224 (3.76), 280 (3.36) nm; IR (KBr) ν_{\max} 3417, 2935, 1712, 1643, 1469 cm⁻¹; ¹H-NMR (600 MHz, CDCl₃) and ¹³C-NMR (150 MHz, CDCl₃) data, see Table 4.1; HRESITOFMS (negative ion mode) m/z 195.0656 ([M - H]⁻, calcd. for C₁₀H₁₁O₄, 195.0658).

4.3.2 2-hydroxymethyl-3-hydroxy-(*E*)-cinnamic acid (25)

White powder: UV (MeOH) λ_{\max} (log ϵ) 217 (4.49), 236 (3.99), 279 (4.03) nm; IR (KBr) ν_{\max} 3417, 2923, 1689, 1623, 1469 cm⁻¹; ¹H-NMR (600 MHz, CDCl₃) and ¹³C-NMR (150 MHz, CDCl₃) data, see Table 4.1; HRESITOFMS (positive ion mode) m/z 217.0474 ([M + Na]⁺, calcd. for C₁₀H₁₀NaO₄, 217.0477).

4.3.3 Colletofuran A (26)

Yellowish oil; [α]_D²³ +14 (c 0.1, MeOH); UV (MeOH) λ_{\max} (log ϵ) 215 (4.62), 224 (3.62), 277 (3.08) nm; IR (KBr) ν_{\max} 3432, 2931, 1639, 1473 cm⁻¹; ¹H-NMR (600 MHz, CDCl₃) and ¹³C-NMR (150 MHz, CDCl₃) data, see Table 4.2; HRESITOFMS (positive ion mode) m/z 317.1368 ([M + Na]⁺, calcd. for C₁₆H₂₂O₅Na, 317.1365).

4.3.4 Colletofuran B (27)

Colorless oil; $[\alpha]_D^{25} +7$ (c 0.1, MeOH); UV (MeOH) λ_{\max} (log ϵ) 215 (4.24), 223 (4.16), 276 (3.44) nm; IR (KBr) ν_{\max} 3432, 2931, 1604, 1465 cm^{-1} ; ^1H -NMR (600 MHz, CDCl_3) and ^{13}C -NMR (150 MHz, CDCl_3) data, see Table 4.3; HRESITOFMS (positive ion mode) m/z 433.2203 ($[\text{M} + \text{Na}]^+$, calcd. for $\text{C}_{22}\text{H}_{34}\text{O}_7\text{Na}$, 433.2201).

4.3.5 Colletofuran C (28)

Colorless oil; $[\alpha]_D^{25} +3$ (c 0.1, MeOH); UV (MeOH) λ_{\max} (log ϵ) 215 (4.20), 222 (4.02), 276 (3.28) nm; IR (KBr) ν_{\max} 3421, 2931, 1604, 1465 cm^{-1} ; ^1H -NMR (600 MHz, CDCl_3) and ^{13}C -NMR (150 MHz, CDCl_3) data, see Table 4.3; HRESITOFMS (positive ion mode) m/z 447.2357 ($[\text{M} + \text{Na}]^+$, calcd. for $\text{C}_{23}\text{H}_{36}\text{O}_7\text{Na}$, 447.2358).

4.3.6 Colletofuran D (29)

Colorless oil; $[\alpha]_D^{25} -25$ (c 0.1, MeOH); UV (MeOH) λ_{\max} (log ϵ) 216 (4.24), 223 (4.18), 276 (3.45) nm; IR (KBr) ν_{\max} 3432, 2931, 1604, 1465 cm^{-1} ; ^1H -NMR (600 MHz, CDCl_3) and ^{13}C -NMR (150 MHz, CDCl_3) data, see Table 4.3; HRESITOFMS (positive ion mode) m/z 433.2201 ($[\text{M} + \text{Na}]^+$, calcd. for $\text{C}_{22}\text{H}_{34}\text{O}_7\text{Na}$, 433.2201).

4.3.7 Colletofuran E (30)

Colorless oil; $[\alpha]_D^{25} -12$ (c 0.1, MeOH); UV (MeOH) λ_{\max} (log ϵ) 215 (4.27), 223 (4.23), 276 (3.49) nm; IR (KBr) ν_{\max} 3421, 2935, 1604, 1465 cm^{-1} ; ^1H -NMR (600 MHz, CDCl_3) and ^{13}C -NMR (150 MHz, CDCl_3) data, see Table 4.3; HRESITOFMS (positive ion mode) m/z 447.2256 ($[\text{M} + \text{Na}]^+$, calcd. for $\text{C}_{23}\text{H}_{36}\text{O}_7\text{Na}$, 447.2358).

4.4 Results and Discussion

All compounds (Fig. 4.1) were isolated using various steps of chromatographic separations. Their planar structures were determined mainly by HRESITOFMS and 1D/2D NMR analyses. The absolute configurations of secondary alcohols on **26–28** were established using the modified Mosher's ester method. The absolute configurations of **27–30** were further verified using the X-ray crystalline sponge.

Compound **24** was isolated as a white powder. Its molecular formula was determined to be $\text{C}_{10}\text{H}_{12}\text{O}_4$ (five degrees of unsaturation), through a combination of HRESITOFMS (m/z 195.0656 $[\text{M} - \text{H}]^-$) and NMR data. The ^{13}C NMR (Table

4.1) spectrum confirmed the presence of 10 carbon resonances, including three methylenes [δ_{C} 28.9 (C-7), 36.9 (C-8), and 56.7 (C-10)]; three methines [δ_{C} 114.4 (C-4), 121.3 (C-6), and 129.8 (C-5)]; three quaternary carbons [δ_{C} 121.8 (C-2), 142.5 (C-1), and 157.6 (C-3)]; and a carbonyl [δ_{C} 176.9 (C-9)]. The ^1H NMR and HMQC data indicated the presence of three methylene protons [δ_{H} 2.57 (t, $J = 7.8$ Hz, H-7), 2.96 (t, $J = 7.8$ Hz, H-8), and 4.74 (s, H-10)], and three aromatic methine protons [δ_{H} 6.65 (d, $J = 7.8$ Hz, H-4), 6.69 (d, $J = 7.8$ Hz, H-6), and 7.01 (t, $J = 7.8$ Hz, H-5)]. The ^1H - ^1H COSY data (Fig. 4.2) showed a spin system from H-4/H-5/H-6, indicating the structure of **24** is contains a 1,2,3-trisubstituted benzene ring. Furthermore, COSY data also showed a cross peak between H-7/H-8, along with HMBC correlations (Fig. 4.2) from H-7 to C-1, C-2, C-6, C-8, and C-9, and from H-8 to C-1, C-7, and C-9, indicating the structure of **24** is also contains a propanoic acid moiety and attached to the benzene ring at C-1. The hydroxy methyl group was attached at C-2 based on HMBC correlation from H-10 to C-1, C-2, and C-3, and the remaining hydroxyl group was attached at C-3 based on its characteristic chemical shift for oxygenated aromatic carbon. Therefore, the structure of **24** was assigned as 3-(3-hydroxy-2-(hydroxymethyl)phenyl)propanoic acid (Fig. 4.1).

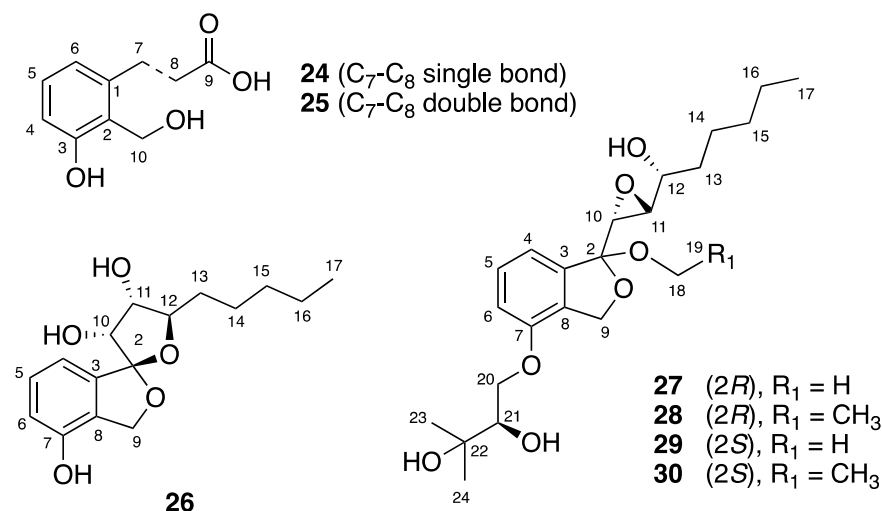


Figure 4.1 The structures of **24**–**30**.

Compound **25** was isolated as a white powder. Its molecular formula (m/z) was two mass units less than the molecular formula of **24**. A comparison of ^{13}C

and ^1H NMR spectral data of **24** and **25** (Table 4.1), revealed that they share similar structure, except for C-7 (δ_{C} 28.9) and C-8 (δ_{C} 36.9), in **24**, were shifted to sp^2 region at δ_{C} 144.1 (C-7) and 121.4 (C-8), in **25**, suggesting that **25** is an unsaturated form of **24** at C-7 and C-8. This deduction was supported by HMBC correlations (Fig. 2) from H-7 to C-1, C-2, C-6, and C-9, and from H-8 to C-1 and C-9. The *trans* geometry of double bond (Δ^7) was determined based on a large coupling constant ($^3J_{7-8} = 16.2$ Hz). Therefore, the structure of **25** was assigned as 2-hydroxymethyl-3-hydroxy-(*E*)-cinnamic acid (Fig. 4.1).

Table 4.1 ^{13}C NMR (150 MHz) and ^1H (600 MHz) spectral data of **24** and **25** (CD_3OD).

Pos.	24		25	
	δ_{C} , type	δ_{H} , mult. (<i>J</i> in Hz)	δ_{C} , type	δ_{H} , mult. (<i>J</i> in Hz)
1	142.5, C		136.8, C	
2	121.8, C		127.1, C	
3	157.6, C		157.6, C	
4	114.4, CH	6.65, d (7.8)	130.0, CH	7.14, d (5.4)
5	129.8, CH	7.01, t (7.8)	117.8, CH	6.85, dd (5.4, 3.0)
6	121.3, CH	6.69, d (7.8)	118.9, CH	7.15, d (3.0)
7	28.9, CH_2	2.57, t (7.8)	144.1, CH	8.11, d (16.2)
8	36.9, CH_2	2.96, t (7.8)	121.4, CH	6.37, d (16.2)
9	176.9, C		170.5, C	
10	56.7, CH_2	4.74, s	55.9, CH_2	4.81, s

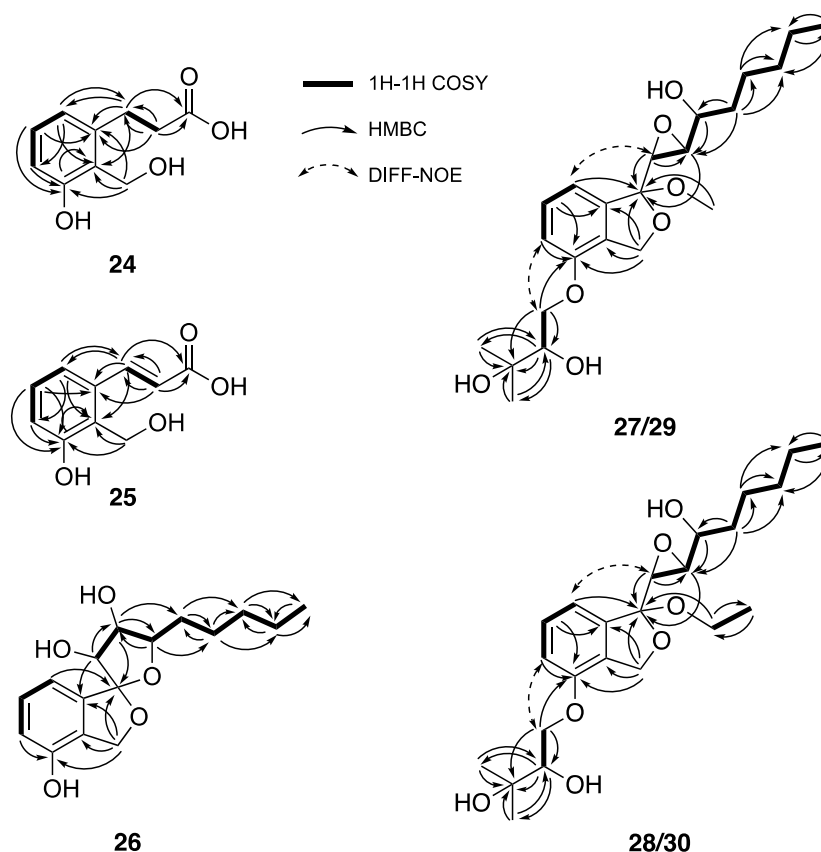


Figure 4.2 The ^1H – ^1H COSY, key HMBC, and key DIFF-NOE correlations of **24**–**30**.

Compound **26** was isolated as a yellowish oil. Its molecular formula was determined to be $\text{C}_{16}\text{H}_{22}\text{O}_5$ (six degrees of unsaturation) through a combination of HRESITOFMS (m/z 317.1368 $[\text{M} + \text{Na}]^+$) and NMR data. The ^{13}C NMR (Table 4.2) spectrum showed the presence of 16 carbon resonances, including one methyl, five methylenes, six methines, and four quaternary carbons. The ^1H NMR (Table 4.2) and HMQC data indicated the presence of three aromatic protons [δ_{H} 6.64 (d, $J = 7.8$ Hz, H-6), 6.83 (d, $J = 7.8$ Hz, H-4), and 7.16 (t, $J = 7.8$ Hz, H-5)], and COSY cross peaks from H-4/H-5/H-6, suggesting the structure of **26** is contained a 1,2,3-trisubstituted benzene. A methyl group [δ_{H} 0.87 (t, $J = 7.2$ Hz, H-17)]; four aliphatic methylene protons [δ_{H} 1.31–1.33 (m, H-15 and H-16), 1.42 (m, H-14), and 1.62 (q, $J = 7.2$ Hz, H-13)]; one oxygenated methylene [δ_{H} 5.04 (d, $J = 12.0$ Hz) and 5.19 (d, $J = 12.0$ Hz), H-9]; and three oxygenated methine protons [δ_{H} 3.92 (dd, $J = 6.0$, 1.8 Hz, H-11), 4.14 (td, $J = 7.2$, 1.8 Hz, H-12), and 4.27 (d, $J = 6.0$ Hz, H-10)] were

also observed in ^1H NMR spectrum of **26**. The oxygenated methylene was attached at C-8 based on HMBC correlations (Fig. 4.2) from H-9 to C-3, C-7, and C-8. Furthermore, the HMBC correlation from H-9 to C-2, constructed the dihydroisobenzofuran core in **26**. The hydroxyl group was attached to C-8 based on its characteristic chemical shift for oxygenated aromatic carbon. Additionally, the COSY data showed a spin system from H-10/H-11/H-12/H-13/H-14/H-15/H-16/H-17, indicating the structure of **26** contains an octyl side chain. This octyl side chain was attached at C-2 based on HMBC correlations from H-10 to C-2 and C-3, and from H-11 to C-2, as well as the NOE correlation from H-10 to H-4. Three oxygens were attached to C-10, C-11, and C-12, based on HMBC correlation of oxygenated methine protons, H-10 to C-11 and C-12, from H-11 to C-10, C-12, and C-13, and from H-12 to H-10, H-11, H-13, and H-14.

Based on the molecular formula of **26**, five unsaturated degrees were attributed to the presence of a dihydroisobenzofuran ring, to fulfil one more unsaturation degree, **26** must contain one more ring on its structure. Based on above discussion, it is likely that the structure of **26** contains oxetane moiety (C-2 to C-11) or tetrahydrofuran moiety (C-2 to C-12). To confirm the connectivity of the ether bond, we prepared the (*S/R*)-MTPA ester of **26**. Based on a comparison of ^1H NMR spectra of **26**, (*S*)-(**26a**), and (*R*)-MTPA ester (**26b**) (Fig. 4.3), H-10 and H-11 were shifted to downfield area, indicating two MTPA esters were attached to C-10 and C-11. Based on this result, we therefore concluded that the structure of **26** contains a tetrahydrofuran moiety with the ether bond at C-2 to C-12. Simultaneously, the absolute configuration of secondary alcohols at C-10 and C-11 were also determined using this method. From $\Delta\delta$ ($\delta_S - \delta_R$) values (Fig. 4.4) of the (*S/R*)-MTPA esters, the absolute configuration of C-10 and C-11 in **26** were determined to be 10*R*,11*S*. The remaining configuration at C-2 and C-12 of **26** were then determined based on diff-NOE experiments. The irradiation of δ_{H} 4.27 (H-10) enhanced the signals of H-3 and H-11, as well as the irradiation of δ_{H} 3.92 (H-11) enhanced the signals of H-10 and H-13, indicating these protons on tetrahydrofuran ring are co-facial and configuration of C-2 must be *R*. This also supported by coupling constants of $^3J_{\text{H}10-\text{H}11} = 6.0$ Hz and $^3J_{\text{H}11-\text{H}12} = 1.8$ Hz, indicating the dihedral angles approximately 60° and 90° for H-10–H-11 and H-11–H-12, respectively (Fig. 4.5.a).

Table 4.2 ¹³C NMR (150 MHz) and ¹H (600 MHz) spectral data of **26** (CDCl₃).

Pos	26	
	¹³ C, type	¹ H, m (J in Hz)
2	115.1, C	
3	138.3, C	
4	114.1, CH	6.83, d (7.8)
5	129.9, CH	7.16, t (7.8)
6	115.9, CH	6.64, d (7.8)
7	149.9, C	
8	126.6, C	
9	70.9, CH ₂	5.04, d (12.0) 5.19, d (12.0)
10	74.7, CH	4.27, d (6.0)
11	74.4, CH	3.92, dd (6.0, 1.8)
12	85.4, CH	4.14, td (7.2, 1.8)
13	34.1, CH ₂	1.62, q (7.2)
14	25.0, CH ₂	1.42, m
15	31.6, CH ₂	1.31-1.33, m
16	22.5, CH ₂	1.31-1.33, m
17	13.9, CH ₃	0.87, t (7.2)

To unambiguously determine the configurations of stereocenter on 1,6-dioxaspiro[4.4]nonane moiety, we also performed quantum mechanical calculations of ¹³C NMR chemical shifts of **26**, using DFT GIAO method at the ωB97XD/631G(d)CHCl₃//B3LYP/631G(d) level of theory, based on structure model from MTPA and NOE results. The calculated data agreed well with the experimental (Fig. 4.5.b) with the mean absolute error (MAE) 2.0 ppm, max error (ME) 3.7 ppm, and correlation coefficient (r^2) 0.9982. These data resulted in the configurations of 2*S*,10*R*,11*S*,12*R*. Therefore, the structure of **26** was assigned as shown in Fig. 4.1 and was named colletofuran A.

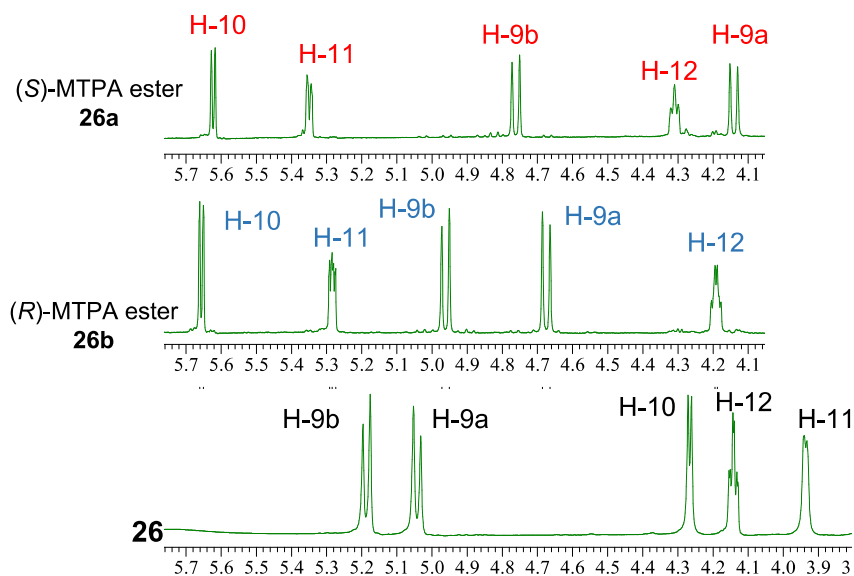


Figure 4.3 The comparison of ^1H NMR spectra of **26**, **26a**, and **26b** (CDCl_3) in ppm.

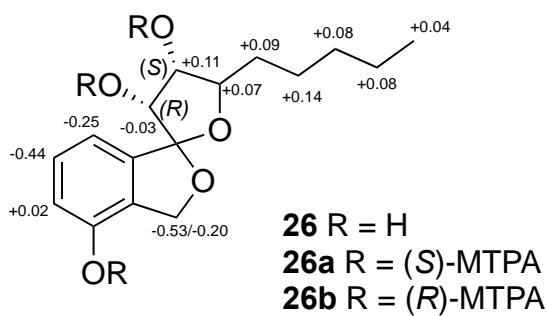


Figure 4.4 Chemical shift differences for (S)-MTPA ester (**26a**) and (R)-MTPA ester (**26b**) of **26** (in ppm).

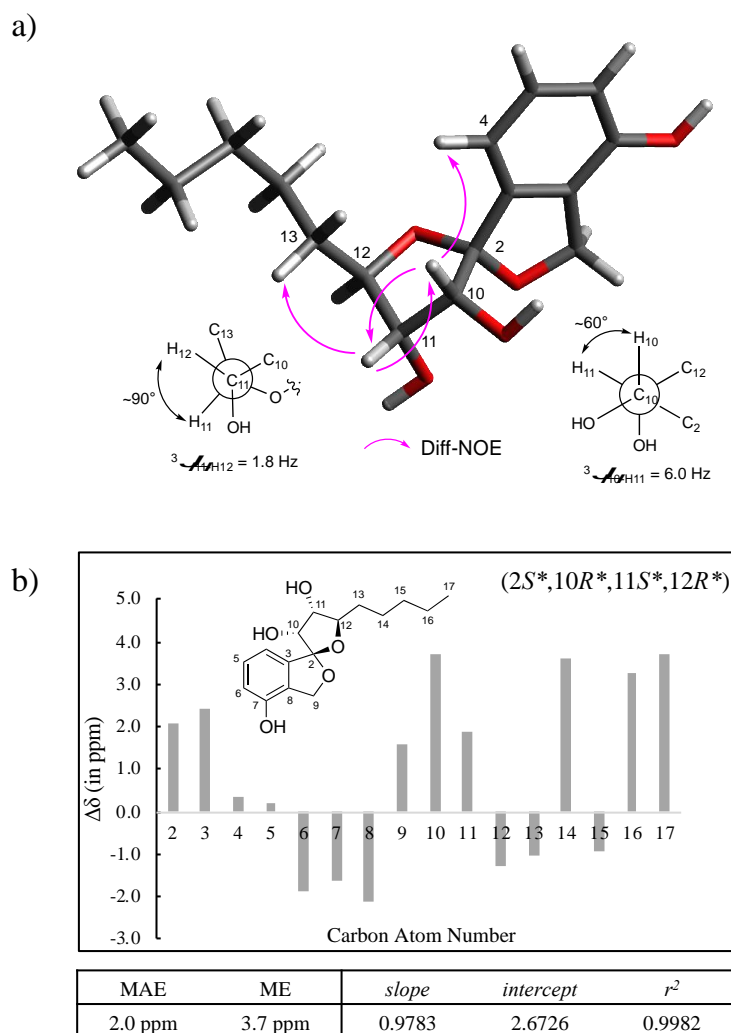


Figure 4.5 a) The key diff-NOE correlations of **26** and Newman projections of dihedral angles between H-10–H-11 and H-11–H-12; b) Comparison between calculated and observed ^{13}C NMR chemical shifts, MAE, ME, and correlation coefficient r^2 for the proposed stereochemical models of **26**. Slope, intercept, and r^2 values determined by least-squares linear regression between the calculated chemical shift and the experimental ^{13}C NMR.

Table 4.3 ¹³C NMR (150 MHz) and ¹H (600 MHz) spectral data of **27-30** (CDCl₃).

	27		28		29		30	
Pos	¹³ C, type	¹ H, m (<i>J</i> in Hz)	¹³ C, type	¹ H, m (<i>J</i> in Hz)	¹³ C, type	¹ H, m (<i>J</i> in Hz)	¹³ C, type	¹ H, m (<i>J</i> in Hz)
2	110.7, C		110.4, C		110.1, C		109.8, C	
3	128.6, C		128.4, C		128.5, C		128.3, C	
4	115.67, CH	7.01, d (7.8)	115.6, CH	6.95, d (7.8)	115.8, CH	7.01, d (7.8)	115.6, CH	6.94, d (7.8)
5	130.0, CH	7.35, t (7.8)	129.9, CH	7.26, t (7.8)	130.1, CH	7.35, t (8.4)	129.9, CH	7.26, t (7.8)
6	111.88, CH	6.89, d (8.4)	111.7, CH	6.80, d (7.8)	111.9, CH	6.90, d (7.8)	111.7, CH	6.82, d (7.8)
7	152.8, C		152.7, C		152.85, C		152.7, C	
8	137.3, C		138.0, C		137.5, C		138.1, C	
9	71.6, CH ₂	5.16, d (12.6)	71.2, CH ₂	5.07, d (12.6)	71.6, CH ₂	5.21, d (13.2)	71.2, CH ₂	5.11, d (12.6))
		5.02, d (12.6)		4.93, d (12.6)		5.10, d (13.2)		5.00, d (13.2)
10	58.0, CH	3.40, d (2.4)	58.7, CH	3.35, d (2.4)	58.9, CH	3.34, d (2.4)	59.0, CH	3.28, d (2.4)
11	58.5, CH	3.11, dd (4.8, 2.4)	58.5, CH	3.03, dd (4.8, 2.4)	58.0, CH	3.17, dd (4.2, 2.4)	58.0, CH	3.03, dd (4.8, 2.4)
12	70.6, CH	3.54, m	70.6, CH	3.56, m	70.3, CH	3.52, m	70.3, CH	3.51, m
13	34.4, CH ₂	1.57, m	34.5, CH ₂	1.50, m	34.5, CH ₂	1.54, m	34.4, CH ₂	1.47, m
14	24.8, CH ₂	1.42, m	24.8, CH ₂	1.40, m	24.8, CH ₂	1.39, m	24.7, CH ₂	1.33, m
15	31.7, CH ₂	1.29, m	31.7, CH ₂	1.23, m	31.7, CH ₂	1.26, m	31.6, CH ₂	1.19, m
16	22.5, CH ₂	1.29, m	22.5, CH ₂	1.23, m	22.5, CH ₂	1.26, m	22.4, CH ₂	1.19, m
17	13.9, CH ₃	0.88, t (7.2)	14.0, CH ₃	0.81, t (6.6)	13.9, CH ₃	0.86, t (6.6)	13.9, CH ₃	0.79, t (6.6)
18	50.1, OCH ₃	3.07, s	58.4, OCH ₂	3.36, m	50.24, OCH ₃	3.07, s	58.3, OCH ₂	3.37, m
19			15.3, CH ₃	3.03, m			15.1, CH ₃	3.00, m
				1.07, t (7.2)				1.06, t (7.2)
20	69.2, CH ₂	4.18, dd (9.6, 2.4)	69.1, CH ₂	4.10, dd (9.0, 2.4)	69.2, CH ₂	4.21, dd (9.6, 2.4)	69.1, CH ₂	4.13, dd (9.6, 3.6)
		4.09, dd (9.6, 7.8)		4.02, dd (9.6, 8.4)		4.10, dd (9.6, 7.8)		4.02, dd (9.0, 7.8)
21	75.7, CH	3.81, dd (7.8, 3.0)	75.7, CH	3.81, dd (7.2, 3.0)	75.7, CH	3.82, m	75.6, CH	3.81, dd (7.2, 3.0)
22	71.6, C		71.6, C		71.6, C		71.5, C	
23	26.6, CH ₃	1.32, s	26.6, CH ₃	1.25, s	26.6, CH ₃	1.34, s	26.5, CH ₃	1.21, s
24	24.8, CH ₃	1.27, s	24.8, CH ₃	1.20, s	24.8, CH ₃	1.29, s	24.8, CH ₃	1.26, s

Compound **27** was isolated as a colorless oil. Its molecular formula was determined to be C₂₂H₃₄O₇ by a combination of HRESITOFMS and NMR data, indicating six degrees of unsaturation. Extensive NMR data analyses (Table 4.3 and Fig. 4.2) revealed that **27** has the same 1-octyl-1,3-dihydroisobenzofuran core as in **26**. The ¹³C and ¹H NMR (Table 4.3) data of **27** showed additional resonances for a methylene [δ_C/δ_H 69.2/4.18 (dd, *J* = 9.6, 2.4 Hz) and 4.09, (dd, *J* = 9.6, 7.8 Hz), C-20]; a methine [δ_C/δ_H 75.7/3.81 (m), C-21]; two methyls [δ_C/δ_H 24.4/1.27 (s), C-24 and 26.6/1.32 (s), C-23]; a quaternary carbon [δ_C/δ_H 71.6]; and a methoxy group [δ_C/δ_H 50.1/3.07 (s)]. The COSY data showed a spin system from H-20/H-

21, along with HMBC correlations from H-23 to C-22 and C-21, from H-24 to C-22 and C-21, from H-21 to C-23, C-24, and C-22, and from H-20 to C-21 and C-22, construct a 2,3-dihydroxy-3-methylbutyloxy moiety. This moiety was attached at C-7, based on the HMBC correlation from H-20 to C-7 (Fig. 4.2). Furthermore, the methoxy group was attached at C-2, based on the HMBC correlation from H-18 to C-2. Based on this discussion, five unsaturated degrees were attributed to the presence of a dihydroisobenzofuran ring. The NMR chemical shift of oxygenated methines C-10 [δ_C/δ_H 58.0/3.40 (d, $J = 2.4$ Hz)] and C-11 [δ_C/δ_H 58.5/3.11 (dd, $J = 4.8, 2.4$ Hz)] are in characteristic lower chemical shift than C-12 [δ_C/δ_H 70.6/3.54 (m)], indicating an epoxy ring is presence in **27**, between C-10 and C-11, along with an alcohol group at C-12, and fulfil the last unsaturation degree.

Compound **27** has five stereocenters on its structure. Coupling constant values and NOE experiments were not provided certain conclusion about its relative configuration, due to flexible bonds. Thus, we prepared (*S*)- and (*R*)-MTPA ester of **27**, to determine the absolute configuration of secondary alcohols at C-12 and C-21. Based on $\Delta\delta$ ($\delta_S - \delta_R$) values (Fig. 4.6) the absolute configuration of C-12 and C-21 in **27** were determined to be 12*R*,21*R*. Next, we intended to determine the complete absolute configuration of **27**, the X-ray Bijvoet technique offers immediate access to data on molecular chirality, but **27** exists as an oil and is not appropriate for the prompt determination by this conventional technique. To the best of our knowledge, the crystalline sponge method is the only way to directly determine the absolute configuration of a compound without crystallization.^{108,109} A single crystal of the porous complex $[(ZnI_2)_2(tpt)_3 \cdot x(\text{solvent})]_n$ [crystalline sponge; tpt = tris(-pyridyl)-1,3,5-triazine]^{110,111} was treated with **27**. The guest-absorbed crystal was subjected to X-ray crystallographic data collection. The crystal structure of **27**/crystalline sponge complex was solved (Fig. 4.7). The absolute configuration of **27** was thus established as 2*R*,10*S*,11*R*,12*R*,21*R* based on the Flack (parsons) [0.171 (9)] parameters, supported above result from the modified Mosher's ester method. Thus, the structure of **27** was determined as shown in Fig. 4.1 and it was named colletofuran B. The possibility of **27** being an artifact on the attachment of methoxy group was avoided by re-isolation of compounds without involving MeOH.

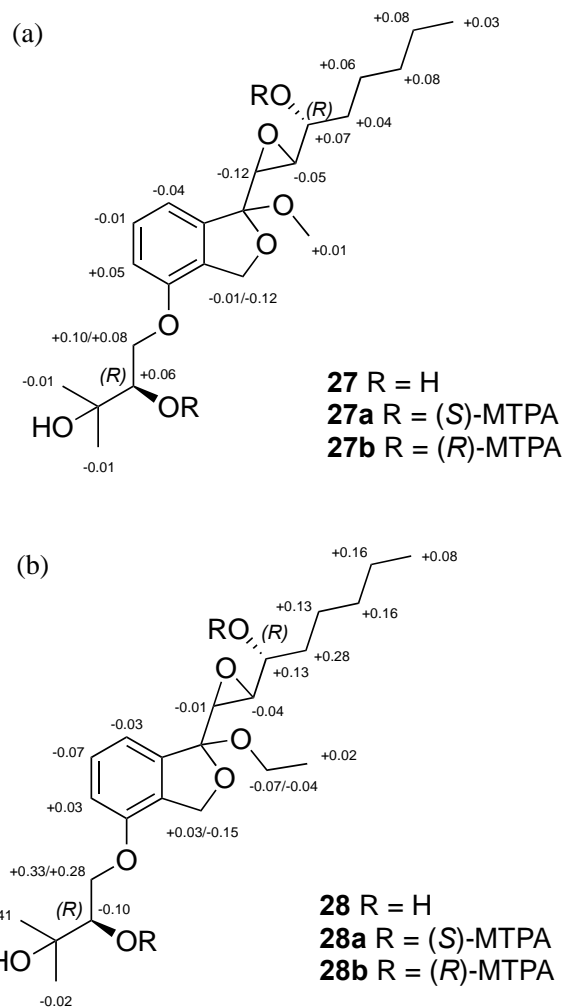


Figure 4.6 Chemical shift differences for a) (S)-MTPA ester (**26a**) and (R)-MTPA ester (**26b**) of **26**, b) chemical shift differences for (S)-MTPA ester (**27a**) and (R)-MTPA ester (**27b**) of **27**, and c) chemical shift differences for (S)-MTPA ester (**28a**) and (R)-MTPA ester (**28b**) of **28** (in ppm).

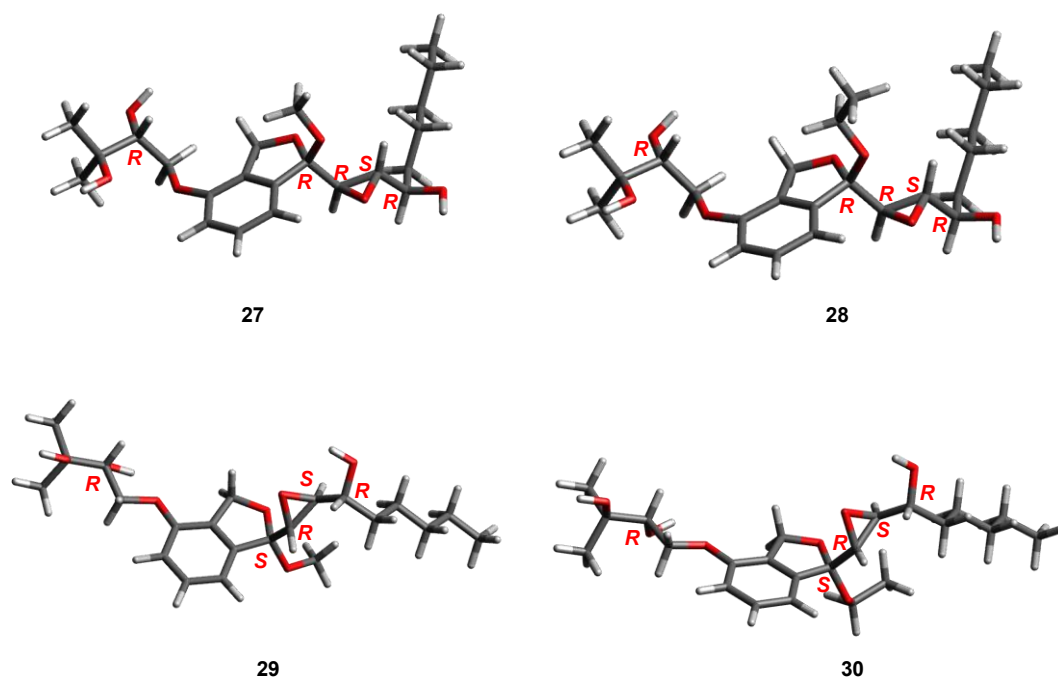


Figure 4.7 3D conformations model for guests **27–30**.

Compound **28** was isolated as a colorless oil. Its molecular formula was determined to be $C_{23}H_{36}O_7$, 14 mass units higher than **27**, based on HRESITOFMS data (m/z 447.2357, $[M + Na]^+$), indicating an additional methyl group was present in **28**. Extensive analysis of 1D/2D NMR revealed the structures of **27** and **28** are similar. A comparison of NMR data of **27** and **28** (Table 4.3) confirmed the additional methyl group [δ_C/δ_H 15.3/1.07 (t, $J = 7.24$ Hz), C-19] is present in **28**. Furthermore, the methoxy group in **27** [δ_C/δ_H 50.1/3.07 (s), C-18], was altered to be an oxygenated methylene in **28** [δ_C/δ_H 58.4/3.36 (m); 3.03 (m), C-18], indicating an ethoxy group was present in **28**, instead of a methoxy group. This deduction was supported by COSY cross peak of H-18/H-19 and HMBC correlation from H-18 to C-2 and C-19, and from H-19 to C-18. The absolute configuration of secondary alcohols at C-12 and C-21 was also determined using the modified Mosher's ester and confirmed these carbons have 12*R*,21*R* configurations. The complete absolute configuration of **28** was established as 2*R*,10*S*,11*R*,12*R*,21*R* [Flack (parsons), 0.201 (11)], using the crystalline sponge method (Fig. 4.7). Therefore, the structure of **28** was determined as shown in Fig. 4.1 and was named colletofuran C.

Compound **29** was isolated as a colorless oil, its molecular formula ($C_{22}H_{34}O_7$) is the same as **27**, based on HRESITOFMS (m/z 433.2201 ($[M + Na]^+$)). The extensive analysis of 1D/2D NMR revealed **29** has the same planar structure as **27** (Table 4.3). A comparison of chemical shifts and coupling constants of those compounds indicating no observable distinct difference. In separation process, they were separated in HPLC (Develosil column) indicated that they were different compounds, supported by different specific rotation, $[\alpha]_D^{25} +7$ (c 0.1, MeOH) for **27** and $[\alpha]_D^{25} -25$ (c 0.1, MeOH) for **29**. Using the crystalline sponge method, we finally confirmed that **29** was an epimer of **27** at C-2 (Fig. 4.7). The complete absolute configuration of **29** was established as 2*S*,10*S*,11*R*,12*R*,21*R* [Flack (parsons), 0.061 (17)] and thus was named colletofuran D (Fig. 4.1).

The molecular formula of **30** ($C_{23}H_{36}O_7$) was the same as **28**. It was isolated as a colorless oil. A comparison of NMR data (Table 4.3), including chemical shift and coupling constants, also revealed that they have the same planar structure. Both compounds were separated by HPLC (Develosil column) and exhibited a different specific rotation ($[\alpha]_D^{25} +3$ (c 0.1, MeOH) for **28** and $[\alpha]_D^{25} -12$ (c 0.1, MeOH) for **30**), indicating that they are different compounds. Using the same crystalline sponge method, we confirmed complete absolute configuration of **30** to be 2*S*,10*S*,11*R*,12*R*,21*R* [Flack (parsons), 0.056 (7)] (Fig. 4.7). Compound **30** is an epimer of **28** at C-2 and was named colletofuran E (Fig. 4.1).

Aphids are a serious insect pest in agriculture worldwide. Most aphids are host-specific, feeding on one or a few closely related plant species. Some of the aphids in greenhouses, however, are polyphagous, e.g. *Aphis gossypii* (Glover), cotton aphid and *Myzus persicae* (Sulzer), green peach aphid.¹¹² These two species have also shown particular ability to develop resistance to different insecticides that comprise the most important groups.¹¹³ Thus, this assay was performed to test the susceptibility of *A. gossypii* and *M. persicae*, against 1-octyl-1,3-dihydroisobenzofuran core present in **26–30**. The commercial insecticide milbemectin was tested as the positive control. As shown in Table 4.4, **29** exhibited strong aphicidal activity ($LC_{50} = 0.5 \mu\text{g/mL}$) against *A. gossypii* and weak activity ($LC_{50} = 118 \mu\text{g/mL}$) against *M. persicae*. In contrast, **30** exhibited moderate aphicidal activity against *M. persicae* ($LC_{50} = 26 \mu\text{g/mL}$), but inactive against *A. gossypii*. Other compounds displayed either weak or no aphicidal activity (LC_{50}

>200 µg/mL) against tested aphids. In general, the data showed dose dependent responses and *M. persicae* was more resistant than *A. gossypii* to the treatments. This is correlated with the ability to overcome various types of plant defenses. These findings indicate the presence of *C. boninense* as an endophyte appears to help the protection against plant pests by providing insecticidal compounds.

Table 4.4 Insecticidal activity of compounds **26–30** against two aphid species

Compound	LC ₅₀ (µg/mL)	
	<i>Aphis gossypii</i> (Glover)	<i>Myzus persicae</i> (Sulzer)
26	1	>200
27	>200	169
28	>200	>200
29	0.5	118
30	>200	26
Milbemectin	0.15	0.75

Chapter 5 Conclusions

The declining trends in microbial metabolites and natural products research, together with the increasing resistance of antibiotics, have been occurred. Renewing natural products research requires unlimited natural resources, including microbial sources. The biggest advantage of microorganisms develops is their incredible adaptability to changes in their environments due to their flexible metabolic power. Their incredible adaptability, requires a variety of biochemical mechanisms and interactions.⁶ These biochemical mechanisms and interactions resulting in the production of various compounds and have served as potential resources to fulfill important demand of new compounds for various human applications. In this study, endophytic fungi are expected to be potential source of new compounds. The endophytic fungi used in this study were isolated from plants collected from Merapi volcano area. It was presumed that during the post-eruption in this area, fungal endophytes were not investigated as metabolite sources. We explored new metabolite sources from the damaged area, which led to the isolation of several fungal strains.

Structure characterizations of new compounds based on NMR can be performed and consider as a powerful tool on a routine basis and often provide high reliability for the planar structure and relative configuration of compounds.¹¹⁴ However, it may still be challenging to determine the absolute stereochemistry. The difference in NMR anisotropy effects between two diastereomers can be used by using chiral derivatization techniques to deduce the absolute configuration.¹¹⁵ One of chiral reagents for this purpose have been developed from the primarily used of Mosher's acid/chloride (α -methoxy- α -(trifluoromethyl)phenylacetic acid/chloride, MTPA/MTPACl), which an aromatic moiety (phenyl-) is essential as a producer of the necessary anisotropy effect.⁶³ This method also has a limitation on the determination of whole absolute structure of several polyfunctional and complex natural products. Thanks to rapid development of computational chemistry, quantum mechanical calculations of chiroptical data¹¹⁵, e.g. electronic circular dichroism, and gauge including atomic orbitals (GIAO) ¹³C NMR chemical shift calculations¹¹⁶, providing useful support in the interpretation of experimental data. The direct X-ray method, developed by Bijvoet is still considered to be the

most reliable method; provided only that a suitable single crystal can be obtained from samples, which many times occurs isolated as oily substances.¹¹⁷ The crystalline sponge method is an X-ray technique that allows the crystallographic study of even oily compounds in small quantities and has therefore been useful in determining the absolute structures of natural products and their derivatives.^{108,118,119}

N. pseudotrichia 120-1NP was isolated from the stem of *Gliricidia sepium*. Seven new compounds, nectrianolins A–C (**1–3**); 6,8-dihydroxy-3,4,7-trimethylisocoumarin (**5**); 8-hydroxy-6-methoxy-3,4,7-trimethylisocoumarin (**6**); nectriaquinone B (**8**); and zythiostromic acid C (**11**), were isolated from the brown rice culture of this strain, along with four known compounds (**4**, **7**, **9**, and **10**). Compounds **1–3** were evaluated for their in vitro cytotoxicity against HL60 and HeLa cell lines by the MTT method. Compounds **1–3** exhibited cytotoxic activity against the HL60 cell lines with IC₅₀ values of 1.7, 1.5 and 10.1 μ M, respectively. Compound **1–3** also exhibited cytotoxicity against the HeLa cell lines with IC₅₀ values of 34.7, 16.6 and 52.1 μ M, respectively. Additionally, compounds **4–11** were evaluated for their antimicrobial activity against *Staphylococcus aureus*, *Pseudomonas aeruginosa*, *Candida albicans*, and *Aspergillus clavatus*, phytotoxicity, and in vitro cytotoxicity.

F. solani B-18 was isolated from an unidentified forest litter. Four new compounds with γ -methylidene-spirobutanolide core, fusaspirols A–D (**12–15**), were isolated from the brown rice culture of *Fusarium solani* B-18. Oxaspirol analogues have been reported to possess various biological activities, **12–15** and its derivatives did not show cytotoxicity against murine macrophage derived RAW264.7 cells. Compounds **12** and **12a** significantly increased the number of mature osteoclasts at the comparable levels to the positive control (kenpaullone) and the negative control (DMSO), suggesting that **12** and **12a** activated a signaling pathway in osteoclastic differentiation. In the scale-up fermentation based on this strain, with the same method, additional four new polyketides, fusopoltides B–E (**20–23**), were isolated along with four known compounds (**16–19**). Fusopoltide B (**20**) is a diastereomer of its co-isolated known compound, fusopoltide A (**19**),

featuring a pentaleno[1,2-*c*]pyran ring system. Fusopoltide C (**21**) and fusopoltides D–E (**22–23**) are incorporated the first natural polyketides featured decahydro-pentaleno[1,2-*c*]pyran and pentaleno[1,2-*c*]furan ring systems, respectively.

C. boninense AM-12-2 was isolated from the stem of *Acacia mangium*. Seven new compounds, 3-(3-hydroxy-2-(hydroxymethyl)phenyl)propanoic acid (**24**), 2-hydroxymethyl-3-hydroxy-(*E*)-cinnamic acid (**25**), and colletofurans A–E (**26–30**), were isolated from brown-rice culture of *Colletotrichum boninense* AM-12-2. Colletofurans A–E (**26–30**) are first natural compounds featured an unprecedented 1-octyl-1,3-dihydroisobenzofuran core. Additionally, colletofuran A (**26**) contained a unique 1,6-dioxaspiro[4.4]nonane ring system. Compounds **24–30** were evaluated for their anti-aphicidal activity.

In this thesis, 30 fungal metabolites, including 22 new compounds and two compounds firstly isolated from fungal culture, were identified. Complex interactions with their host may involve the presence of these fungi in volcanic areas. The interactions possibly related to their chemistry in some respects and have been shown to produce secondary metabolites that are new, attractive, and biologically active. Although certain new compounds exhibited no activity in bioassay, the new chemistry faced difficulties in the determination of the structure that had to be addressed. These results also disclosed that endophytic fungi from Merapi volcano area harbor an enormous reservoir of new compounds for drug discovery.

References

1. Butler MS. *J Nat Prod*. 2004; 67: 2141–2153.
2. Demain AL, Zhang L. In *Natural Products* Humana Press: Totowa, NJ, 2005; pp 3–29.
3. Newman DJ, Cragg GM. In *Natural Products in Medicinal Chemistry* 2009; pp 3–27.
4. Gaynes R. *Emerg Infect Dis*. 2017; 23: 849–853.
5. Cragg GM, Newman DJ. *Biochim Biophys Acta - Gen Subj*. 2013; 1830: 3670–3695.
6. Bérday J. *J Antibiot (Tokyo)*. 2012; 65: 441–441.
7. Hong J. *Curr Opin Chem Biol*. 2011; 15: 350–354.
8. Newman DJ, Cragg GM. *J Nat Prod*. 2016; 79: 629–661.
9. Atanasov AG, Waltenberger B, Pferschy-Wenzig EM, Linder T, Wawrosch C, Uhrin P, Temml V, Wang L, Schwaiger S, Heiss EH, Rollinger JM, Schuster D, Breuss JM, Bochkov V, Mihovilovic MD, Kopp B, Bauer R, Dirsch VM, Stuppner H. *Biotechnol Adv*. 2015; 33: 1582–1614.
10. Demain AL, Sanchez S. *J. Antibiot. (Tokyo)*., 2009, 62, 5–16.
11. Mishra BB, Tiwari VK. *Eur J Med Chem*. 2011; 46: 4769–4807.
12. Martinez-Klimova E, Rodríguez-Peña K, Sánchez S. *Biochem Pharmacol*. 2017; 134: 1–17.
13. Venugopalan A, Srivastava S. *Biotechnol Adv*. 2015; 33: 873–887.
14. Yu H, Zhang L, Li L, Zheng C, Guo L, Li W, Sun P, Qin L. *Microbiol Res*. 2010; 165: 437–449.
15. Kusari S, Hertweck C, Spiteller M. *Chem Biol*. 2012; 19: 792–798.
16. Schulz B, Boyle C, Draeger S, Römmert A-K, Krohn K. *Mycol Res*. 2002; 106: 996–1004.
17. Pusztahelyi T, Holb IJ, Pócsi I. *Front Plant Sci*. 2015; 6: 1–23.
18. Gupta S, Chaturvedi P, Kulkarni MG, Van Staden J. *Biotechnol Adv*. 2019: 107462.
19. Cragg GM, Newman DJ. *Biochim Biophys Acta - Gen Subj*. 2013; 1830: 3670–3695.
20. DeJong JHM, Liu Y, Bollon AP, Long RM, Jennewein S, Williams D, Croteau RB. *Biotechnol Bioeng*. 2006; 93: 212–224.

21. Demain AL, Vaishnav P. *Microb Biotechnol.* 2011; 4: 687–699.
22. Stierle A, Strobel G, Stierle D. *Science (80-)*. 1993; 260: 214–216.
23. Uzma F, Mohan CD, Hashem A, Konappa NM, Rangappa S, Kamath P V., Singh BP, Mudili V, Gupta VK, Siddaiah CN, Chowdappa S, Alqarawi AA, Abd-Allah EF. *Front Pharmacol.* 2018; 9: 1–37.
24. Kusari S, Singh S, Jayabaskaran C. *Trends Biotechnol.*, 2014, 32, 304–311.
25. Strobel GA, Hess WM, Ford E, Sidhu RS, Yang X. Taxol from fungal endophytes and the issue of biodiversity, 1996, vol. 17.
26. Wang J, Li G, Lu H, Zheng Z, Huang Y, Su W. *FEMS Microbiol Lett.* 2000; 193: 249–253.
27. Kumaran RS, Muthumary J, Hur BK. *J Biosci Bioeng.* 2008; 106: 103–106.
28. Yang H-X, Ai H-L, Feng T, Wang W-X, Wu B, Zheng Y-S, Sun H, He J, Li Z-H, Liu J-K. 2018.
29. Tang J-W, Kong L-M, Zu W-Y, Hu K, Li X-N, Yan B-C, Wang W-G, Sun H-D, Li Y, Puno P-T. 2019.
30. Liu H, Tan H, Chen Y, Guo X, Wang W, Guo H, Liu Z, Zhang W. *Org Lett.* 2019; 21: 1063–1067.
31. Strobel G a. *Microbes Infect.* 2003; 5: 535–544.
32. Martinez-Klimova E, Rodríguez-Peña K, Sánchez S. *Biochem. Pharmacol.*, 2017, 134, 1–17.
33. Alvin A, Miller KI, Neilan B a. *Microbiol Res.* 2014; 169: 483–495.
34. Pambudi NA. *Renew. Sustain. Energy Rev.*, 2018, 81, 2893–2901.
35. Voight B, Constantine EK, Siswamidjoyo S, Torley R. *J Volcanol Geotherm Res.* 2000; 100: 69–138.
36. Cronin SJ, Lube G, Dayudi DS, Sumarti S, Subrandiyo S, Surono. *J Volcanol Geotherm Res.* 2013; 261: 244–259.
37. Sunardi, Sulistijorini, Setyawati T. *Biotropia (Bogor)*. 2017; 24: 35–46.
38. Sholikha M, Djohan TS, Subagja J, Kurniati T. *IOP Conf Ser Mater Sci Eng.* 2018; 434: 012291.
39. Karadimou E, Kallimanis AS, Tsiripidis I, Raus T, Bergmeier E, Dimopoulos P. *Ecosphere.* 2018; 9.
40. Sutomo, Hobbs RJ, Cramer VA. *Trop Plant Res.* 2015; 2: 204–214.
41. Redman RS, Sheehan KB, Stout RG, Rodriguez RJ, Henson JM. *Science.*

- 2002; 298: 1581.
42. Twizeyimana M, Forster H, McDonald V, Wang DH, Adaskaveg JE, Eskalen A. *Plant Dis.* 2013; 97: 1580–1584.
 43. Gutiérrez M, Theoduloz C, Rodríguez J, Lolas M, Schmeda-Hirschmann G. *J Agric Food Chem.* 2005; 53: 7701–7708.
 44. Wang RS, Gong T, Zhu P, Cheng K Di. *J Chinese Pharm Sci.* 2012; 21: 183–186.
 45. Awakawa T, Kaji T, Wakimoto T, Abe I. *Bioorganic Med Chem Lett.* 2012; 22: 4338–4340.
 46. Sheldrick GM. *Acta Crystallogr. Sect. A Found. Crystallogr.*, 2008, 64, 112–122.
 47. Flack HD, Bernardinelli G. *J Appl Cryst.* 2000.
 48. Shiono Y, Murayama T, Takahashi K, Okada K, Katohda S, Ikeda M. *Biosci Biotechnol Biochem.* 2005; 69: 287–92.
 49. Tanaka AK, Sato C, Shibata Y, Kobayashi A, Yamashita K. *Agric Biol Chem.* 1974; 38: 1311–1315.
 50. Chen S, Liu Y, Liu Z, Cai R, Lu Y, Huang X, She Z. *RSC Adv.* 2016; 6: 26412–26420.
 51. Geng W-L, Wang X-Y, Kurtán T, Mándi A, Tang H, Schulz B, Sun P, Zhang W. *J Nat Prod.* 2012; 75: 1828–1832.
 52. Medentsev AG, Akimenko VK. *Phytochemistry*, 1998, 47, 935–959.
 53. Forcina GC, Castro A, Bokesch HR, Spakowicz DJ, Legaspi ME, Kucera K, Villota S, Narváez-Trujillo A, McMahon JB, Gustafson KR, Strobel SA. *J Nat Prod.* 2015; 78: 3005–3010.
 54. Carroll J, Jonsson EN, Ebel R, Hartman MS, Theodore R. Holman A, Crews P. *J Org Chem.* 2001; 66: 6847–6851.
 55. Yu S, Deng Z, Proksch P, Lin W. *J Nat Prod.* 2006; 69: 1330–1334.
 56. Shiono Y, Koyama H, Murayama T, Koseki T. *Phytochem Lett.* 2015; 14: 143–147.
 57. Hirose A, Maeda H, Tonouchi A, Nehira T, Hashimoto M. *Tetrahedron.* 2014; 70: 1458–1463.
 58. Fu Y, Wu P, Xue J, Wei X. *J Nat Prod.* 2014; 77: 1791–1799.
 59. Spruit CJP. *Recl des Trav Chim des Pays-Bas.* 2010; 68: 309–324.
 60. Kesteleyn B, De Kimpe N. *J Org Chem.* 2000; 65: 640–644.

61. Nielsen LB, Wege D. *Org Biomol Chem*. 2006; 4: 868.
62. Zhou Z-Y, Liu R, Jiang M-Y, Zhang L, Niu Y, Zhu Y-C, Dong Z-J, Liu J-K. *Chem Pharm Bull (Tokyo)*. 2009; 57: 975–8.
63. Seco JM, Quiñoá E, Riguera R. *Chem Rev*. 2004; 104: 17–118.
64. Sassa T, Yoshikoshi H. *Agric Biol Chem*. 1983; 47: 187–189.
65. Zhang L, Shen Y, Wang F, Leng Y, Liu JK. *Phytochemistry*. 2010; 71: 100–103.
66. Aburai N, Yoshida M, Ohnishi M, Kimura K. *Phytomedicine*. 2010; 17: 782–788.
67. Saeed A. *Eur J Med Chem*. 2016; 116: 290–317.
68. Baker RA, Tatum JH, Nemec S. *Mycopathologia*. 1990; 111: 9–15.
69. Xuan Nguyen H, Thanh Thi Nguyen M, Anh Nguyen T, Thi Nguyen NY, Anh Thi Phan D, Ho Thi P, Huu Phan Nguyen T, Hoang Dang P, Trung Nguyen N, Ueda J, Awale S. *Fitoterapia*. 2013; 91: 148–153.
70. Schöffler A, Liermann JC, Kolshorn H, Opatz T, Anke H. *Zeitschrift für Naturforsch C*. 2009; 64: 25–31.
71. Liu C, Shen G-N, Luo Y-H, Piao X-J, Jiang X-Y, Meng L-Q, Wang Y, Zhang Y, Wang J-R, Wang H, Xu W-T, Li J-Q, Liu Y, Wu Y-Q, Sun H-N, Han Y-H, Jin M-H, Cui Y-D, Fang N-Z, Jin C-H. *Int J Biochem Cell Biol*. 2018.
72. Klaus V, Hartmann T, Gambini J, Graf P, Stahl W, Hartwig A, Klotz L-O. *Arch Biochem Biophys*. 2010; 496: 93–100.
73. Pessôa MG, Paulino BN, Mano MCR, Neri-Numa IA, Molina G, Pastore GM. *Appl Microbiol Biotechnol*. 2017; 101: 3493–3511.
74. Shiono Y, Ariefta NR, Anwar C, Matsjeh S, Sappapan R, Murayama T, Koseki T, Kawamura T, Uesugi S, Kimura K ichi. *Phytochem Lett*. 2016; 17: 232–237.
75. Kyekyeku JO, Kusari S, Adosraku RK, Bullach A, Golz C, Strohmman C, Spiteller M. *Fitoterapia*. 2017; 119: 108–114.
76. Shweta S, Zuehlke S, Ramesha BT, Priti V, Mohana Kumar P, Ravikanth G, Spiteller M, Vasudeva R, Uma Shaanker R. *Phytochemistry*. 2010; 71: 117–122.
77. Chowdhury NS, Sohrab MH, Rana MS, Hasan CM, Jamshidi S, Rahman KM. *J Nat Prod*. 2017; 80: 1173–1177.

78. Takemoto K, Kamisuki S, Chia PT, Kuriyama I, Mizushima Y, Sugawara F. *J Nat Prod.* 2014; 77: 1992–1996.
79. Doi J, Hirota A, Nakagawa M, Sakai H, Isogai A. *Agric Biol Chem.* 1985; 49: 2247–2248.
80. Halgren TA. *J Comput Chem.* 1996; 17: 490–519.
81. Frisch, M. J.; Trucks, G. W.; Schlegel, H. B.; Scuseria, G. E.; Robb, M. A.; Cheeseman, J. R.; Scalmani, G.; Barone, V.; Mennucci, B.; Petersson, G. A.; Nakatsuji, H.; Caricato, M.; Li, X.; Hratchian, H. P.; Izmaylov, A. F.; Bloino, J.; Zheng, G.; Sonnenb DJ. *Gaussian 09, Revis. E.01*, 2009.
82. Wijeratne EMK, Gunaherath GMKB, Chapla VM, Tillotson J, De La Cruz F, Kang MJ, U'Ren JM, Araujo AR, Arnold AE, Chapman E, Gunatilaka AAL. *J Nat Prod.* 2016; 79: 340–352.
83. Kutrzeba LM, Li XC, Ding Y, Ferreira D, Zjawiony JK. *J Nat Prod.* 2010; 73: 707–708.
84. Hashimoto M, Tsushima T, Murakami T, Nomiya M, Takada N, Tanaka K. *Bioorg Med Chem Lett.* 2008; 18: 4228–4231.
85. Rether J, Erkel G, Anke T, Sterner O. *J Antibiot (Tokyo).* 2004; 57: 493–495.
86. Hirota A, Nakagawa M, Hirota H. *Agric Biol Chem.* 1991; 55: 1187–1188.
87. Oh H, Swenson DC, Gloer JB, Shearer CA. *J Nat Prod.* 2003; 66: 73–79.
88. Akiba Y, Mizuta A, Kakihara Y, Nakata J, Nihara J, Saito I, Egusa H, Saeki M. *Biochem Biophys Reports.* 2016; 5: 253–258.
89. Letarouilly JG, Broux O, Clabaut A. *Genomics.* 2018.
90. Coudert AE, de Vernejoul M-C, Muraca M, Del Fattore A. *Int J Endocrinol.* 2015; 2015: 1–8.
91. Kornsakulkarn J, Dolsophon K, Boonyuen N, Boonruangprapa T, Rachtawee P, Prabpai S, Kongsaree P, Thongpanchang C. *Tetrahedron.* 2011; 67: 7540–7547.
92. Chen K, Sun W, Bie Q, Liu X, Chen C, Liu J, Xue Y, Wang J, Luo Z, Zhu H, Zhang Y. *Tetrahedron Lett.* 2018; 59: 2679–2682.
93. Tsai I, Lin W, Huang M, Chen T-L, Chen I. *Helv Chim Acta.* 2001; 84: 830–833.
94. Chen J-J, Chen P-H, Liao C, Huang S, Chen I. *J Nat Prod.* 2007; 70: 1444–1448.

95. Chen J, Zhang T, Zhang Q, Liu Y, Li L, Si J, Zou Z, Hua H. *J Agric Food Chem.* 2018; 66: 3408–3416.
96. Cheng MJ, Lee KH, Tsai IL, Chen IS. *Bioorganic Med Chem.* 2005; 13: 5915–5920.
97. Chung C-Y, Hwang T-L, Kuo L-M, Kuo W-L, Cheng M-J, Wu Y-H, Sung P-J, Chung M-I, Chen J-J. *Int J Mol Sci.* 2013; 14: 22395–22408.
98. Cheng MJ, Tsai IL, Chen IS. *J Chinese Chem Soc.* 2003; 50: 1241–1246.
99. Ramachandran PV, Krzeminski MP, Reddy MVR, Brown HC. *Tetrahedron Asymmetry.* 1999; 10: 11–15.
100. Xiao WJ, Chen HQ, Wang H, Cai CH, Mei WL, Dai HF. *Fitoterapia.* 2018; 130: 180–183.
101. Hertweck C. *Angew Chemie - Int Ed.* 2009; 48: 4688–4716.
102. Damm U, Cannon PF, Woudenberg JHC, Johnston PR, Weir BS, Tan YP, Shivas RG, Crous PW. *Stud Mycol.* 2012; 73: 1–36.
103. Feng L, Wang J, Liu S, Zhang X-J, Bi Q-R, Hu Y-Y, Wang Z, Tan N-H. *J Nat Prod.* 2019; 82: 1434–1441.
104. Bang S, Lee C, Kim S, Song JH, Kang KS, Deyrup ST, Nam SJ, Xia X, Shim SH. *J Org Chem.* 2019; 84: 10999–11006.
105. Dallery JF, Le Goff G, Adelin E, Iorga BI, Pigné S, O’Connell RJ, Ouazzani J. *J Nat Prod.* 2019; 82: 813–822.
106. Biradha K, Fujita M. *Angew Chemie - Int Ed.* 2002; 41: 3392–3395.
107. Gray SM. *Curr Protoc Microbiol.* 2008; 10: 16B.1.1–16B.1.10.
108. Inokuma Y, Yoshioka S, Ariyoshi J, Arai T, Hitora Y, Takada K, Matsunaga S, Rissanen K, Fujita M. *Nature.* 2013; 495: 461–466.
109. Hoshino M, Khutia A, Xing H, Inokuma Y, Fujita M. *IUCrJ.* 2016; 3: 139–151.
110. Biradha K, Fujita M. *Angew Chemie - Int Ed.* 2002; 41: 3392–3395.
111. Matsuda Y, Mitsunashi T, Lee S, Hoshino M, Mori T, Okada M, Zhang H, Hayashi F, Fujita M, Abe I. *Angew Chemie - Int Ed.* 2016; 55: 5785–5788.
112. Vuong PT, Kim J, Song Y. *J Asia Pac Entomol.* 2001; 4: 41–44.
113. Foster SP, Denholm I, Rison J-L, Portillo HE, Margaritopoulos J, Slater R. *Pest Manag Sci.* 2012; 68: 629–633.
114. Breton RC, Reynolds WF. *Nat Prod Rep.* 2013; 30: 501.
115. Allenmark S, Gawronski J. *Chirality.* 2008; 20: 606–608.

- 116. Barone G, Gomez-Paloma L, Duca D, Silvestri A, Riccio R, Bifulco G. *Chemistry*. 2002; 8: 3233–3239.
- 117. Flack HD, Bernardinelli G. *Chirality*. 2008; 20: 681–690.
- 118. Hoshino M, Khutia A, Xing H, Inokuma Y, Fujita M. *IUCrJ*. 2016; 3: 139–151.
- 119. Zigon N, Hoshino M, Yoshioka S, Inokuma Y, Fujita M. *Angew Chemie*. 2015; 127: 9161–9165.

Acknowledgements

First of all, I would like to express my profound appreciation to Prof. Dr. Yoshihito Shiono, for giving me this opportunity and excellent working conditions and facilities to pursue my doctoral study in Yamagata University, as well as his patient guidance, helpful suggestions, kindhearted discussion, and comprehensive supports for my study and life in Tsuruoka.

I am deeply indebted to Prof. Dr. Takuya Koseki (Yamagata University) and Prof. Dr. Ken-ichi Kimura (Iwate University) for their unforgettable support and help in my research and scientific advices.

My sincere appreciation goes to Prof. Dr. Masaru Hashimoto for his scientific advices and help, as PhD referee.

During my PhD study, I received many helps, supports, and happiness from day to day, therefore I would like to express my profound gratitude to all laboratory members:

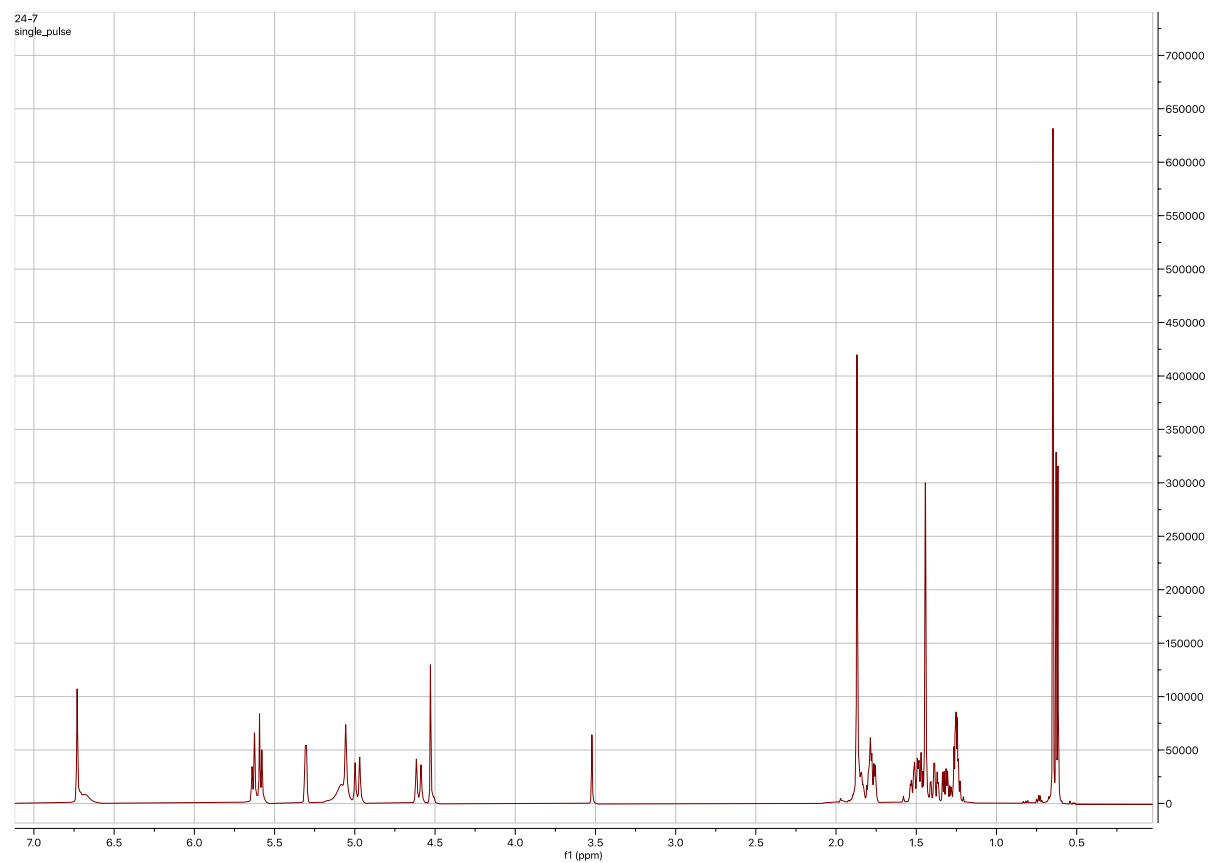
- Mrs. Priska Kristiana, Mrs. Hasna Tazkia Nikmawahda, and Mr. Muhlisun Azim, for their help on fungi screening and experiments.
- I enjoyed the time here with Mr. Takuma Suzuki, thanks for help on structure determination and his assistance on daily life in Tsuruoka. Special thanks also for Mr. Nakamura Tomoki, Mr. Kyotaro Ichikawa, and Mr. Yasuhiro Yokoyama, for all of their help.
- I would like to thank all–present and past–members of Laboratory of Fermentation Products, Yamagata University.
- Special thanks to visiting researchers Prof. Dr. Unang Supratman, Dr. Alain Meli Lannang, Dr. Abdou Tchoukoua, Prof. Dr. Samir Abdelgaleil, Dr. Yenny Febriani Yun, Dr. Rani Maharani, Dr. Desi Harneti, Dr. Hadi Kuncoro, and Mr. Deden Indradinata for their help and support.
- Great time spend with Indonesian students, Mr. Ferry Ferdiansyah Sofian and Ms. Nurrizka Kurniawati, as well as all students on JASSO program in the same lab.

I am grateful to Ministry of Education, Culture, Sports, Science, and Technology of Japan, for financial support during my study in Japan.

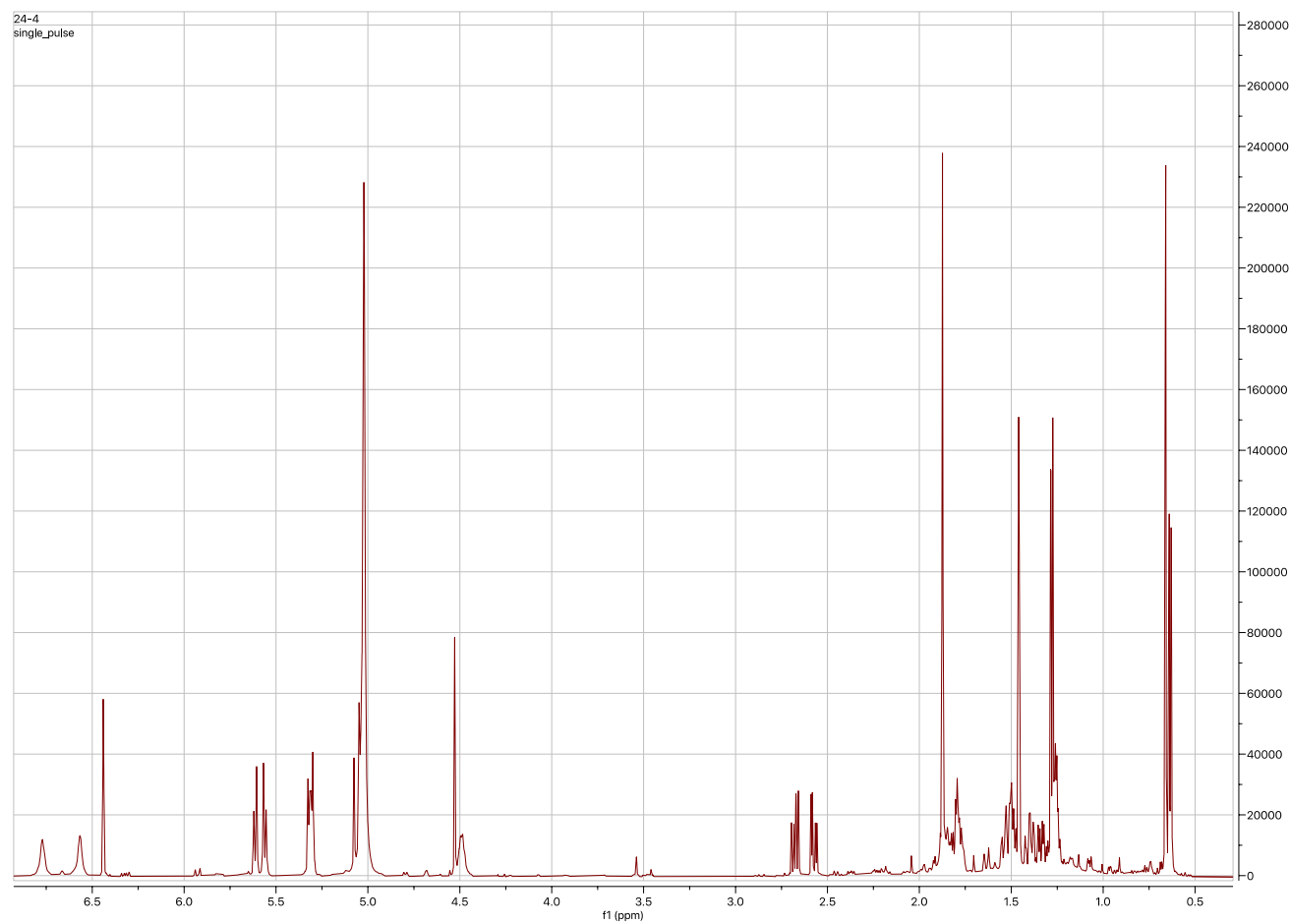
In the end, I would like to express my deepest thankfulness and appreciation to my family, my wife Endah Perananingtyas—my children Fatih Jayawardhana Ariefta and Farha Hayukinara Ariefta, for their enormous encourages and supports to finish this study.

Supplemental Data

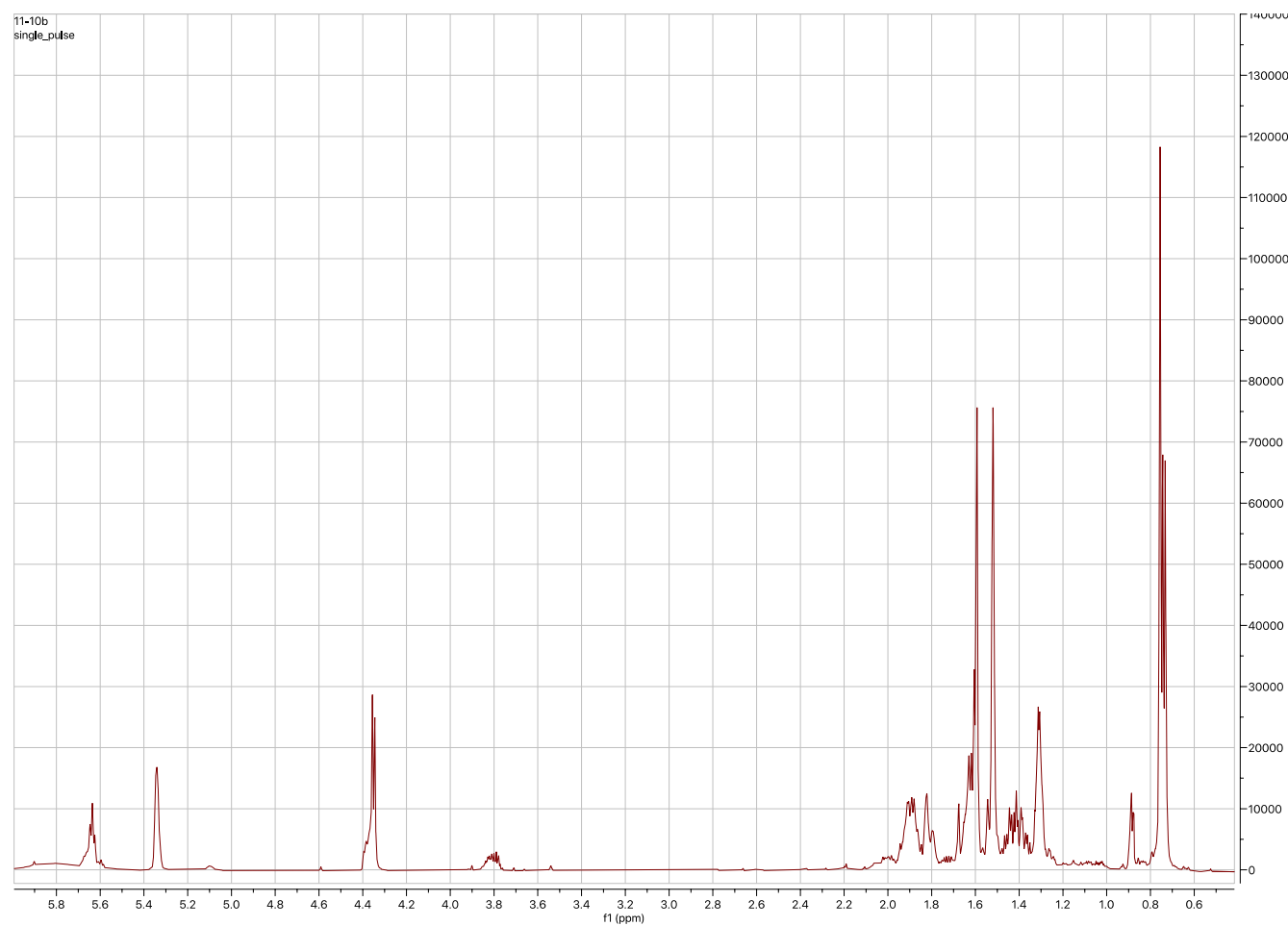
Appendix. 1. ^1H NMR spectrum of **1** (Pyridine- d_5 , 600 MHz).



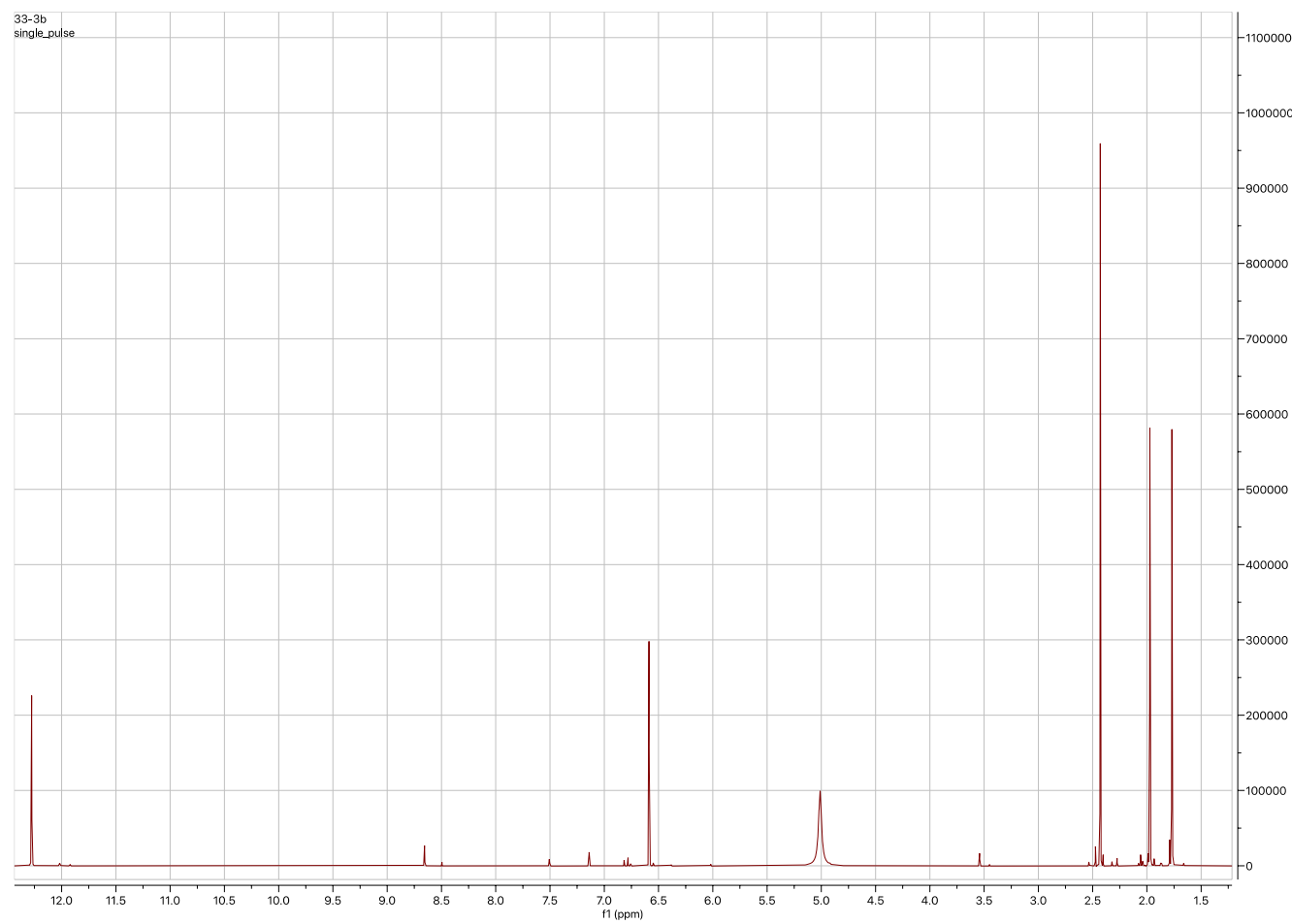
Appendix 2. ^1H NMR spectrum of **2** (Pyridine- d_5 , 600 MHz).



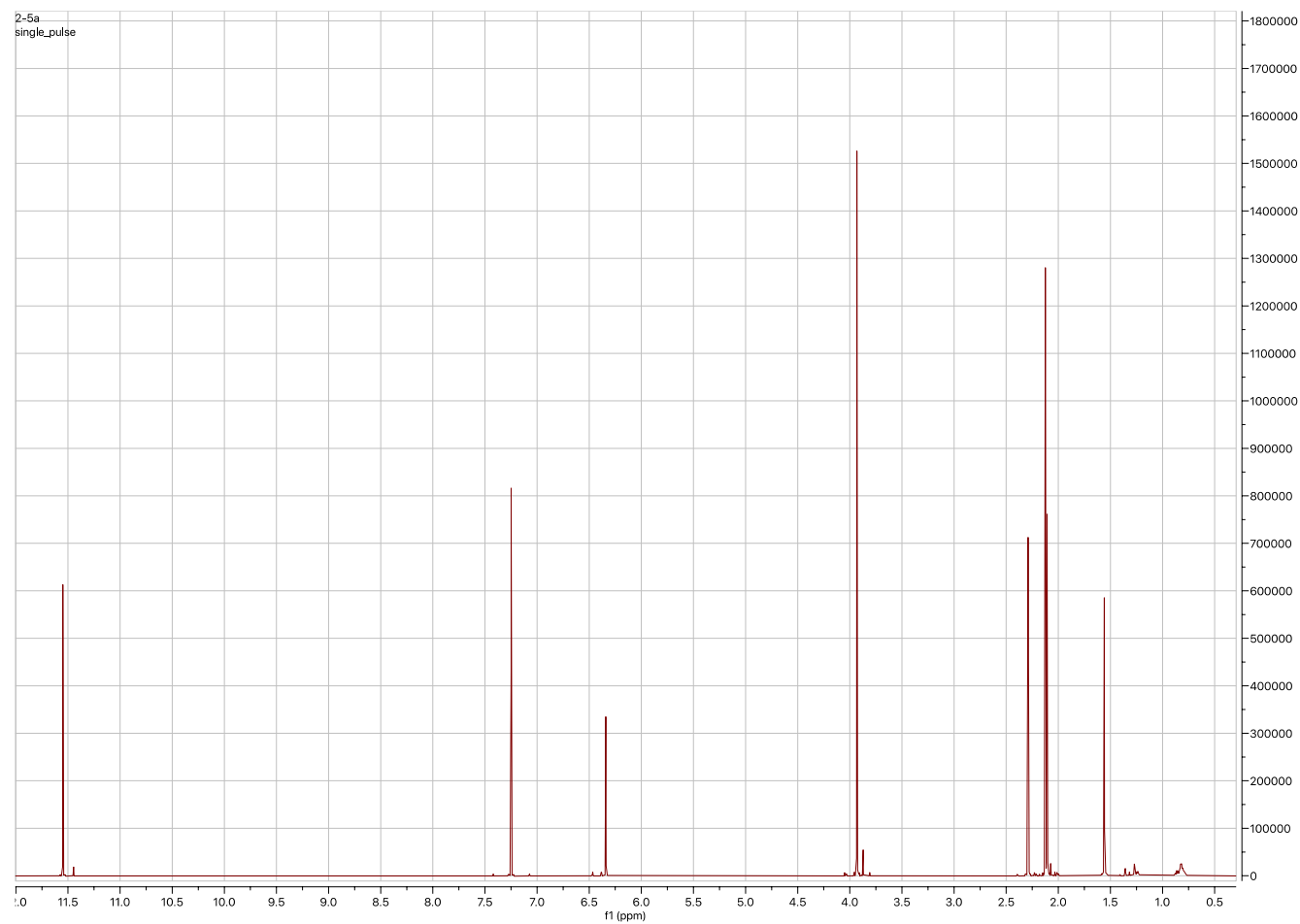
Appendix 3. ^1H NMR spectrum of **3** (Pyridine- d_5 , 600 MHz).



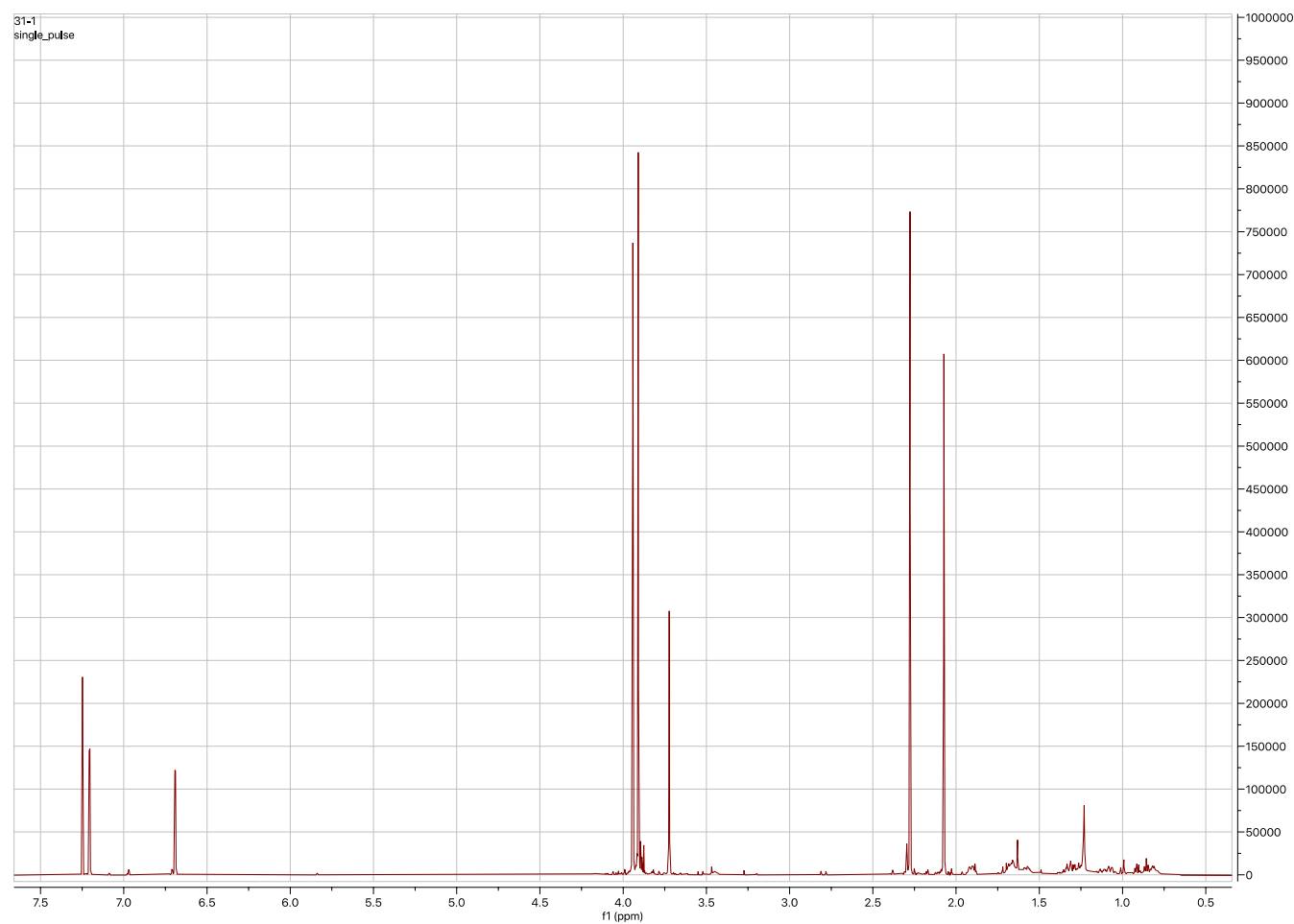
Appendix 4. ^1H NMR spectrum of **5** (Pyridine- d_5 , 600 MHz).



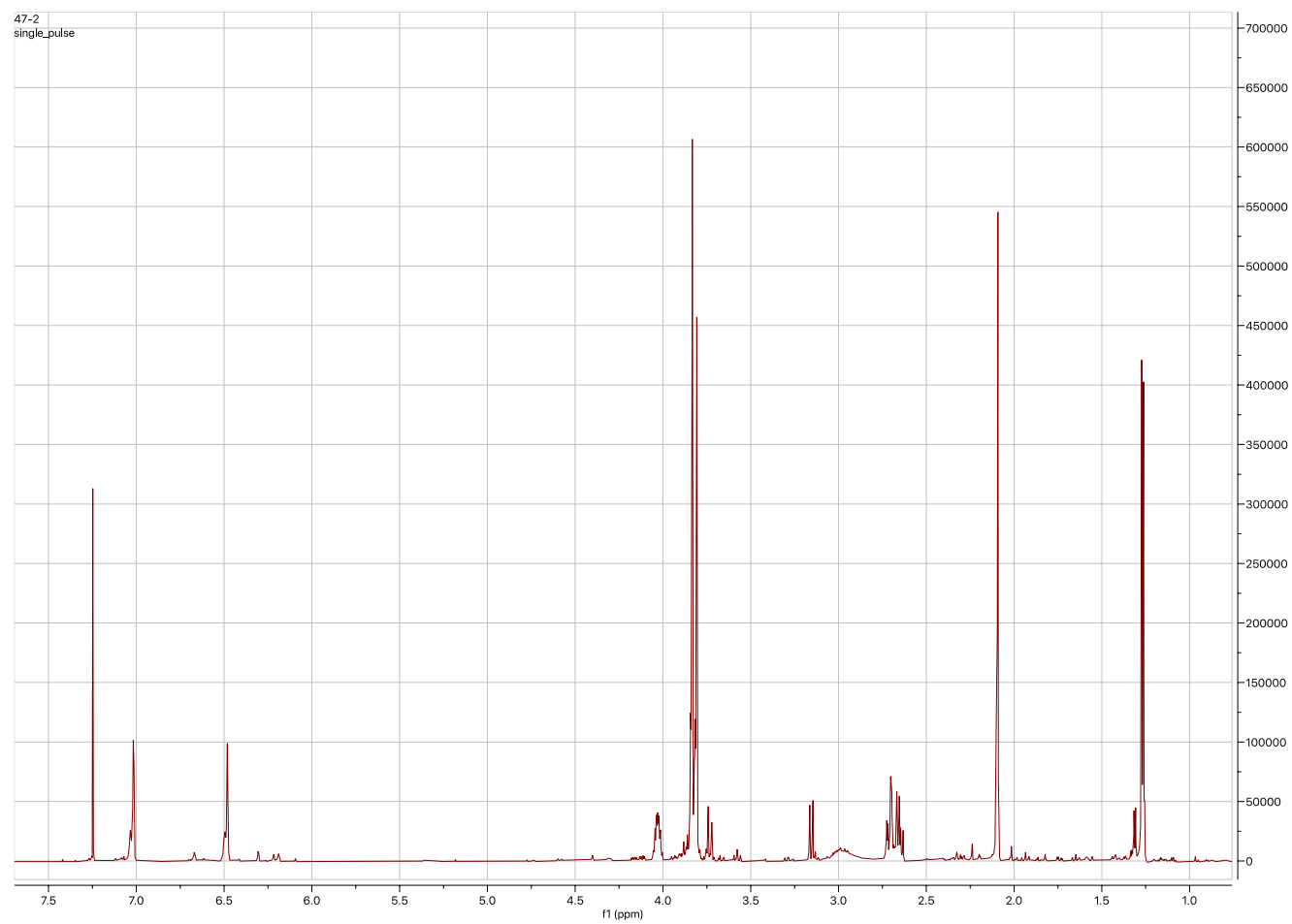
Appendix 5. ^1H NMR spectrum of **6** (CDCl_3 , 600 MHz).



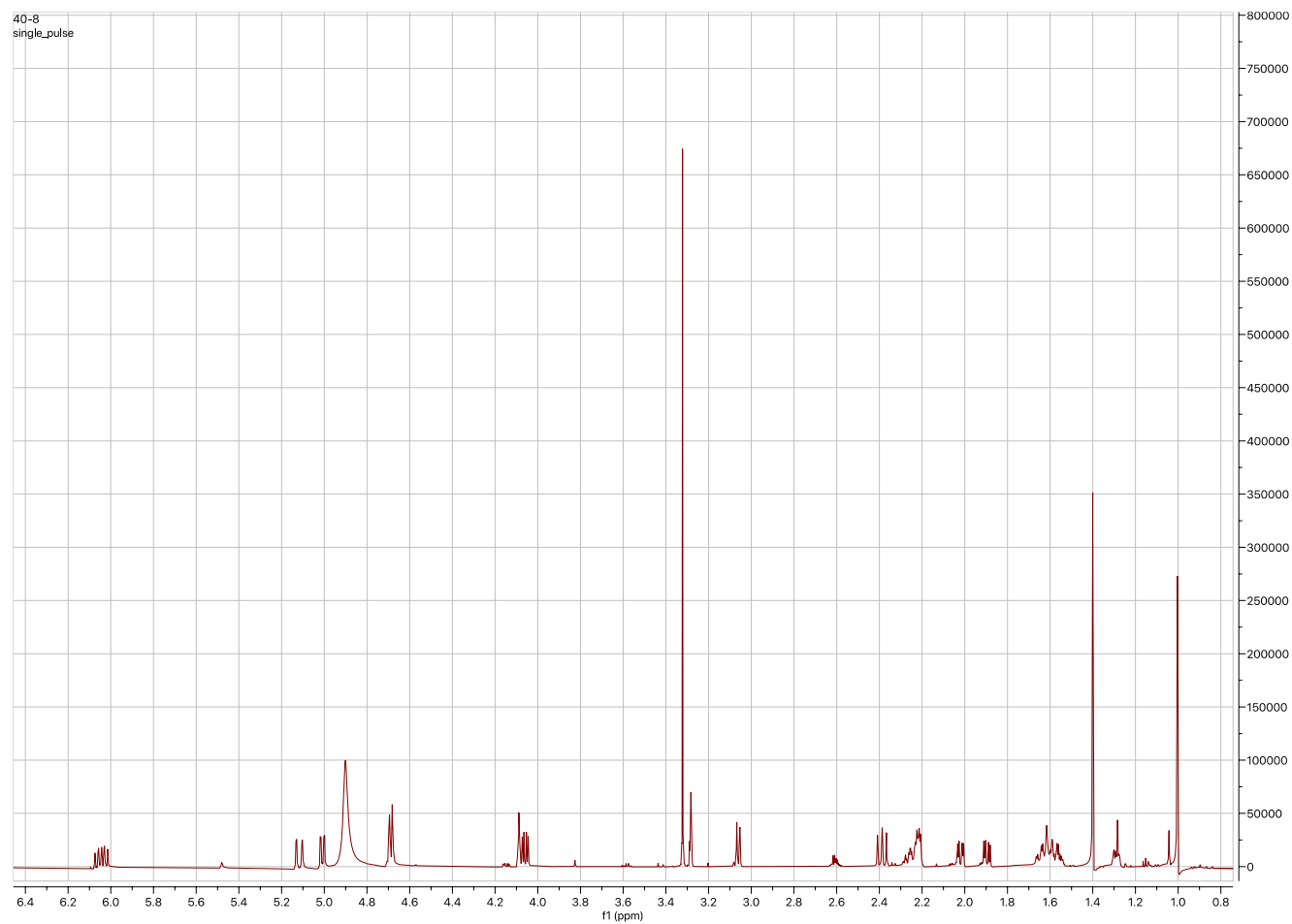
Appendix 6. ^1H NMR spectrum of **7** (CDCl_3 , 600 MHz).



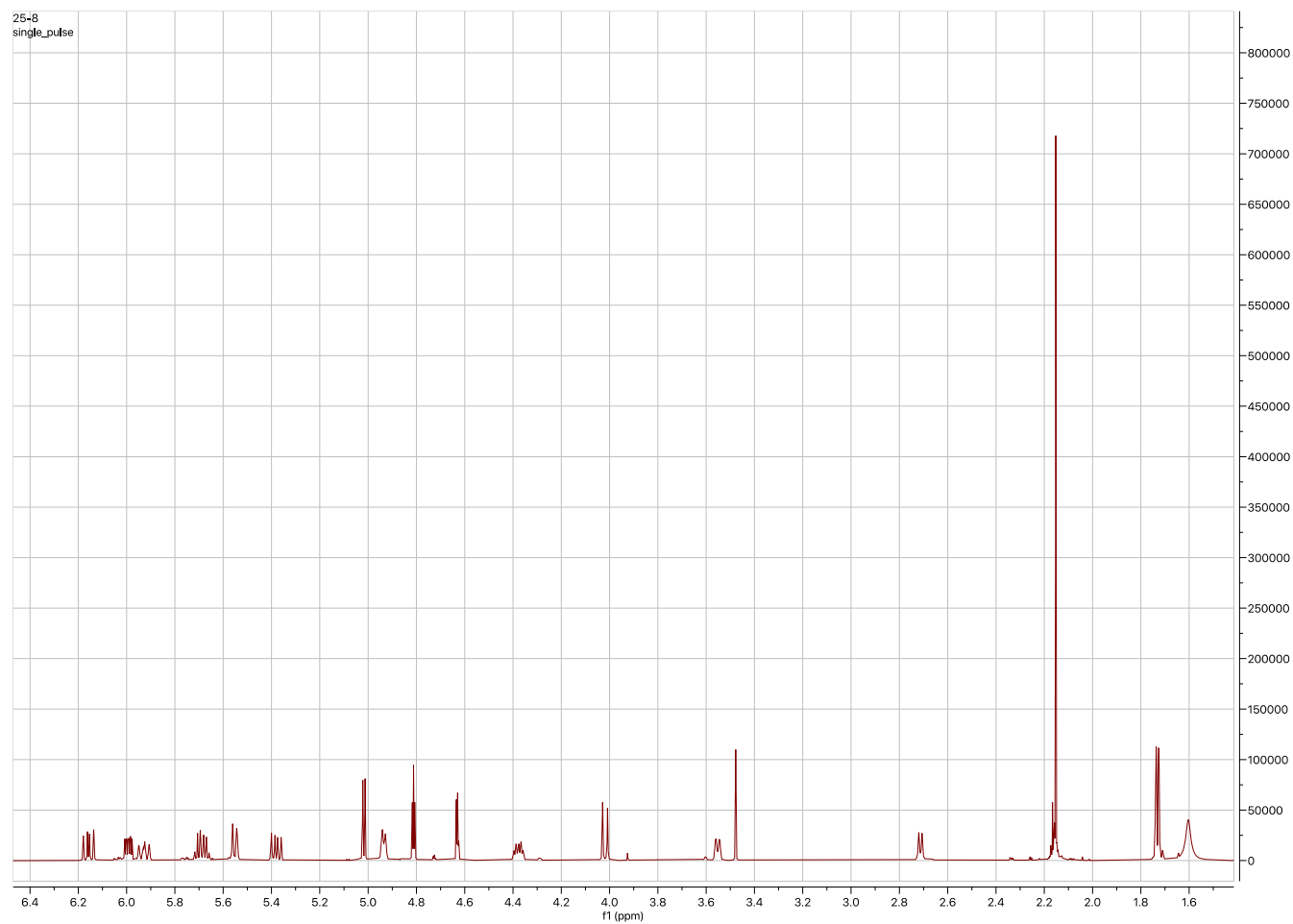
Appendix 7. ^1H NMR spectrum of **8** (CDCl_3 , 600 MHz).



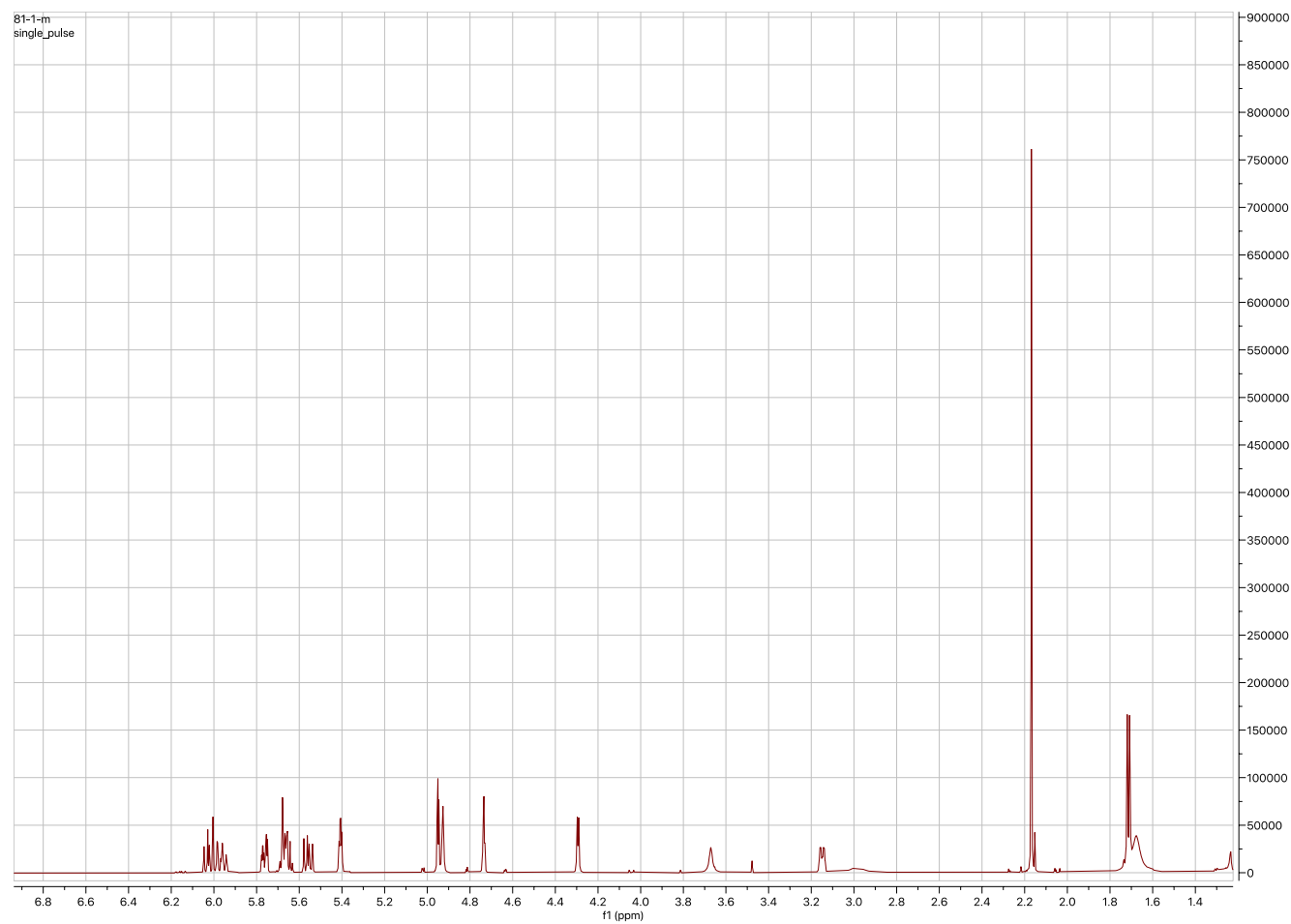
Appendix 8. ^1H NMR spectrum of **11** (CD_3OD , 600 MHz).



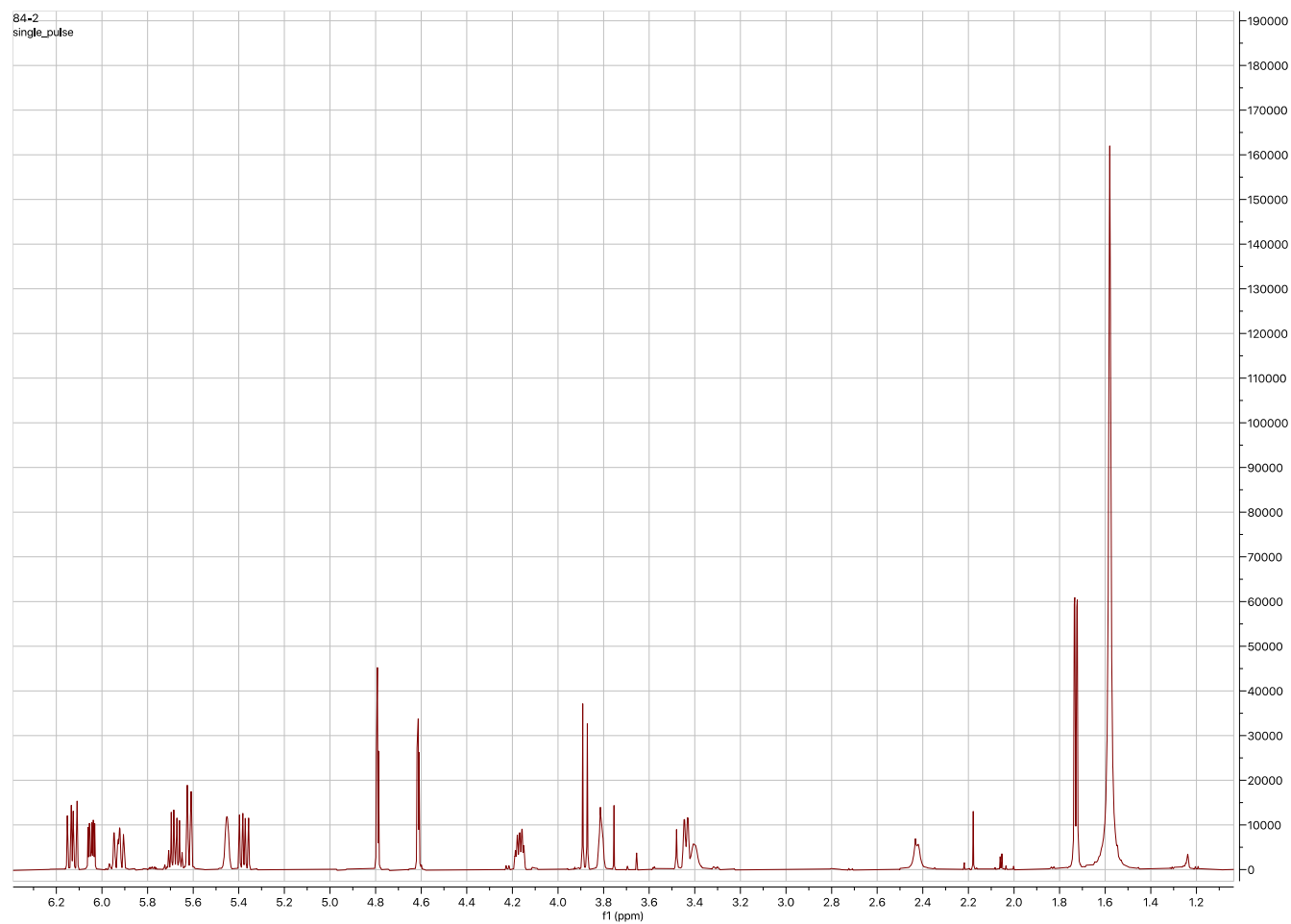
Appendix 9. ^1H NMR spectrum of **12** (CDCl_3 , 600 MHz).



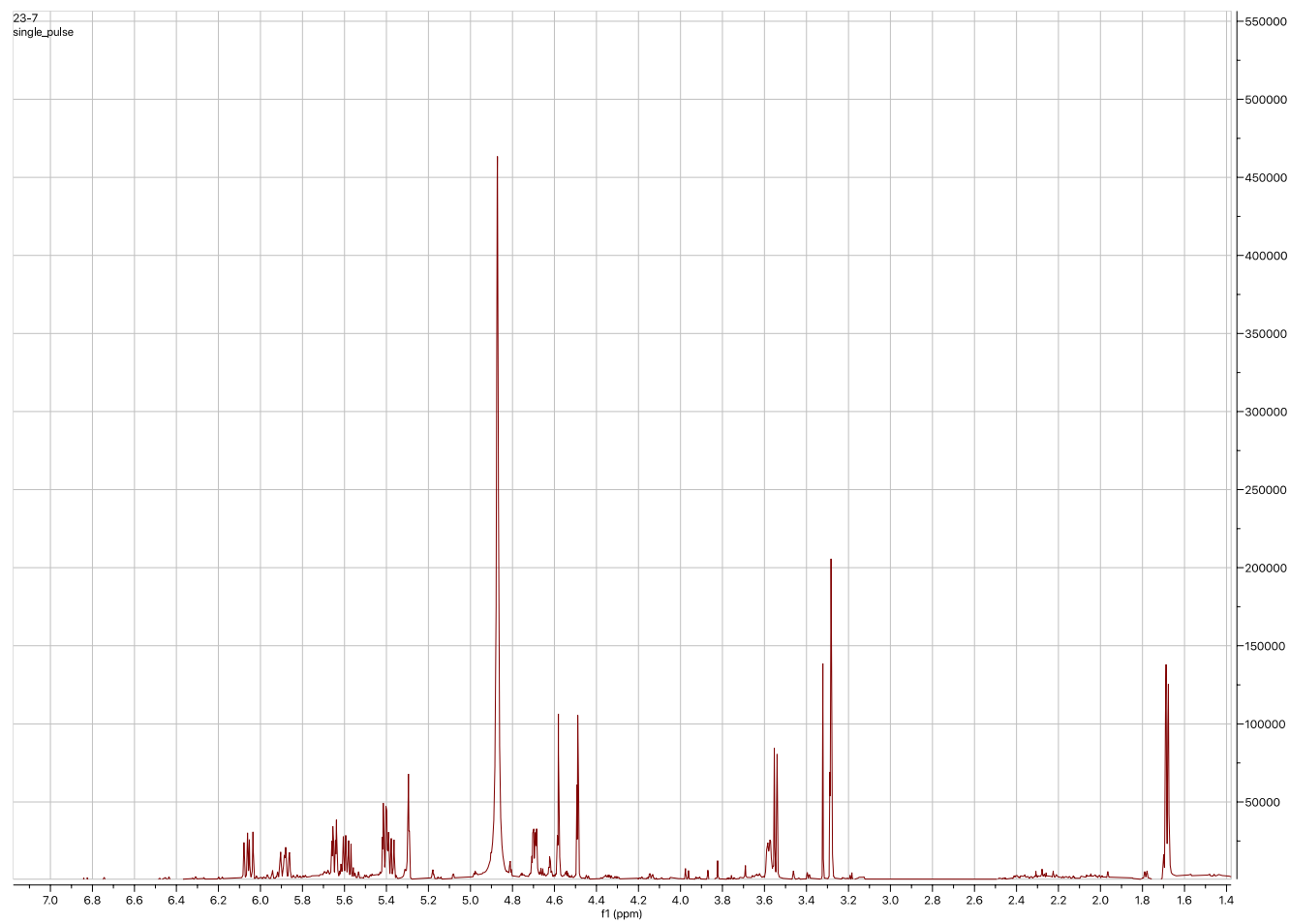
Appendix 10. ^1H NMR spectrum of **13** (CDCl_3 , 600 MHz).



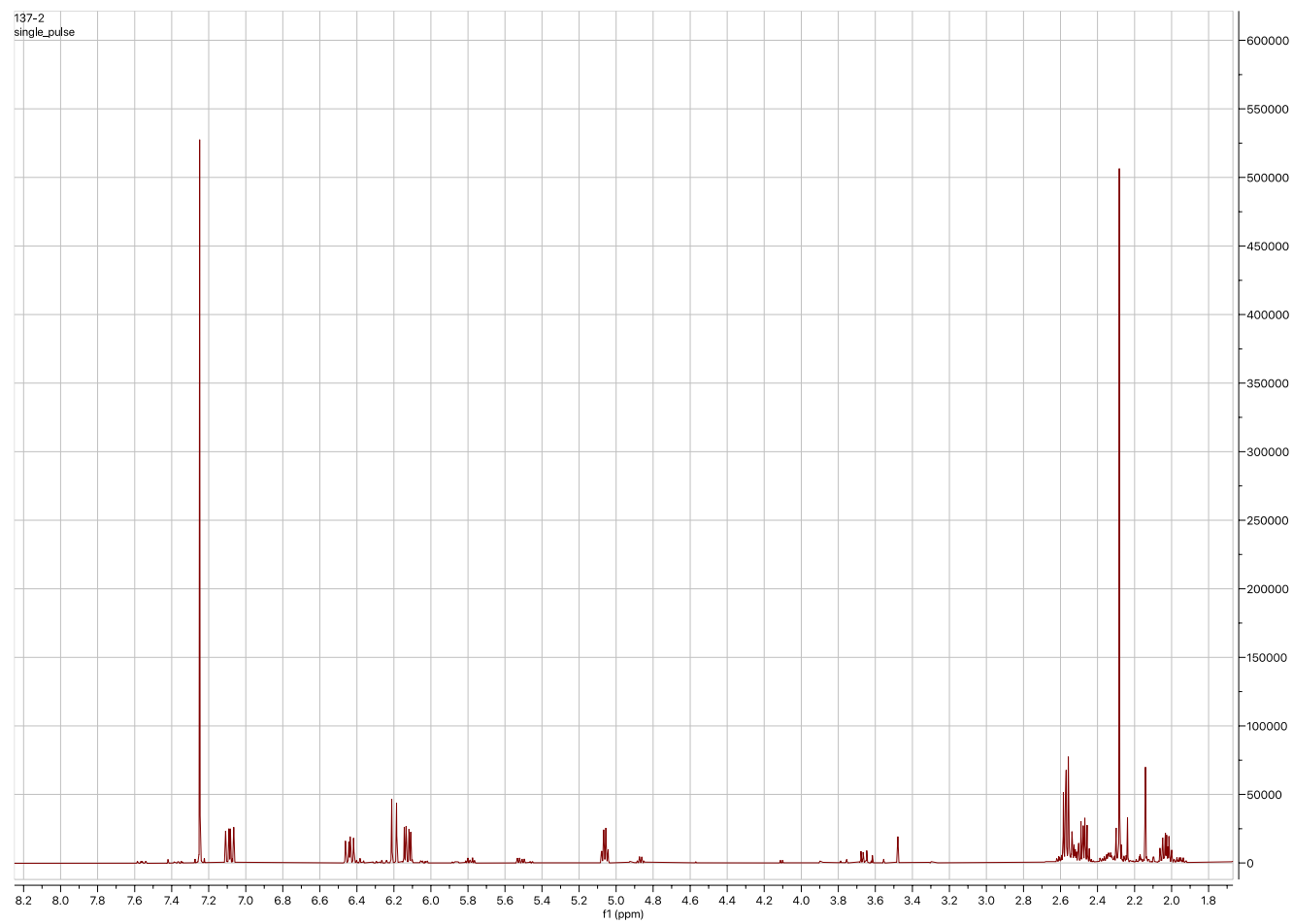
Appendix 11. ^1H NMR spectrum of **14** (CDCl_3 , 600 MHz).



Appendix 12. ^1H NMR spectrum of **15** (CD_3OD , 600 MHz).



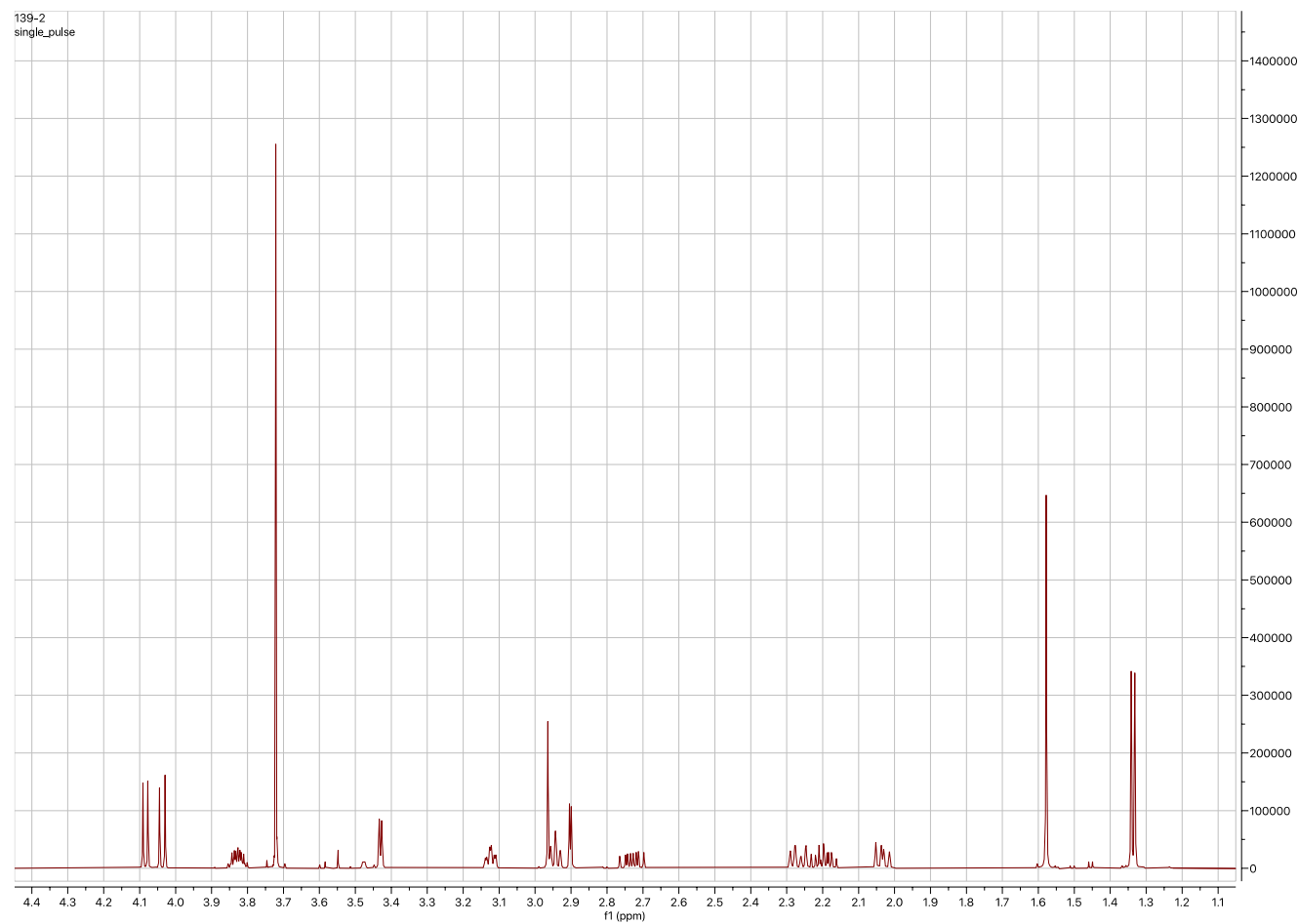
Appendix 13. ^1H NMR spectrum of **18** (CDCl_3 , 600 MHz).



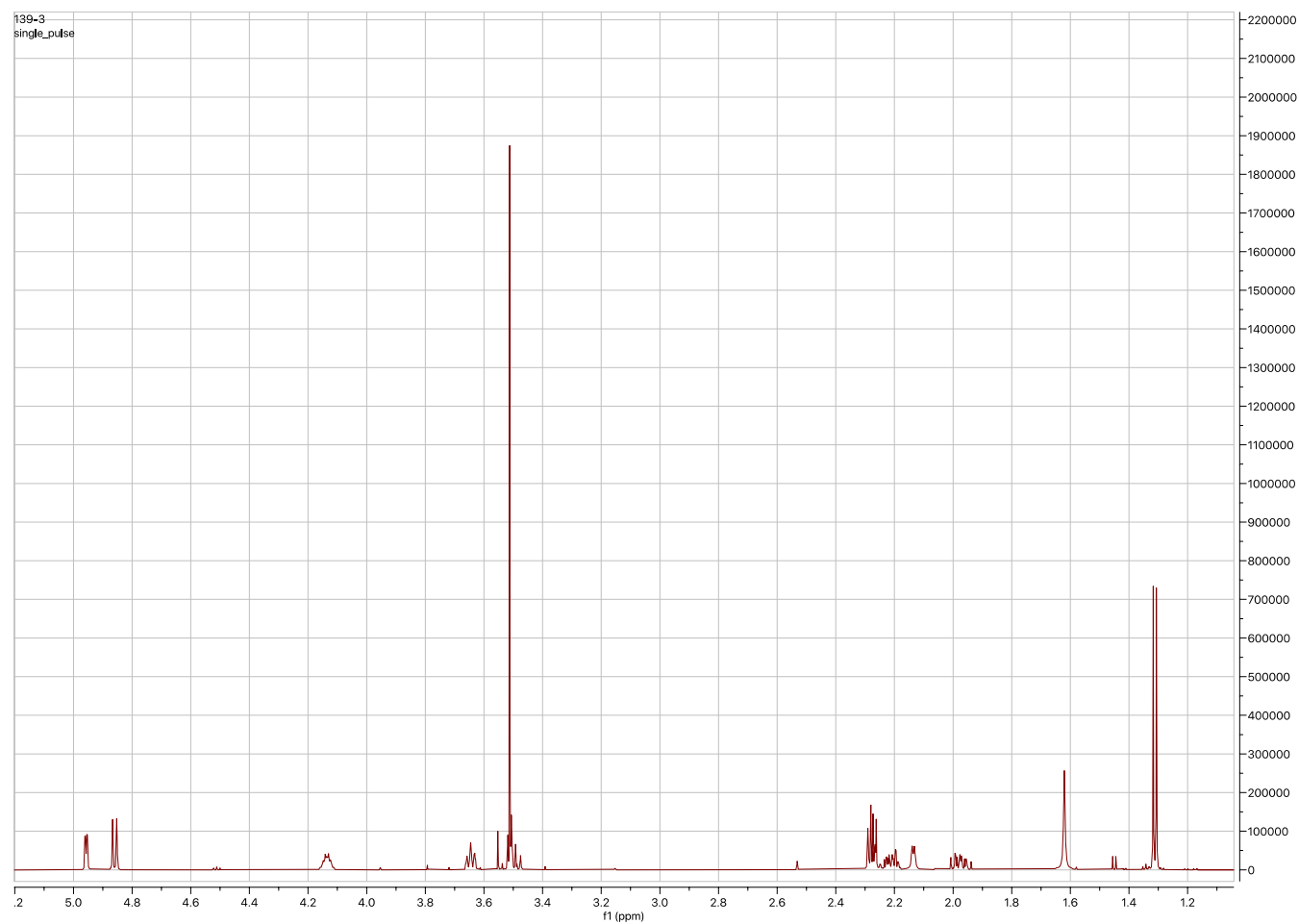
Appendix 14. ^1H NMR spectrum of **20** (CDCl_3 , 600 MHz).



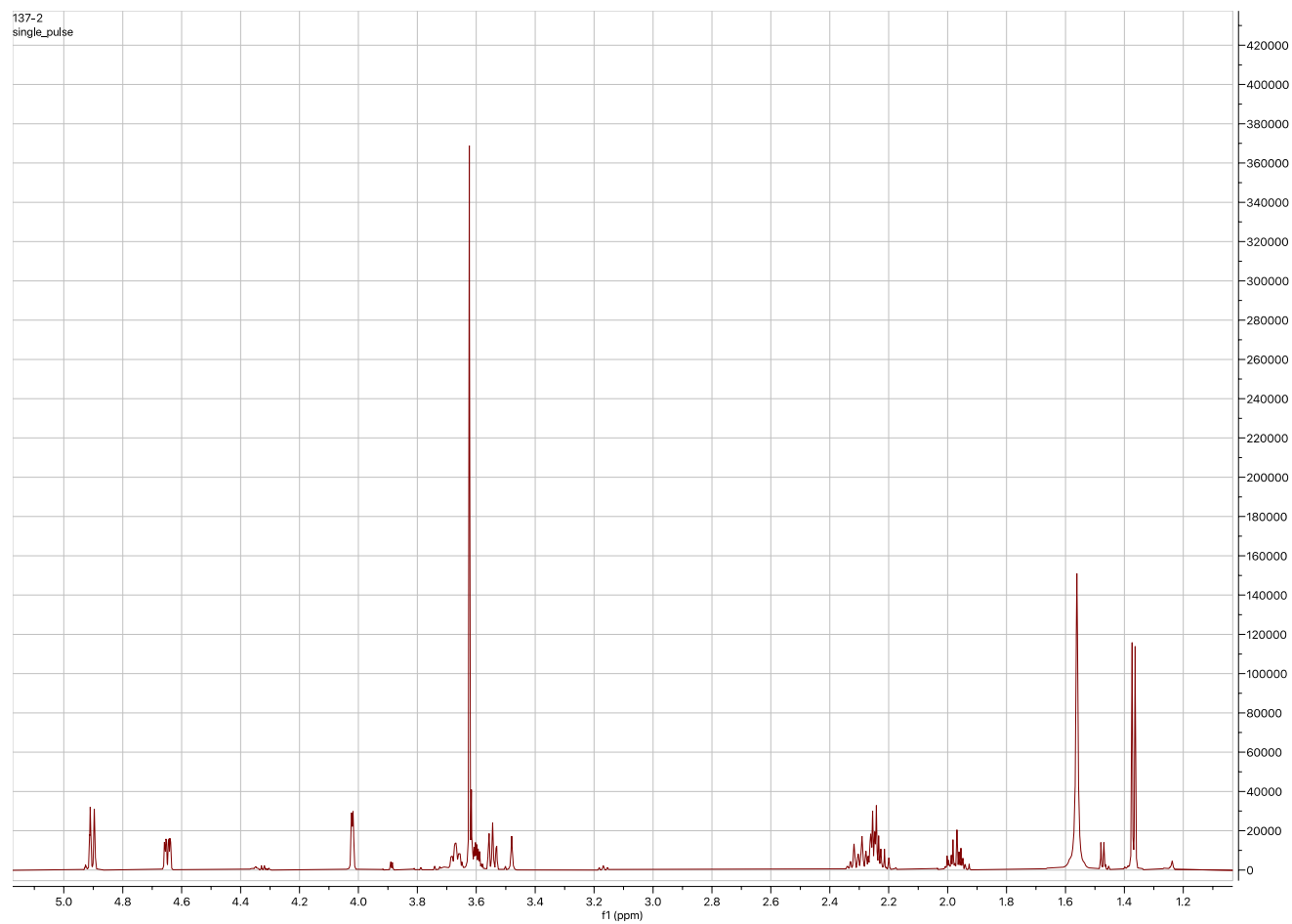
Appendix 15. ^1H NMR spectrum of **21** (CDCl_3 , 600 MHz).



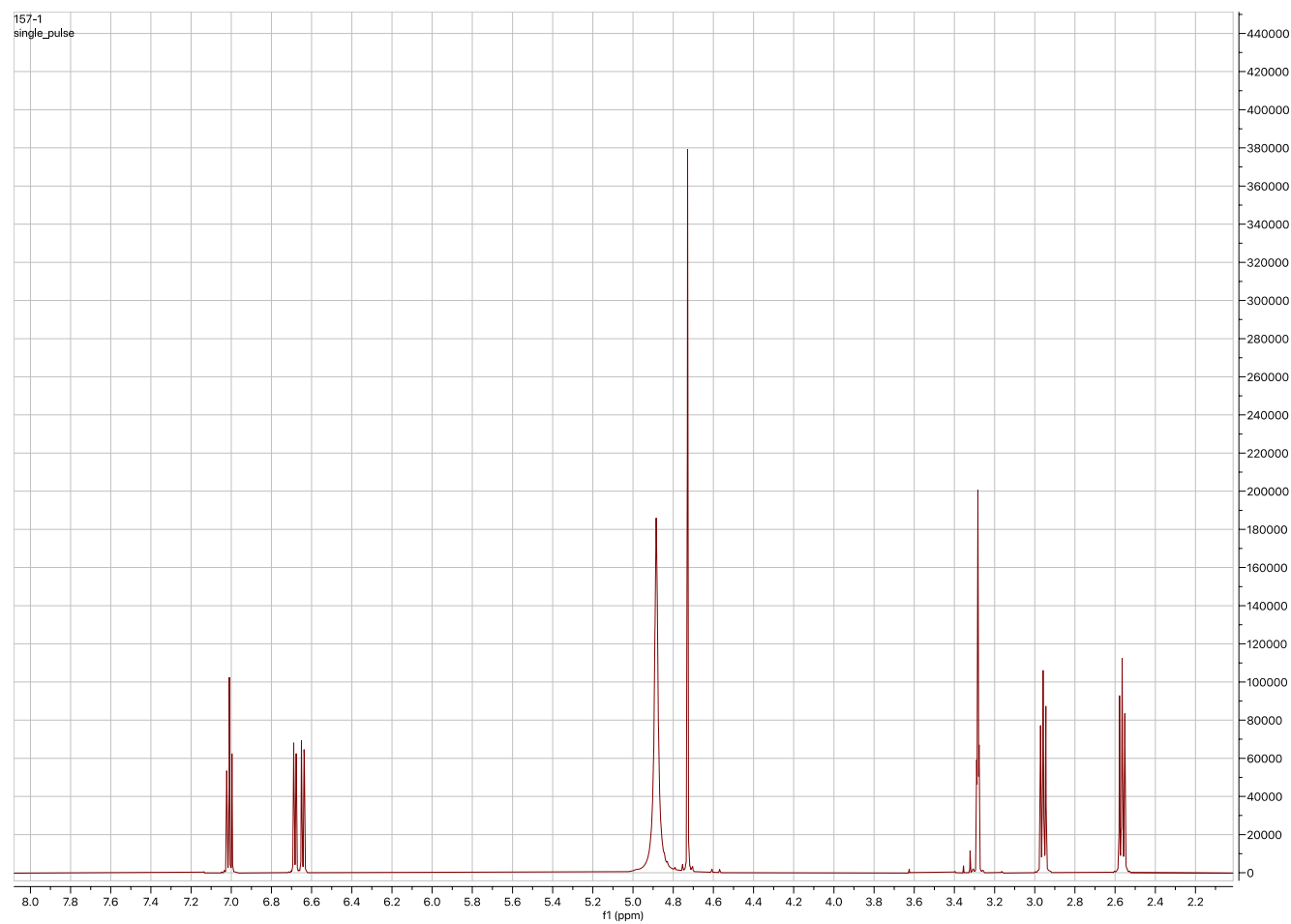
Appendix 16. ^1H NMR spectrum of **22** (CDCl_3 , 600 MHz).



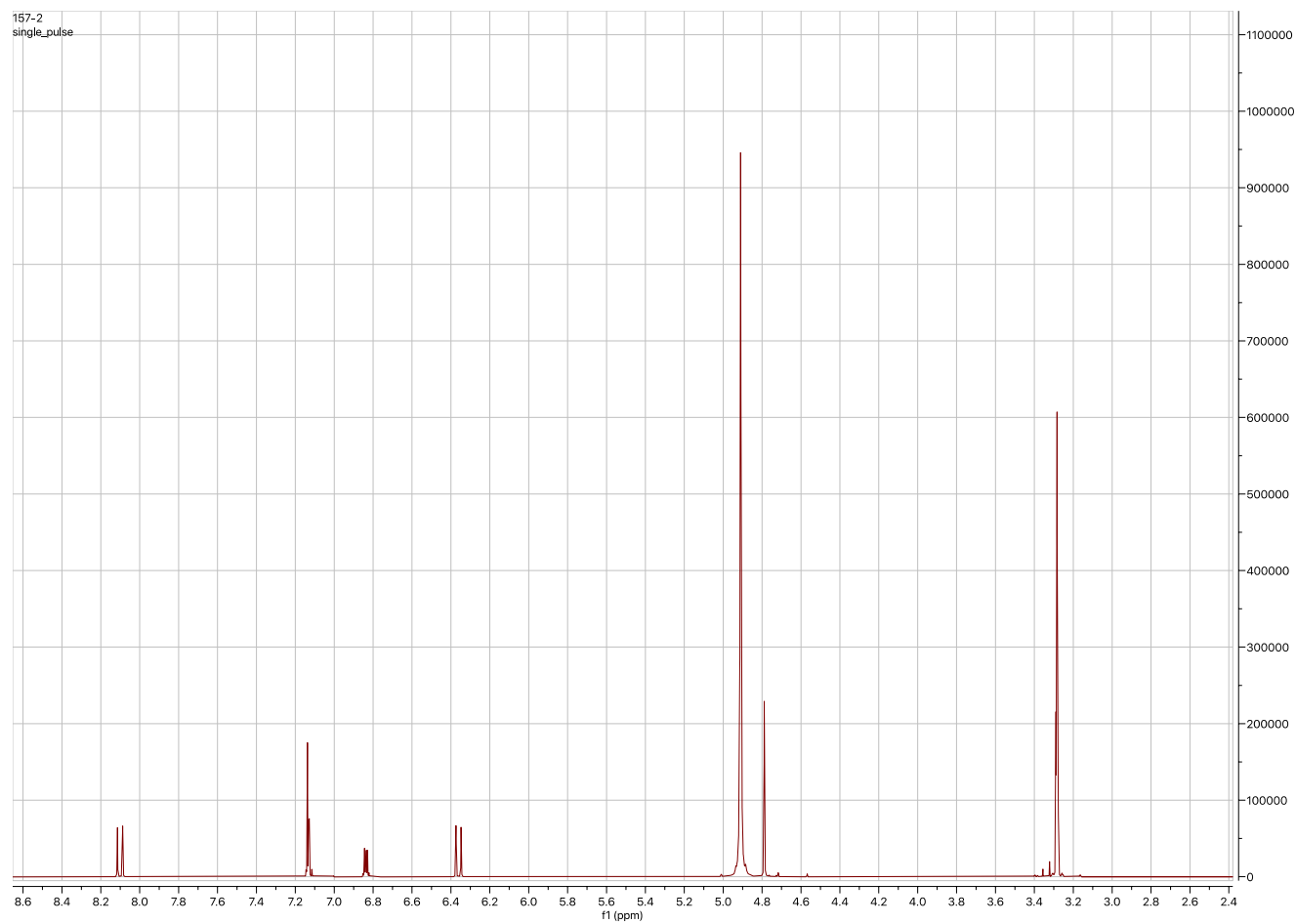
Appendix 17. ^1H NMR spectrum of **23** (CDCl_3 , 600 MHz).



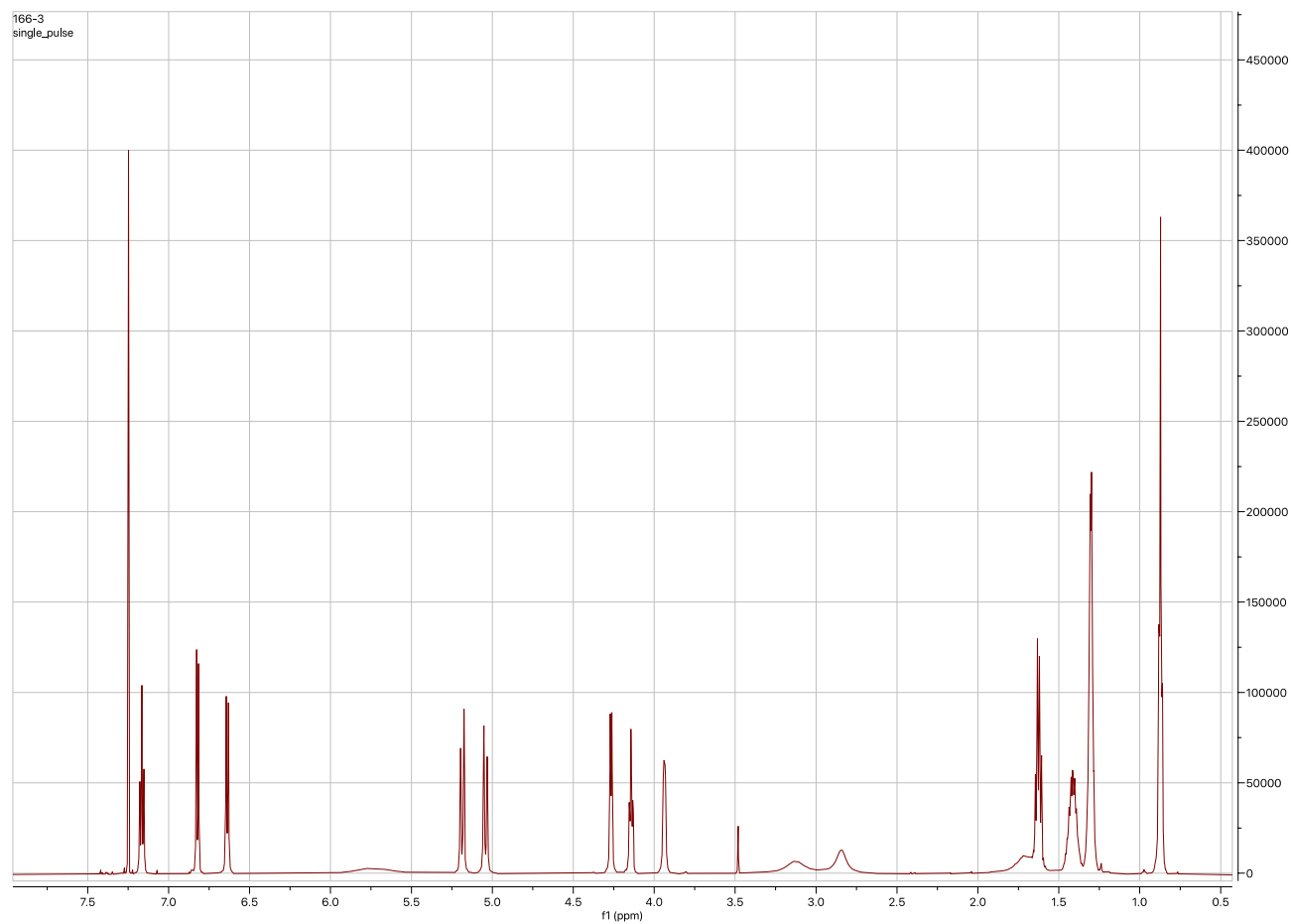
Appendix 18. ^1H NMR spectrum of **24** (CD_3OD , 600 MHz).



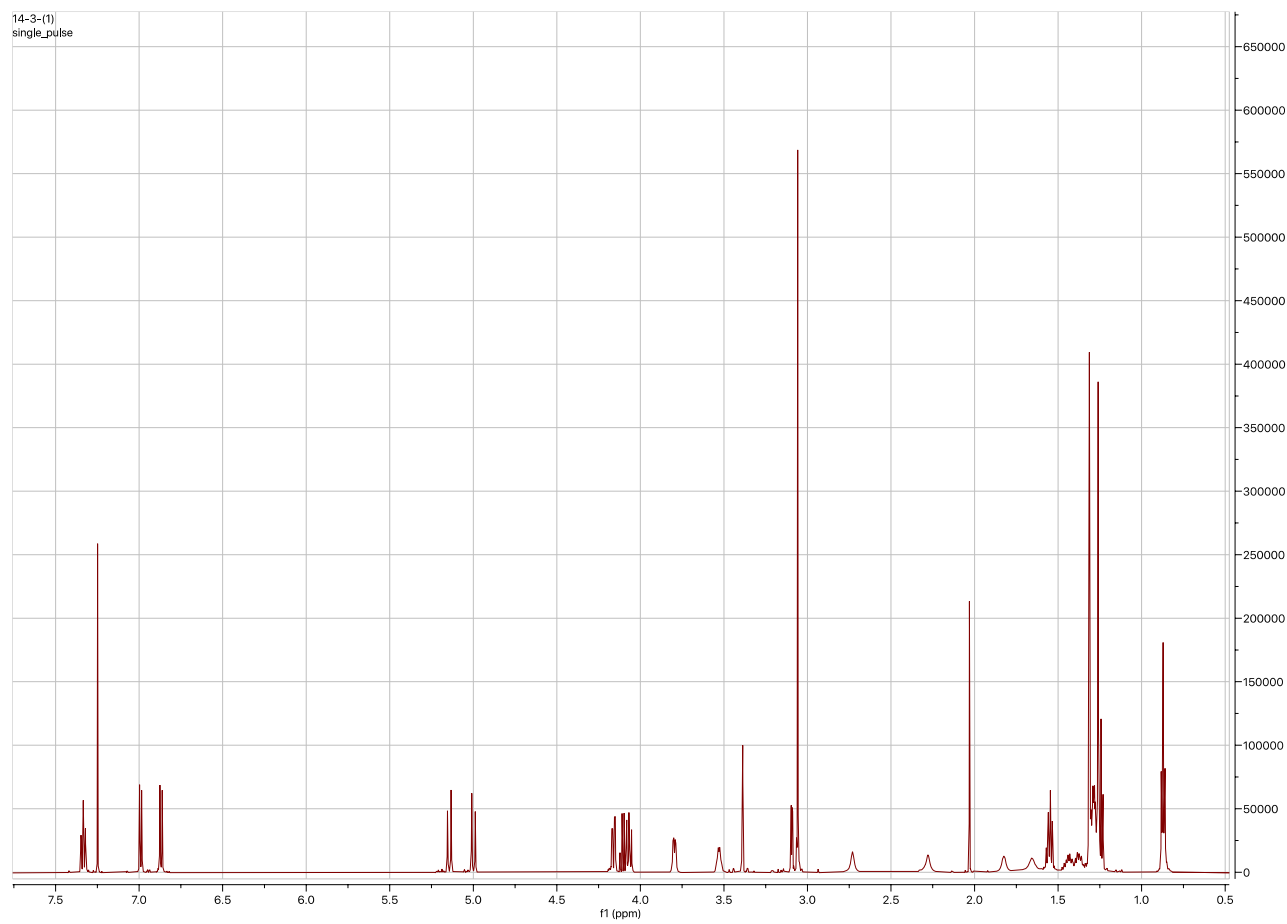
Appendix 19. ^1H NMR spectrum of **25** (CD_3OD , 600 MHz).



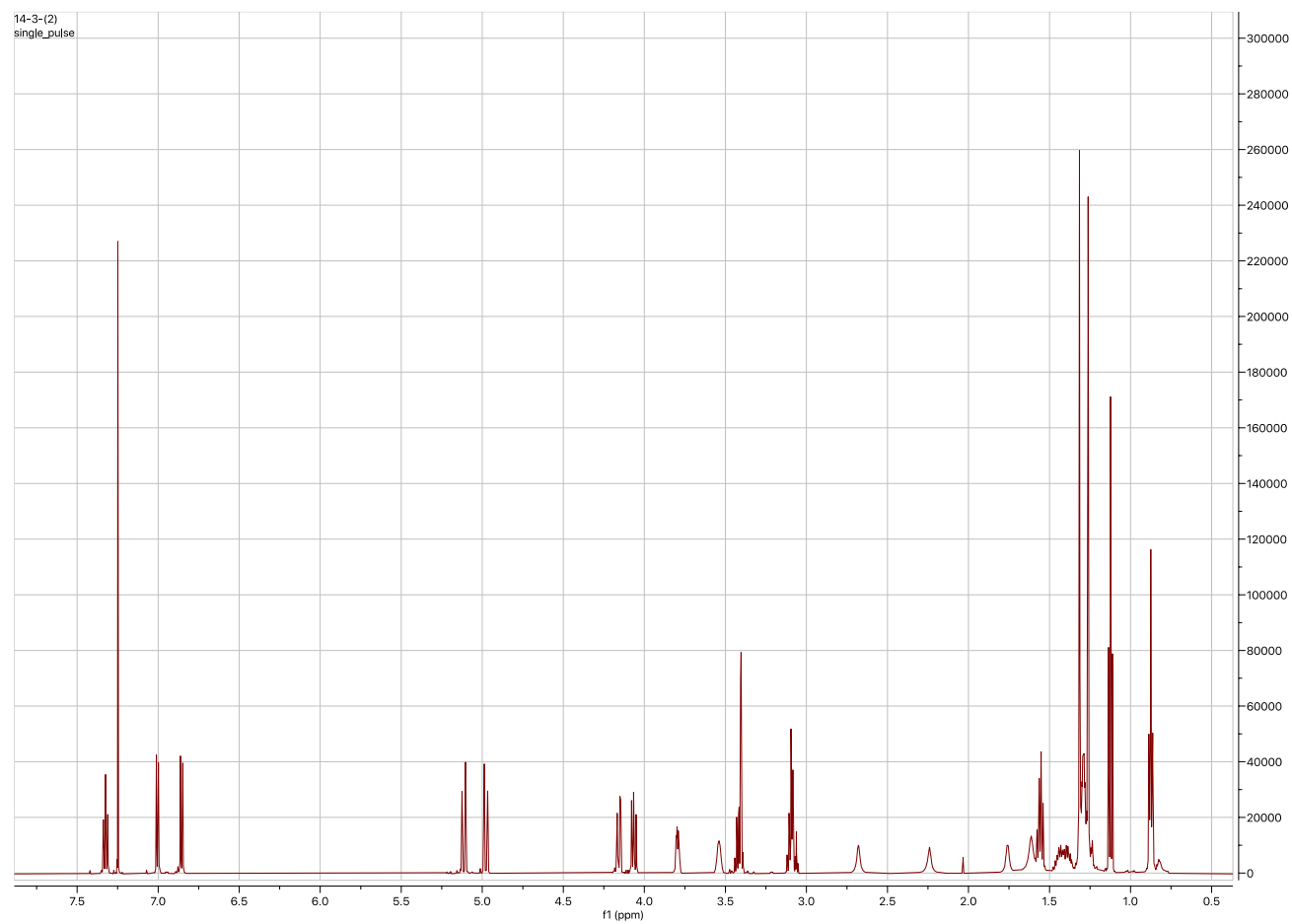
Appendix 20. ^1H NMR spectrum of **26** (CDCl_3 , 600 MHz).



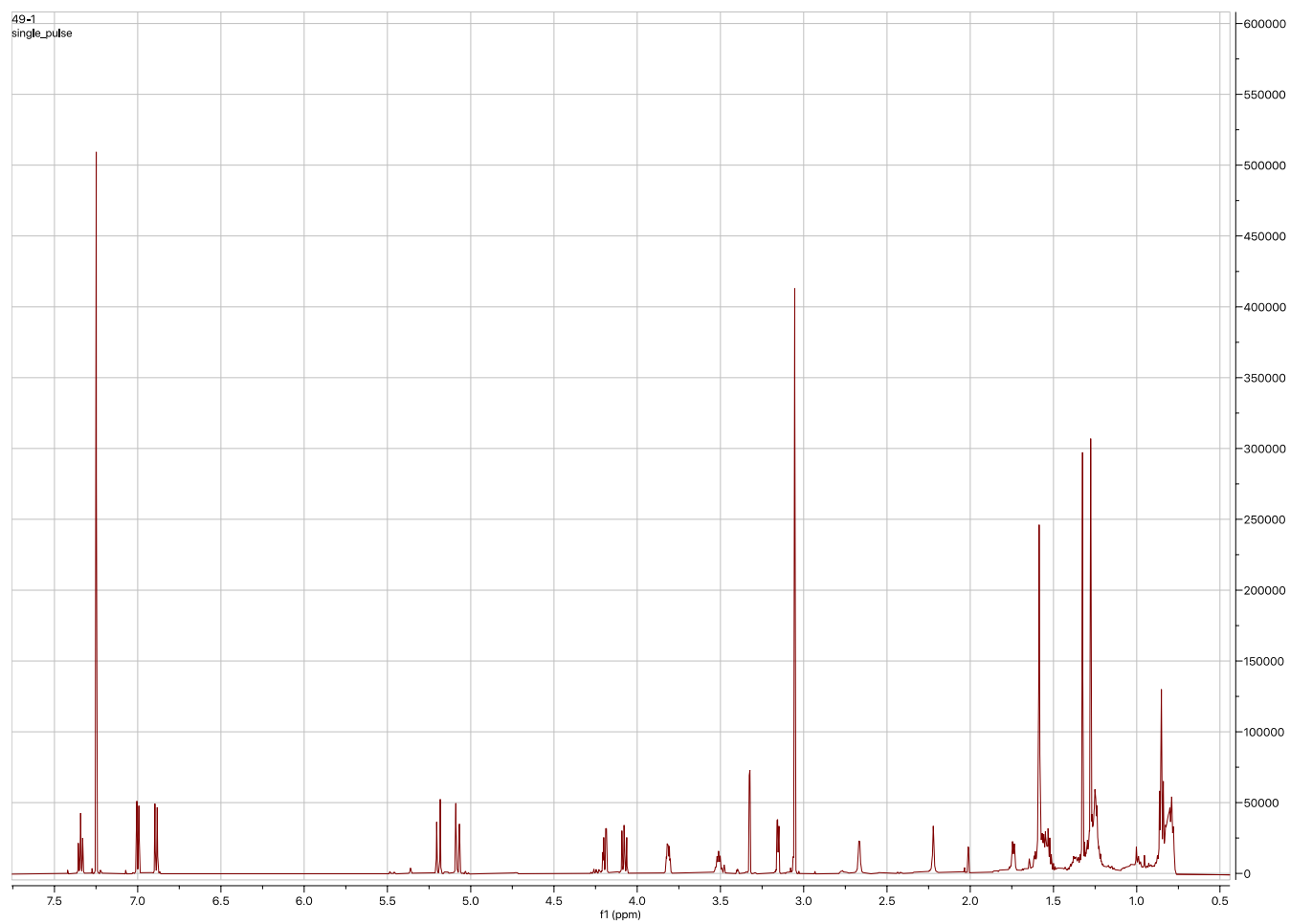
Appendix 21. ^1H NMR spectrum of **27** (CDCl_3 , 600 MHz).



Appendix 22. ^1H NMR spectrum of **28** (CDCl_3 , 600 MHz).



Appendix 23. ^1H NMR spectrum of **29** (CDCl_3 , 600 MHz).



Appendix 24. ^1H NMR spectrum of **30** (CDCl_3 , 600 MHz).

